

Instituto Tecnológico y de Estudios Superiores de Monterrey

Campus Monterrey

School of Engineering and Sciences



An analysis of the technical challenges to produce a Digital Twin of FDM parts

A dissertation presented by

Alan Mauricio Guajardo Treviño

Submitted to the

School of Engineering and Sciences

in partial fulfillment of the requirements for the degree of

Doctor of Philosophy

In

Engineering Science

Major in Advanced manufacturing

Monterrey Nuevo León, Aug 5^h, 2022

@2022 by Alan Mauricio Guajardo Treviño
All rights reserved

Dedication

I would like to express my deepest gratitude to my family, friends, advisor, and thesis committee for believing in me. Thanks for all your unconditional confidence, support, patience, and encouragement. You were my main motivation for pushing through this work.

Acknowledgements

I would like to thank Tecnológico de Monterrey support on tuition, the cyber-physical consortium for the help and equipment and CONACYT with the support for living.

An analysis of the technical challenges to produce a Digital Twin of FDM parts

By

Alan Mauricio Guajardo Treviño

Abstract

A Digital Twin (DT) is a digital representation containing all relevant information of a physical entity with synchronization between the entity and its virtual representation. The Digital Twin is mainly used to monitor, control and predict a part or process. Many challenges exist in implementing Digital Twins in the Additive Manufacturing (AM) fabrication process. However, recent advancements in sensorization and simulation make DT more useful for AM processes and ease its adoption. While FDM parts are commonly used in non-load bearing functions, with the aid of DT, it is possible to improve the mechanical properties and geometrical accuracy of the parts, which can help expand their use in engineering applications. This work evaluates the challenges and benefits of creating a Digital Twin for FDM products and proposes a methodology for gathering the relevant information.

List of Figures

Figure 1. Phases of the product life cycle.....	17
Figure 2. Digital Twin for manufacturing framework [36]	20
Figure 3. Workflow of Digital Twin for manufacturing	21
Figure 4. Workflow to obtain elements for Digital Twins.....	23
Figure 5. Functional view of Digital Twin for manufacturing [36] [58]	25
Figure 6. Life cycle evolution of DT for FDM	27
Figure 7. Functional view of Digital Twin for FDM [36] [58]	28
Figure 8. Deviation between CAD model, slicer model, and scan of the printed part.	38
Figure 9. IWT specimen measurements.....	42
Figure 10. Deposition paths for the parts with IWT of 0.5 mm and IWT 0.8 in three different slicing software.....	43
Figure 11. Images of the actual experimental specimens and their manufacturing defects.....	43
Figure 12. Details of defects in the reticle of the specimens.	44
Figure 14. (a) Q150R-ES Rotary Pumped Coater from Quorum (b) SEM EVO MA 25 by Zeiss.....	45
Figure 15. Specimen mounted on Metrotom 800 CT-Scan	46
Figure 16. Comparison of reticle center. (a) Thin 0.5, (b) Thin 0.6, (c) Thin 0.8	47
Figure 17. Comparison of raster width. (a) Thin 0.5, (b) Thin 0.8, (c) Thin 0.8.....	47
Figure 18. SEM images of the boundary between rasters.....	48
Figure 19. SEM images of layer and raster gaps	49
Figure 20 SEM images of rasters and volume cells	50
Figure 21. SEM images of print layers sliding	50
Figure 22 SEM images of air gaps	51
Figure 23. SEM images of print layer defect.....	51
Figure 24. SEM images of discontinuous carbon fiber strands.....	52
Figure 25. Post mortem CT scan of ASTM d695 specimen. (a) top view, (b) Lateral view, (c) front view.....	53
Figure 26 Post mortem CT scan of isogrid specimen. (a) top view, (b) Lateral view, (c) front view (d) STL.....	54
Figure 27. 1W geometry, all dimensions are in mm.	62
Figure 28. 2W geometry, all dimensions are in mm.	63
Figure 29. Printing orientations (a) 1W Horizontal. (b) 1W Vertical. (c) 2W Horizontal. (d) 2W Vertical.....	63
Figure 30. Specimens on the print bed.....	64
Figure 31. HandyScan Black Elite from Creaform	65
Figure 32. Locations of inspected surfaces for 1W.....	65
Figure 33. Locations of inspected surfaces for 2W.....	66
Figure 34. Location of future tolerances for specimens	66
Figure 35. Digimat-AM printer setup.....	67
Figure 36. Digimat-AM fabrication setup	68
Figure 37. Simulation 2W deformed geometry exported as STL	68

Figure 38. Deformed geometry superimposed in CAD model	69
Figure 40. Result of simulated deformed 2W horizontal from Digimat-AM	70
Figure 40. Tolerance deviation results based on GD&T	76
Figure 42. Flatness tolerance deviation results based on GD&T	77
Figure 43. Cylindricity tolerance deviation results based on GD&T	78
Figure 44. Perpendicularity tolerance deviation results based on GD&T	79
Figure 45. Point cloud differences result in the average of printed parts against CAD models for all specimens	82
Figure 46. Results of average feature deviation between simulations and scanned parts. H: Horizontal, V: Vertical, M: Machine	83
Figure 47. Temperature prediction from thermal simulation of 1W specimen	84
Figure 48. Thermal image from the deposition of 1W specimen	84
Figure 49. Basic model and simulation conditions, defect free (solid) case.	92
Figure 50. Model with raster gaps simulation conditions.	92
Figure 51. Compressive load vs contraction of the different IWT specimens (0.5, 0.6, 0.8, 1.0, 1.5). Solid lines show experimental results, dashed and dotted lines represent Nonlinear Static Simulations (NLS), with overlap represented as a solid structure	94
Figure 52. Buckling simulation results of solid models IWT 0.8, 1.0 and 1.5	95
Figure 53. Buckling simulation results of models with raster gaps and voids IWT 0.8, 1.0 and 1.5	95
Figure 54. Experimental specimens during the test. (a) The onset of buckling occurs when the internal structure begins to collapse; (b) Buckling of the full structure	96

List of Tables

Table 1. Additive manufacturing families	33
Table 2. deviation result summary	55
Table 3 2W machine 1 geometrical tolerance deviation based on GD&T	70
Table 4 1W machine 1 geometrical tolerance deviation based on GD&T	71
Table 5 2W machine 2 geometrical tolerance deviation based on GD&T	73
Table 6 1W machine 2 geometrical tolerance deviation based on GD&T	74
Table 7 Machine1 2W point cloud differences	79
Table 8 Machine 1 1W point cloud differences	80
Table 9 Machine 2 2W point cloud differences	81
Table 10. Machine 2 1W point cloud differences	81
Table 11. Experimental tests and the simulation results	93

Contents

Chapter 1.....	11
1.1 Introduction	11
1.1 Discussion.....	28
1.2 Conclusion	29
1.3 Motivation.....	30
1.4 Objective	30
1.5 Scope.....	30
1.6 Research Question.....	31
1.7 Solution overview	31
1.8 Main Contributions	31
Chapter 2.....	32
2.1 Introduction	32
2.2 Inspection devices.....	40
2.3 Methodology.....	41
2.3.1 Large isogrid specimens	41
2.3.2 Thin isogrid specimens	44
2.4 Results	47
2.5 Discussion.....	54
2.6 Conclusions.....	55
Chapter 3.....	56
3.1 Introduction	56
3.2 Creation of FDM specimens for tolerance performance inspection	62
3.3 Surface inspection of printed specimens.....	64
3.4 Thermo-mechanical simulation	67
3.4.1 Results.....	70
3.5 Thermal simulation	83
3.5.1 Results.....	84
3.6 Discussion.....	85
3.7 Conclusion	86
Chapter 4.....	87
4.1 Introduction	87

4.2	Methodology.....	90
4.3	Results	93
4.4	Discussion.....	96
4.5	Conclusions.....	97
Chapter 5	Conclusion and future work	98
Bibliography.....		100
Published papers.....		113
Curriculum Vitae.....		114
Appendix A.....		115

Chapter 1

1.1 Introduction

Digital Twins are becoming a topic of interest in both the literature and the industry; recent technological advances have led them to be used in various industries to simulate real-world scenarios. To better understand the challenges of creating Digital Twins, it's essential to first define what a Digital Twin is, what elements constitute it and how it has been implemented for FDM in the literature. This chapter seeks to propose a model to describe a DT and analyze the challenges of implementing Digital Twins in additive manufacturing.

The recent advances in technology have led to the emergence and evolution of digital technologies, such as Cyber-Physical Systems (CPS), Internet of Things (IoT), Internet of Services (IoS), Big Data, Cloud Computing, Semantic Web, and Virtualization [1]. A Digital Twin (DT) is a blend of these and many other technologies. These technologies are in the direction of constant evolution. Hence, a DT is thought to continuously evolve with these technologies [2]. The Digital Twin technology is increasingly being explored as a way to improve the performance of physical entities with the use of computational techniques and themselves enabled by the virtual counterpart [3]. Digital Twins are often the best solution to support remote human interaction with physical machines and overcome the challenge of geographical distance [4].

Digital Twin development is still at its early stage. Within literature, there is no consistent view on what the Digital Twin is and how the concept is evolving; there are various definitions in the literature [5] [6] [7] [8]. Digital Twins lack an accurate, broadly accepted definition [9]. The idea of Digital Twins was born from NASA's Apollo program, where a hardware twin that consisted of 2 identical space vehicles was developed [10]. The original description of a Digital Twin defines it as a representation of a physical entity containing information about that entity [11]. The original idea of a Digital Twin consists of a system that can have a subset of two systems, the physical system present in the real world and a virtual system that exists in the virtual space that contains all the essential information of the physical system [10]. Digital Twins generally now have three components, a physical product in real space, a virtual representation of that product in the Virtual space, and the connections of data and information that connect the virtual and real products together [12]. A Digital Twin can contain a collection of the relevant data, algorithms, and models of a part or process, and it includes the properties, conditions, and behavior of the real-life object to a certain extent [13] [14] [15].

The Digital Twin has the following characteristics [16]:

- Contains process data, operational data, and behavioral descriptions through multiple simulation models.

- Develops with the actual system throughout the lifecycle and integrates existing knowledge.
- It is used to explain the operation and derive a solution related to the real system.

A Digital Twin must support many different functions [17]:

- Asset analysis and status prediction:
 - Monitor the various deformations of the material.
 - Estimate the reliability of the asset.
 - Monitor system abnormalities.
- Digital reflection of the asset's lifecycle:
 - Asset lifecycle management. Maintain a continuous flow of data about the various stages of the asset lifecycle.
 - A long-term study of a system that predicts behavior and performance under the influence of the external environment.
 - Virtual launch of an asset.
- Resource management:
 - Optimal resource management,
 - Cooperate with other resources for optimal plant management.
- Decision support based on technical and statistical analysis:
 - System optimization in the engineering phase.
 - Lifecycle optimization based on the forecast of past and future asset status and future state prediction.

Digital Twins shall provide [17]:

- Physical objects and Digital Twins.
- Capacity to extend the process hierarchy.
- Capacity to create different interfaces for distinct hierarchy levels.
- Capacity to increase a model's complicatedness by both hierarchy levels addition, adding hierarchies at both levels, and adding details to each phase of the process.
- Capacity to represent different types of processes using the same display composition.
- Capacity to display different visualization scales with different hierarchical levels and different amounts of detail at any stage of the process.
- A framework that connects various modeling methods of assets with cross-cutting digital models.
- A semantic model that structures all plant-related information and clearly describes the control logic of different types of manufacturing processes.

The benefits of using digital twins are diverse [18]:

- Real-time or offline optimization of working parameters.
- Simplify monitoring of job parameters and automatic management of data flow.

- Predict and prevent machine flaws.

Rasheed et al. [19] summarized the following eight complementary values of Digital Twins:

- Personalized products and services.
- Real-time monitoring and control.
- Predictive maintenance and planning.
- More efficient and safer performance.
- Better and more efficient decision support system.
- Situational and Risk Assessment.
- Greater synergy and collaboration within and between teams.
- Better documentation and communication.

Digital Twins can use any model that accurately represents the physical object being twinned [20].

The main components that constitute a Digital Twin of an object are [20]:

- Object model.
- Object data.
- A way to actively update or adjust the model according to the data.

The following criteria are used to differentiate a Digital Twin from other digital modeling and simulation techniques [12]:

1. The virtual representation consists of an instance of the physical Entity.
2. The physical system's data and information are used to update the virtual representation's states.

Digital Twin could be confused with simulation models; the main distinction between a simulation model and a Digital Twin is that the former tracks the present and past states of a single instance of the physical system while the latter predict future states of a physical system based on a set of initial assumptions [12].

A Digital Twin approach would use the test data from the prototype to update parameters in the model of the prototype, use the updated model to predict performance in use, and then update the design [20].

In the development phase, a Digital Twin can consist of an exact CAD representation of the part and multi-body and finite element method simulations to accurately mirror the behavior in the virtual space [13].

Osho et al. [23] realized that due to the varied applications of the DT concept, a single solution or platform for a DT is unrealistic. Thus they presented a generalized

framework for the development of a DT for FDM, which is defined by its maturity in 4 phases:

- 1 Representation.
- 2 Replication.
- 3 Reality.
- 4 Relational.

In the first phase, a basic digital twin would just need to interpret the physical system, represent its significant features and collect data from the physical entity. In the final phase, the digital twin would have some autonomy and be able to communicate in both directions with the cyber-physical system to make decisions and carry out activities in real-time.

Based on the standard and the literature, a Digital Twin of an FDM part is:

- Digital representation of an observable manufacturing element that consists of an exact CAD representation, a sufficiently accurate finite element method simulation, and a way to update the model [7][8][9].

The implementation of DT technology in production systems has shown great potential for enabling advanced management of production data [24]. The ability to continuously physically monitor production machines, parts, and processes during part construction, providing the opportunity to keep quality and process indicators under constant control while creating the means to detect quality deviations and other problems early so that the process can be rectified immediately whenever possible, or stopped early to avoid wasting resources again [25] A Digital Twin can assess the current conditions of the part being manufactured and additionally have the authority and ability to take corrective actions through a built-in feedback loop system [26]. AM processes are often optimized using offline modeling and monitoring tools, while the adaptability and real-time decision support provided by Digital Twins have not been fully achieved [27]. Digital Twins play a transformative role in not only the way we design and operate intelligent cybernetic systems but also in the way we enhance the modularity of multidiscipline systems to address fundamental barriers not addressed by current development modeling practices [19]. In the future, the importance of DT technology will continue to grow, driven by needs such as a more stringent throughput, productivity and cost reduction goals, mass customization in production, verification, faster and smarter system validation, a higher degree of reconfiguration, and tighter integration. All of this, across the entire production ecosystem, including the consumption space [28].

Rasheed et al. [19] summarized the enabling technologies of Digital Twins:

- Physics-based model.
- Data-Driven Model.
- Combined evaluation and modeling.

- Machine-human interface.
- framework and platforms.

Providing additional modular sensor nodes for 3D printers helps detect deviations from intended printing early. Printing defects can be detected using a video camera, remote monitoring with acoustic emissions, or sensor data [29]. Built-in sensors can monitor a variety of physical phenomena associated with cyber-physical systems, such as vibration and energy consumption [30].

DT can greatly aid in the additive manufacturing process. However, there are many challenges when implementing a Digital Twin in FDM. There is no broad consensus on a definition, implementation framework, or protocol [9]. In the literature, scarce research has explored the creation and implementation of DTs for manufacturing [31]. High quantities of data are acquired through the lifecycle of industrial production, yet these data are hysteric and isolated from each other, resulting in inefficient utilization of these precious resources [32].

High-performance Applications often require products that meet strict functional and geometric specifications. This is reflected in the increasing demands of quality assurance requirements and the growing challenges of improving the robustness of the FFF process [25]. Consumer-grade 3D printers do not detect printing errors because they are designed primarily with no feedback mechanisms [29]; it might not even be feasible to place sensors in these systems intrusively after they are fabricated [30]. In the case of Digital Twins for Cyber-Physical Cloud Manufacturing (CPCM) system, much effort is underway to adapt them. Because of the large number of applications that must be processed concurrently, the number of information requests via cloud servers may exceed available computers' capacity [4]. Full physical simulation of the whole production line will take up a lot of time, space, and cost [33]

Rasheed et al. [19] summarized the common challenges for implementing Digital Twins”:

- Real-time simulations, latency, estimation, and automation.
- Transparency and interpretability.
- Data management, compression, and improved data quality.
- Extrapolation ability.
- Combine, assimilate, and combine large-scale data
- Data transmission, communication protocols, and data security.

Bartsch et al. [34] performed a systematic review to investigate the current state of the art and progress of the implementation of the DT. He identified 3 main challenges for achieving the goal of implementing a complete DT in AM:

- Standardization and consistent use of terminology.

- Current production-process models are too complex for even high-end computers to achieve real-time prediction and multiscale modeling or lack accuracy and reliability.
- Common frameworks and corresponding physical and virtual interfaces are needed to connect the different systems.

To implement Digital Twins, 3 steps are primarily followed [35]:

- A Digital Twin Prototype (DTP) includes initial planning and analysis data as well as physical system implementation processes.
- A Digital Twin of each property of the physical object.
- All Digital Twins of system properties should be integrated.

A critical gap in the twinning between the physical world and a virtual model is the real-time monitoring data synchronization for a Digital Twin in the design [33].

One of the main problems encountered when implementing Digital Twins is accurately describing the characteristics of the physical system, and the digital model must be correctly calibrated to accurately perform optimization and error predictions [18]. To implement Digital Twins in FDM, the partial models should be synchronized to represent the whole life cycle of the product or process [36]. The Digital Twin's vision refers to a comprehensive physical and functional description of an entity, product, or system that contains almost all information that may be needed in all current and subsequent lifecycle phases [14].

A Digital Twin made for manufacturing could help enhance the process, improve the design, monitor production, schedule maintenance, and predict hindrances.

- Digital Twins of old products can be rehashed to aid in the inception of new products.
- By comparing defective products' twins, it may be possible to determine if there is an inherent defect in the rest of the products.
- Digital Twins may assist in enhanced iteration processes.

When implementing a new asset, the main goal is to create or improve a product or its manufacturing process to meet the customer's needs [37]. Product lifespan determines the AMP life scope, and the two most commonly used life scopes are [38]:

- Cradle-to-gate: it extends from the acquisition of the raw materials to the instance it leaves the factory.
- Cradle-to-grave: it extends from the acquisition of the raw materials, utilization, and finally the disposal.

A product life cycle consists of 6 phases, and these phases are [37]:

- Design
- Fabrication of product
- Delivery of Product
- Use of Product
- Product refurbishment
- Disposal and Recycling

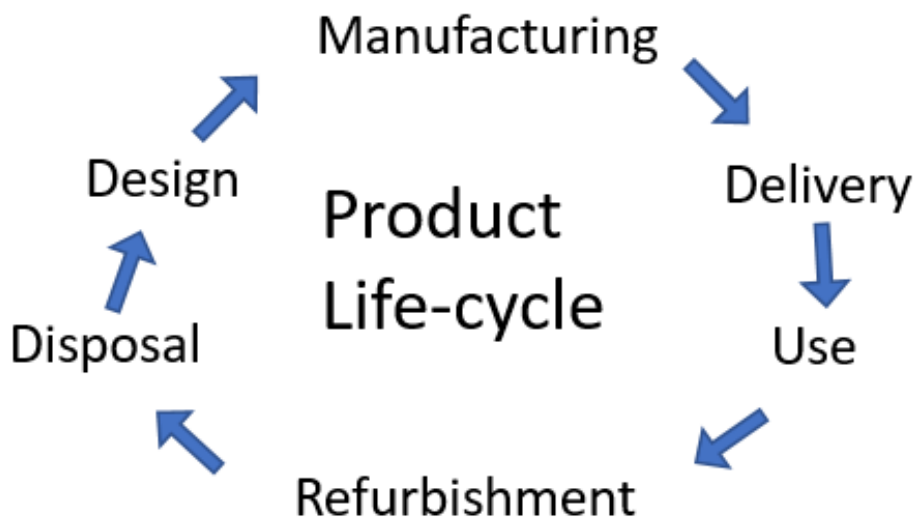


Figure 1. Phases of the product life cycle

Demand for a broader range of products coupled with reduced product lifecycles has spurred the emergence of mass customization models [39]. Unlike requirements for larger batch sizes, market demand is now becoming customer-focused, requiring smaller batch sizes with shorter life cycles [40]. Diversity is often achieved at different stages of the product life cycle. It can be achieved during design, assembly, the sales and distribution stages, and through modifications during the use phase. In addition, diversity in the manufacturing process can be achieved, e.g. by rapid prototyping [41]. Since additive manufacturing processes yield lower production rates compared to conventional manufacturing, it becomes necessary to constantly monitor the whole process and make the needed adjustments to increase the number of acceptable parts; therefore, increasing the overall quality of the process. Yet, in the literature, most emphasis on Digital Twins is set on a single phase of the lifecycle; 5% of studies concentrate on the full lifecycle [32].

The diverse implementations of Digital Twins in additive manufacturing are presented in the following review of the literature.

Cai et al. [42] presented a methodology of using augmented reality (AR) technique to communicate layout information between an AM system made of robotic arms

and its corresponding Digital Twin for toolpath planning and simulation. Two desktops made up their prototype system. To ascertain the spatial relationship between various components in the system, such as the camera, markers, robotic arms, and part substrate, transformation matrices and AM robotic arms have been developed. They concluded that the suggested methodology enables quick recovery of position information from the physical system layout into the Digital Twin and makes it easy to deploy a layout chosen in the Digital Twin using simulation and optimization into the physical system.

Mandolla et al. [43] Proposed blockchain Digital Twins that improve reliability, transparency, and protection of AM product components, where components are printed exactly when needed and use blockchain to securely send data to validated 3D printers, therefore saving inventory, import, and logistics costs. When digital is developed, it can more accurately represent the life cycle of AM products by not only simulating and monitoring the entire manufacturing process to avoid printing errors but also better assessing mechanical properties. Parts can be used more reliably with the application of this technology.

In order to forecast the spatial and temporal fluctuations of metallurgical factors that affect the structure and characteristics of components in laser-based directed energy deposition, Knapp et al. [44] built and validated a Digital Twin for the AM process. Users choose different parameters for the Digital Twin. Additionally, the Digital Twin would forecast estimates for crucial factors such as transitory temperature bounds, the geometrical features of molten pools, and changes in the cooling and solidification rates over time and space.

To improve the production planning of an FDM process, Stavropoulos et al. [27] looked into the combination of empirical and theoretical models. They supplied a platform that supported Digital Twins and gathered insights while offering optimization services to future networked AM manufacturers. For the purpose of production planning, the cycle time, the energy use, and the connection were taken into account. They concluded that the models on display give users the knowledge required to raise the caliber of their output while reducing the amount of material wasted on defective products.

For in situ real-time monitoring of the powder bed fusion (LPBF) and directed energy deposition (DED) 3D printing manufacturing processes as well as material defect forecast, Gaikwad et al. [45] developed a Digital Twin. To identify potential anomalies in the AM process, they integrated physics-based predictions, in-situ sensor data, and machine learning. They found that, compared to using only the theoretical model's predictions or in-situ sensor data alone, augmenting the insight into the process physics gained through a theoretical model with real-time information from in-situ sensor data in a machine learning framework, leads to higher statistical fidelity of detecting process flaws.

For performance tracking and anomaly identification in AM processes, Balta et al. [46] presented a Digital Twin architecture. The DT has a versatile function block that

may be used for a variety of tasks, including performance monitoring and anomaly detection, and is able to record both the functional and continuous dynamics of an AM process. As a novel contribution, Signal Temporal Logic (a formalization to specify propositions on a signal measured from an underlying system) specifications are suggested for anomaly identification in AM processes.

The following statements about the state-of-the-art trends for DTs in manufacturing were condensed by Moyne et al. [28]:

- Even if they don't refer to them as DT, several manufacturing industries already successfully use them.
- Less devoted Digital Twins are typically not utilized during actual manufacturing.
- The quality, throughput, and cost challenges in some industries have led to DT improvements.
- The majority of the DTs in use in factory operations are dedicated DTs, each with a specified purpose.
- DT technology cooperation amongst DT application domains is frequently lacking.
- Manufacturing is starting to investigate and gain from merging and abstracting DT solutions.

There is extensive work in process monitoring for FDM:

- Monitoring the position of the extruder nozzle with encoders [47]
- Monitoring the filament length with attached encoders [48]
- Monitoring filament extrusion with encoders [49]
- Monitoring the creation of thermal stresses during deposition with Bragg sensors attached to the part [50]
- Capturing filament temperature and pressure with sensors to optimize print flow [51]
- Monitoring the pressure and temperatures of the extrusion with sensors in the nozzle [51]
- Capturing the hotend temperatures with thermal imaging [52]
- monitoring the print layer development with thermal imaging [53]
- Detecting extruder anomalies with acoustic emissions [54]
- Detecting machine problems with acoustic emissions [55]
- Detecting step lost with accelerometers on the machine [56]
- Monitor vibrations in the extruder with accelerometers to detect nozzle obstruction [57]

The previous Literature review shows that although challenging, the implementation of Digital Twins is seeing a boom in manufacturing, among other areas, thanks partly to lowering costs in sensorizations, data management, simulation, and digitalization.

According to ISO 23247 [36], a Digital Twin for manufacturing is “a digital representation of an observable manufacturing element with synchronization between the element and its digital representation.” Digital Twin exists along the life-cycle of the product. Digital Twins aid with identifying abnormalities in manufacturing processes to attain functional objectives such as [36]:

- real-time control.
- predictive maintenance.
- in-process adaptation.
- Big Data analysis.
- machine learning.

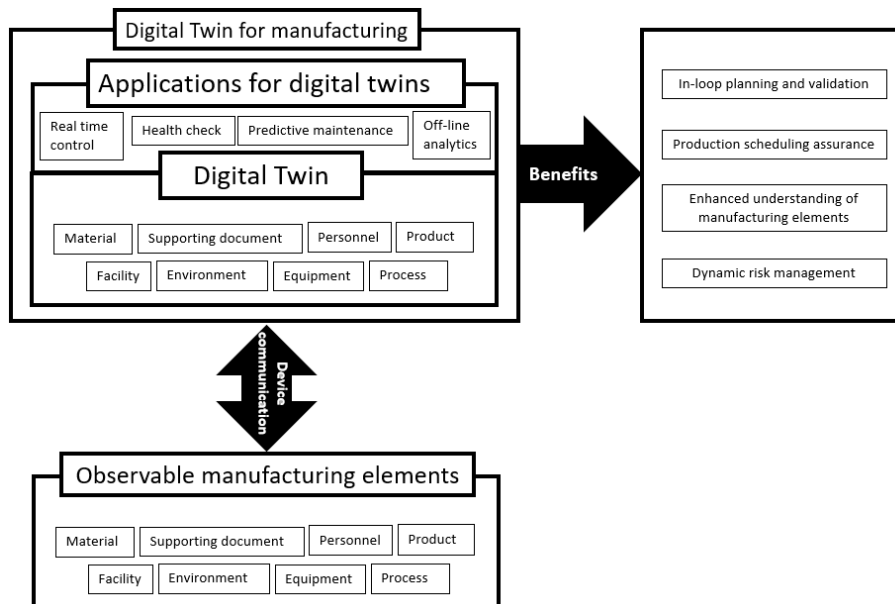


Figure 2. Digital Twin for manufacturing framework [36]

Figure 2 shows the physical entities that communicate with their virtual counterparts and the benefits of DT implementation. Observable manufacturing elements like material, product, and processes are digitalized through varying methods like sensors and scanners, and the applications enable benefits such as:

- Process planning.
- Production Scheduling.
- Simulation and Prediction.
- Managing risks.

Many elements would need to be accurately digitalized to create a full DT, thus making the creation of Digital Twin an arduous and challenging task. In this work, the focus will be set on FDM products.

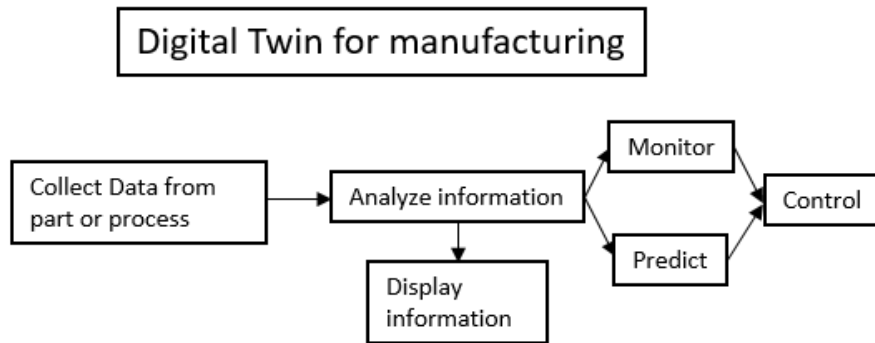


Figure 3. Workflow of Digital Twin for manufacturing

As seen in Figure 3, A Digital Twin in manufacturing is capable of collecting the data from a part or process, analyzing the information, displaying it, then using the information to monitor and predict the behavior and, based on that, decide to implement corrective measurements or change the entire process from the beginning.

DTs of products and processes are more convenient when using digital representations that can be shared throughout the product life cycle. You can use CAD, CAM, CAI, and CNC systems to create data for Digital Twin modeling and view the results of the Digital Twin [36]. In FDM, you can use the original CAD of the modeled part, perform thermo-mechanical simulations to preview predicted deformation during fabrication, use those results to create a geometry that will compensate for the expected geometric distortion, print the part, scan the fabricated part, and compare the Original CAD against the simulated warped geometry and the actually printed geometry to iterate into a more precise compensated geometry.

To generate a Digital Twin for FDM, you need:

- CAD model
- FEA model
- Fabrication data
 - Toolpath
 - Thermal images
- Finished part data
 - CT scans
 - SEM images
 - Surface scan

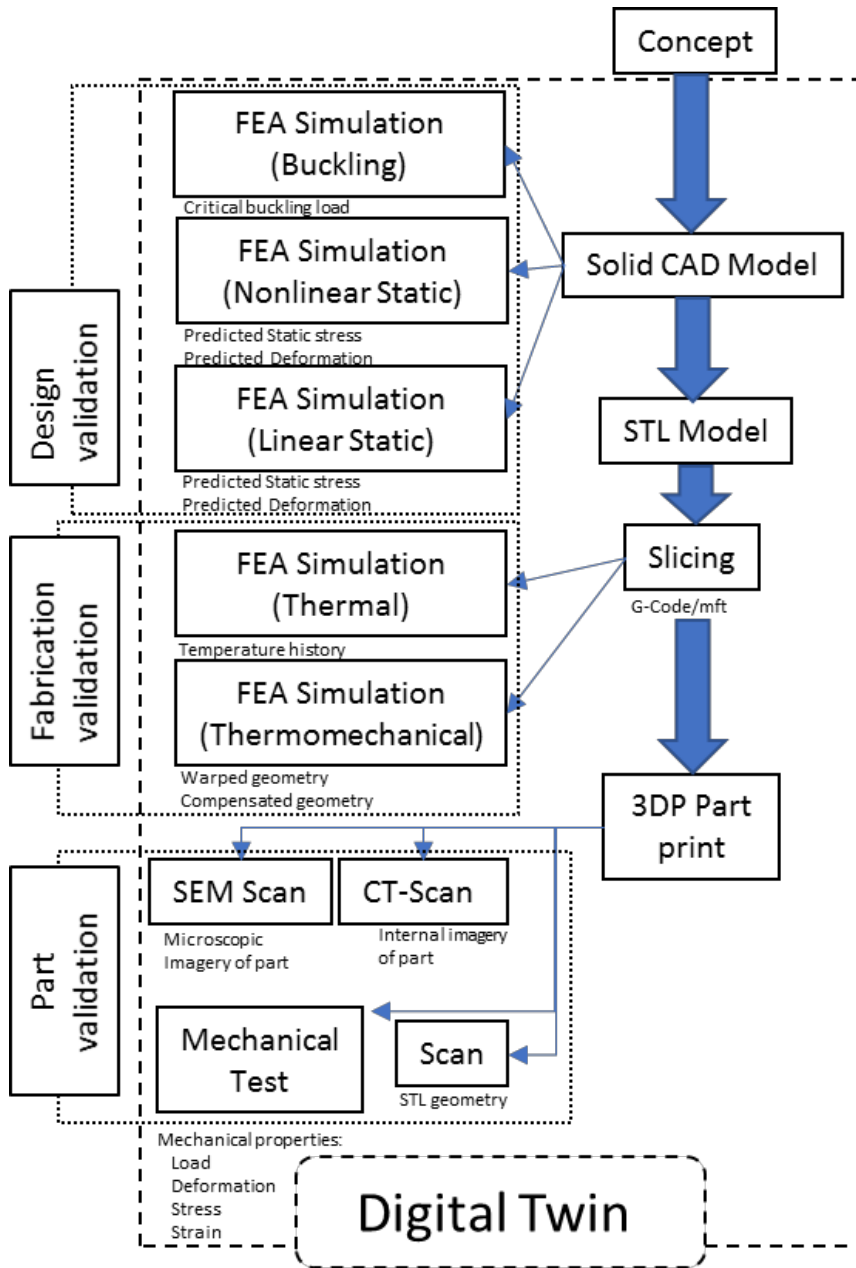


Figure 4. Workflow to obtain elements for Digital Twins

As seen in Figure 4, to create an FDM part, First the product is conceptualized, then Designed in CAD software, an STL is exported, sliced to create the toolpath the printer will be following, and finally, the part is printed. Data is collected through design, fabrication, and part validation phases. Many processes are required to be conducted to obtain all the elements to create a Digital Twin for an FDM part. Equipment like the CT-Scan, SEM microscope, and the universal machine is expensive and difficult to use. Furthermore, the elements gathered need to be correctly obtained and detailed for the DT to be accurate.

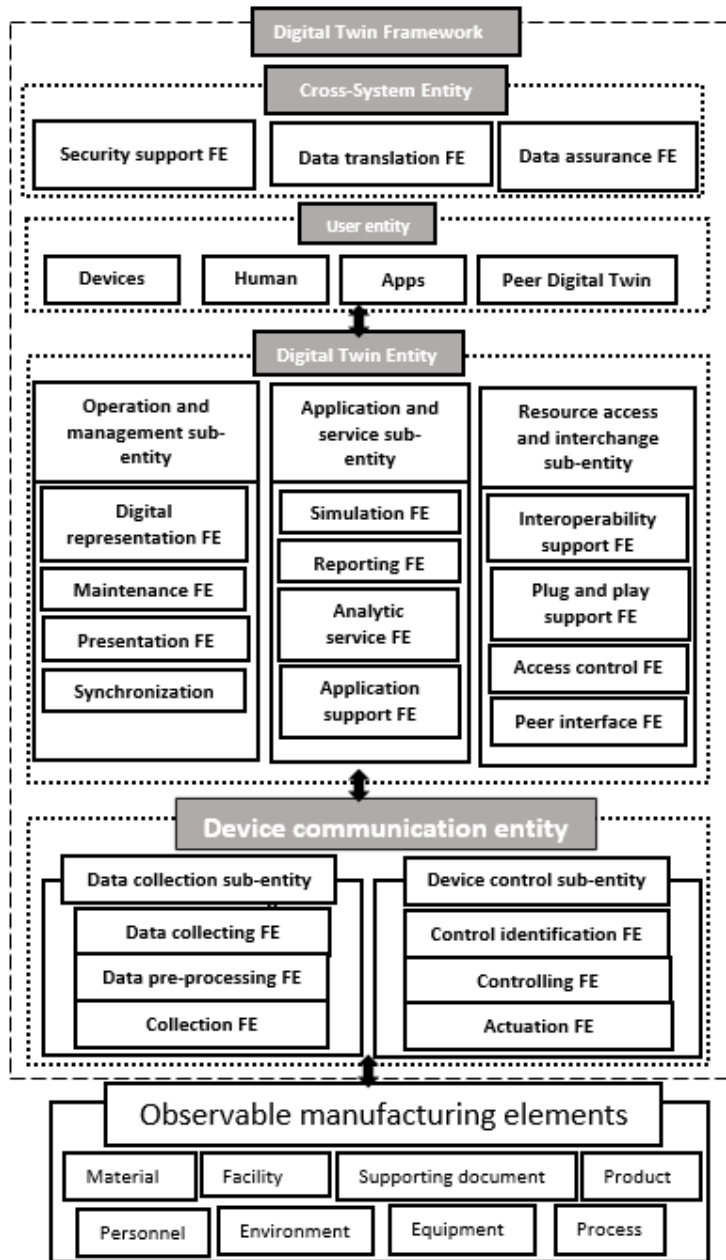


Figure 5. Functional view of Digital Twin for manufacturing [36] [58]

As seen in Figure 5, many entities, sub-entities, and functional entities (FEs) exist in the Digital Twin framework that communicates with the Observable manufacturing Elements (OME) in diverse ways. The functional view of the Digital Twin reference architecture consists of [58]:

- User entity
 - User interface FE: interfaces the user entity to the Digital Twin entity.
- Digital Twin entity
 - Operation and management sub-entity
 - Synchronization FE: synchronizes the status of the Digital Twin with its OME.
 - Presentation FE: presents information.
 - Digital representation FE: models the information of an OME to represent its characteristics.
 - Maintenance FE: keeps the DT operational.
 - Application and service sub-entity:
 - Analytic service FE: manages and analyses the data collected from the OMEs, as well as results from simulations.
 - Reporting FE: reports simulation predictions, production results, and data analytics results.
 - Application support FE: aids in implementing applications such as open and closed loops and predictive and reactive maintenance applications.
 - Resource access and interchange sub-entity
 - Interoperability support FE: enables integration between DTs and other systems.
 - Access control FE: manages the access of the OMEs.
 - Plug and play support FE: provides connection of an OME to its Digital Twin.
 - Peer interface FE: issues interfaces to other DTs.
- Device communication entity
 - Data collection sub-entity
 - Data collecting FE: gathers information from OMEs.
 - Data pre-processing FE: preprocesses collected information by filtering or aggregation.
 - Collection identification FE: recognizes what information is needed from the OMEs.
 - Device control sub-entity

- Controlling FE: commands OMEs by sending orders to devices in their language.
 - Actuation FE: activates an OME in response to a solicitation from the user or Digital Twin entity.
 - Control identification FE: recognizes an OME to control it uniquely and unambiguously.
- Cross-system entity
 - Data assurance FE: guarantees the accuracy and integrity of information.
 - Security support FE: ensures the Digital Twin including authentication, authorization, confidentiality, and integrity.
 - Data translation FE: enables translation of traded data between entities.

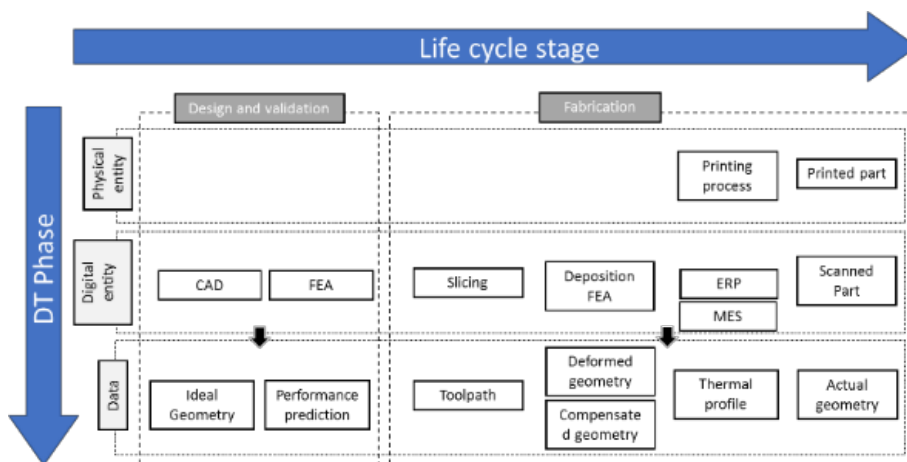


Figure 6. Life cycle evolution of DT for FDM

As shown in Figure 6, as the part goes through design and validation, and fabrication phases, digital entities are being created; these entities have essential information about the 3D part, like the predicted mechanical performance or the expected deformed geometry.

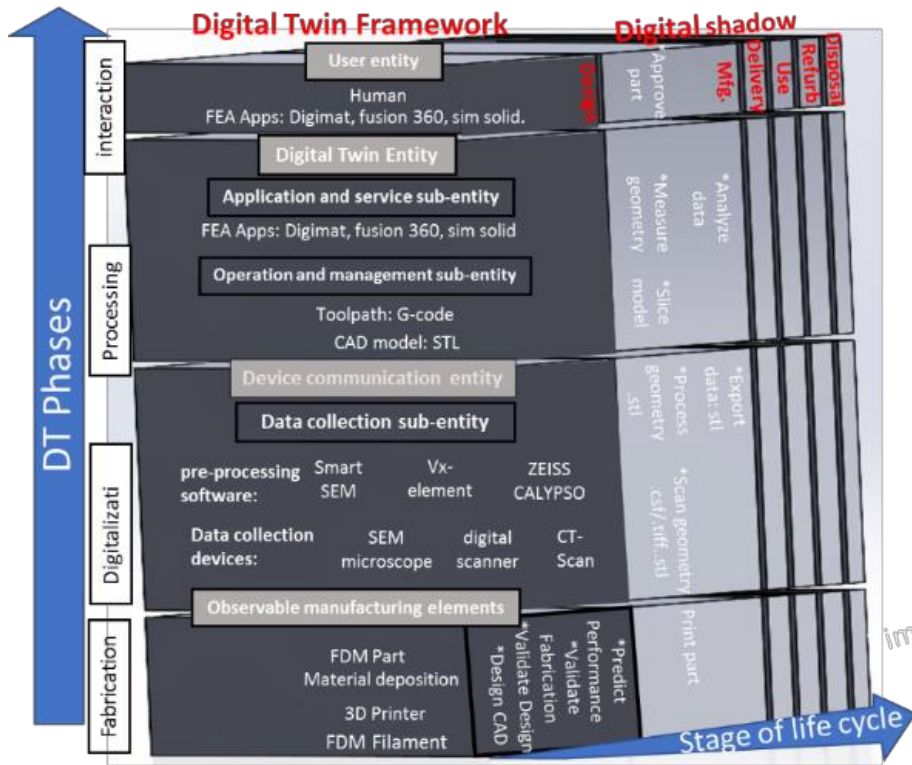


Figure 7. Functional view of Digital Twin for FDM [36] [58]

Figure 7 shows how During the fabrication phase, observable manufacturing elements are digitalized, and their data is collected, using that data simulations are being performed to predict the behavior of the part and the printing process, and the results are examined and experimentally valeted to finally let the user decide if the part is approved

For this work, digital elements are only collected from the design and manufacturing stage. The communication between the observable manufacturing elements and the Digital Twin used in this study is not performed in real-time or automatically; relevant information is collected and used for FEA simulations

1.1 Discussion

As seen in Figure 7, the process of creating a Digital Twin of the fabrication process and printed part is extensive, many elements need to be created, and data

needs to be collected accurately. a CAD model, FEA model, Fabrication toolpath, CT-scans, SEM images, and surface scans are required. Figure 7 explains how the elements are collected in each phase.

1.2 Conclusion

A Digital Twin for manufacturing is a virtual representation of a product or a process containing all relevant information of the physical entity with synchronization between the entity and its digital representation.

The Digital Twin has a user entity where the person gives input and gets output; the Digital Twin entity, where the physical part or process is represented with its behavior, and a device communication entity that handles data collection, simulation, and control of the system, the cross-system entity that aids on the transfer of between entities, and finally the observable manufacturing elements, that are the physical entities being virtualized by the Digital Twin.

Digital Twins in manufacturing are mainly used to monitor, control, and predict a manufacturing process. The Digital Twin, when implemented correctly, can assist in increasing the efficiency and effectiveness of a process; in FDM, this would mean less lead time when designing a new component, fewer geometrical deviations of the part compared to the designed model, and adequate mechanical behavior for the intended application.

A Digital Twin is not an exact copy, as models always have a certain level of abstraction and only represent physical reality with an error margin [15]. As there is no Digital Twin that perfectly emulates all the product's life cycle, there are many challenges that complicate the creation of a Digital Twin for FDM.

1.3 Motivation

The motivation for this thesis surges from the boom seen in the literature on the use of Digital Twins to optimize manufacturing processes. Fused Deposition Modeling (FDM) is widely used as a method for prototyping and small patch production, having cost and time advantages in small fabrication numbers and capable of developing complex shapes without cost increase. However, FDM has many drawbacks like lower geometrical accuracy and mechanical properties compared to traditional manufacturing, as such, DT seems like a viable option to increase the performance of parts fabricated by FDM.

This thesis works to assess the challenges of creating a Digital Twin for FDM parts

1.4 Objective

The main goal of this work is to analyze the technical challenges of producing a Digital Twin for FDM parts and explain how to obtain the elements needed for a Digital Twin of an FDM part.

1.5 Scope

The scope of this work is a Digital Twin for FDM that only covers the design and fabrication phase. It does not cover other phases of the product life cycle. This work could be adapted to work with other manufacturing processes and phases

1.6 Research Question

What are the challenges for producing a Digital Twin for FDM? what elements are required to produce a Digital Twin for FDM.

1.7 Solution overview

The solution is to obtain the elements of a Digital Twin for FDM parts and analyze the challenges of integrating the elements into a DT. This may help to illustrate the challenges in other processes and for other phases.

Comentado [LGFU1]: Justificado es muy largo.

1.8 Main Contributions

The main contributions of this work are the analysis of the technical challenges of producing a Digital Twin for FDM, the improved model of a Digital Twin for FDM, and the operations to obtain the elements needed for an improved DT model.

Chapter 2

2.1 Introduction

One of the main qualities of a Digital Twin is that it virtually represents the physical entity it is based on, be it by geometry or behavior. However, accurate representation of the physical entities is limited by the complexity of the system. The FDM parts being fabricated are not an exact copy of the model created by the designer, FDM parts are built by melting plastic filament with a programmed toolpath, which creates rasters, and print layers during fabrication parts undergo complex thermomechanical profiles that create thermal stresses, leading to geometric deviations. Furthermore, environmental and machine variations may cause printing defects to arise. All these geometric variations are not present in the CAD model. In this chapter, the FDM fabrication process strategy will be inspected to understand how parts deviate geometrically from the design model.

A manufacturing process is an act of turning any material into a product with different shapes and sizes, be it by changing or not the material properties of the final product [59]. The selection and design of manufacturing processes are critical aspects of the quality and economic efficiency of industrial output. [60]. Conventional manufacturing processes can be classified into [61]:

- Subtractive
 - Machining
 - Grinding and finishing
 - Unconventional machining
- Constant mass processes
 - Casting
 - Metal forming
 - Powder metallurgy process
 - Heat treatment
- Additive
 - Welding
 - Joining
 - 3D printing

The American Society for Testing and Materials (ASTM) defines additive manufacturing (AM) as “a process of joining materials to make objects from 3D model data, usually layer upon layer” [62]. 3D printing is a set of advanced manufacturing methods that produce physical items from 3D CAD models that are digitally sliced into 2D cross sections in a discrete point-by-point, line-by-line, or layer-by-layer additive manner [63]. The rapid development of additive manufacturing (AM) has led to many different names for the field, including 3D printing (3DP), additive fabrication (AF), additive layered manufacturing (ALM), rapid

casting, rapid manufacturing (RM), rapid prototyping (RP), rapid tooling and solid free form fabrication (SFF). An attempt to standardize the terminology has been made in ISO/ASTM 52900 [64].

One of the most widely used processes is fused filament fabrication (FFF) or fused deposition manufacturing (FDM), an AM technique based on the multilayer deposition of melted thermoplastic [65]. Parts are created in the FDM technique by extruding molten filament through a heated nozzle [66]. The mechanical qualities of the created pieces are one of the process's limits in engineering applications. Because the printing process has a direct impact on the part's quality, applications that allow users to regulate it are required [67].

According to the basic principle of manufacturing, AM is classified into seven categories; namely, binder jetting, material extrusion, directed energy deposition, material jetting, powder bed fusion, sheet lamination, and vat photo-polymerization [68], which are described in Table1 shown below.

Table 1. Additive manufacturing families

Family	Alternative Names:	Description	Advantages & Limitations	Typical Materials
Photopolymerization	Scan, Spin, and Selectively Photo cure Stereolithography Digital Light Processing Continuous Liquid Interface Production	A laser or projector is used to selectively expose a vat of liquid photopolymer resin to light, causing polymerization to start and turning the exposed areas into solid parts.	Advantages: A good degree of precision and intricacy The finished surface is smooth accommodates extensive build zones Limitations: Needs support and post-curing	UV curable Photopolymer Resins
Powdered Fusion	Selective Heat Sintering Selective Laser Melting Selective Laser Sintering	Powdered materials are selectively consolidated by melting them together	Advantages: substantial complexity Powder acts as a support material	Powders, Plastics, Sand Metal, and Ceramic.

	<p>Direct Metal Laser</p> <p>Multi Jet Fusion Sintering</p> <p>Electron Beam Melting</p>	<p>using a heat source such as a laser or electron beam. The unfused powder surrounding the consolidated part acts as a support material for overhanging features.</p>	<p>a variety of materials can be used</p> <p>Limitations:</p> <p>Needs post-processing; the machine is challenging to clean; employ caution while using x-rays.</p>	
Binder Jetting	3D Printing, Voxel-jet Ex-One	<p>To construct parts layer by layer, liquid bonding agents are selectively put onto thin layers of powdered material. Both organic and inorganic materials are used as binders. After being printed, pieces made of metal or powdered ceramic are usually burned in a furnace.</p>	<p>Advantages:</p> <p>Enables printing in colors</p> <p>extremely productive</p> <p>use a variety of materials</p>	<p>Sand, Powdered Plastic, Glass, Metal, and Ceramic.</p>
Material Jetting	Smooth Curvatures Printing Polyjet	<p>To create pieces, material droplets are</p>	<p>Advantages:</p> <p>Excellent precision</p>	<p>Polymers, Photopolymers, Waxes</p>

	Multi-Jet Modeling	placed one layer at a time. Both jetting thermally molten materials that afterward solidify in ambient temperatures as well as jetting photo-curable resin and curing it with UV light are common kinds.	enables elements to be fully colored and enables the use of multiple materials in one part. Limitations: wax-type materials and a lengthy production time are weaknesses.	
Sheet lamination	Ultrasonic Additive Manufacturing Laminated Object Manufacture Selective Deposition Lamination	To create an object, sheets of material are piled and bonded together. Adhesives, chemicals (for paper or plastic), ultrasonic welding, or brazing are all possible lamination techniques (metals). After the object is formed, unused areas are ripped out layer by	Advantages: Rapid volumetric growth relatively affordable (non-metals) allows for various metal foil combinations, including those with embedding elements.	Metal Tapes Paper and Plastic Sheets,

		layer and eliminated.		
Material extrusion	Fused Deposition Modeling Fused Filament Fabrication	A nozzle or aperture is used to extrude the material in tracks or beads, which are then assembled into multi-layer sculptures. Heated thermoplastic is a common	Advantages: Affordable and cost-effective allows for a variety of hues Suitable for usage in an office setting. Good structural qualities. Limitations: A slower process than SLA and a subpar finish	Pellets, Thermoplastic Filaments, and Liquids.
Directed energy deposition	Direct Metal Deposition Laser Metal Deposition Laser Engineered Net Shaping	Using an energy source like a laser or electron beam, powder or wire is fed into a melt pool that has been created on the surface of the part, where it binds to the underside part or layers. Essentially, this is a type of automated	Advantages: Not constrained by axis or direction efficient for improvements and feature addition Several materials combined into one component Highest rates of single-point deposition Limitations: Requires polish, but	Metal Powder, metal Wire with ceramics

		build-up welding.	only for little portions.	
Hybrid	AMBIT	Combining CNC machining with laser metal deposition (a type of DED), which combines additive manufacturing and "subtractive" machining, enables products to take advantage of both techniques.	Advantages: High Productivity and a smooth surface finish DED's material and geometric freedoms Automated support finishing, inspection, and removal.	Metal Powder, metal wire with the addition of ceramics

AM allows for the flexible preparation of very complex and precise structures that would be impossible to achieve using traditional fabrication methods like casting and machining [63]. The main advantages of 3D printing are as follows [69]:

- Avoiding the use of molds or equipment.
- Reduction of waste material, lowering cost and ambient pollution.
- Great variety of working materials that can be used, from plastics to metals.

3D printing is praised as a disruptive technology that will permanently change manufacturing [70], since it offers a new manufacturing path that overcomes the constraints of traditional methods for processing materials [71]. Early applications of additive manufacturing were concentrated on models and prototypes. As technology progressed, AM became increasingly important in the production of quick and soft tooling. Today, it's also used to make end-of-life parts and goods [72]. AM is linked with clever and efficient technology, which has a wide range of applications in industrialized economies around the world [73]. 3D printing can produce parts with very intricate and complicated geometries that require no post-processing, are manufactured from custom-made materials and composites, have near-zero material waste, and can be used with a wide range of materials including metals [74].

Construction, aerospace, food, soft robotics, automotive, biomedical equipment, prosthetic implants, health care, printed electronics, biomimetic designing, water treatment, energy harvesting, and desalination have all seen increased use of 3D printing in recent years [75]. This technique has been used in a variety of situations. The medical industry, for example, employs 3DP technology to create high-quality bone and joint grafts as well as anatomical models for research and analysis. Architects utilize 3DP to build complicated 3D models for their clients, and airfoils are printed using 3DP in the aerospace sector [76].

In the product development phase of product design and manufacturing, additive manufacturing technology has made a significant contribution [77]. However, essential information like process repeatability and uniformity of made goods is missing from the AM process, preventing it from being regarded as a legitimate manufacturing process [78].

Sensors and intelligent data acquisition assist in the improvement of any asset's life cycle, from design to production, distribution, and maintenance, all the way to recycling [79]. Real-time three-dimensional form measurement techniques are becoming increasingly relevant as artificial intelligence and robots progress [80].

There are some process parameters that directly affect the geometry built by slicing software; by increasing the layer thickness, you, therefore, decrease the number of layers the part will be made of, and also, each layer will be thicker by changing the object orientation, the layers will slice the part in a different direction, nozzle size will make each raster road to have a different circumference, infill density and infill pattern will change the geometry of the internal structure. Other parameters, however, do not change the sliced geometry but will indirectly change the final part geometry by affecting the deposition process. Extruder temperature, print speed, and the filament material used will have a diverse effect on the printed part's geometry.

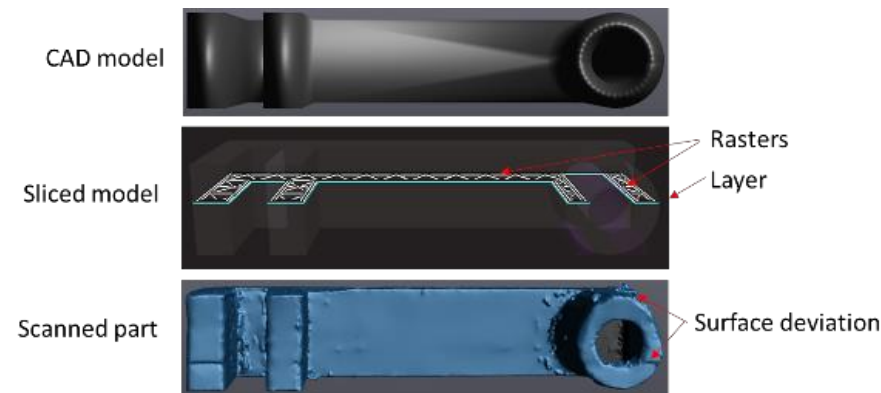


Figure 8. Deviation between CAD model, slicer model, and scan of the printed part.

As seen in Figure 8, the sliced model introduces internal structures, which are not present in the original CAD model, and the printed part exhibits those structures as well as deviations in the surface of the geometry. The STL model created from the scanning process has imperfections, as the software makes approximations to unite the triangles. certain measuring errors are caused by shadows, dust, and other environmental sources.

The following literature review demonstrates how process parameters deviate the internal structure as well as indirectly affect the final geometry of FDM parts.

Peng et al. [81] employed mathematical techniques to model the effects of printing ABS FDM parts in dimensional accuracy and validated the results with experiments. They concluded that layer thickness has a positive effect on dimensional deviation, and lower geometric deviation was shown in parts with thicker layers.

Padhi et al. [82] investigated the impact of process parameters on the precision of ABSP 400-printed FDM parts. They found that layer thickness of 0.178 mm, the orientation of 0, raster angle of 0, raster width of 0.4564 mm, and air gap of 0.008 mm are the best process parameters.

Qattawi et al. [83] studied the influence of process parameters on the accuracy and mechanical properties of FDM parts made of PLA. They concluded that increasing extruder temperature and layer height has a direct effect on increasing deviation, and Although they could not determine exactly how the orientation affected the deviation, they found that orientation has a significant effect on geometrical accuracy, while infill density and infill geometry has almost no effect on deviation. The study also confirmed that the raster bond is stronger than the layer bond, resulting in greater mechanical strength; they also found that increasing infill density and extruder temperature has a positive influence on stiffness.

Tanoto et al. [84] studied the effects of object orientation on mechanical strength and geometric deviation of FDM ABS parts. They concluded that orientation has different effects on different features; some features were better in one orientation and showed to be worse in another. They also concluded that the stiffness depends on the orientation of the force with respect to the print layers, with better tensile strength when the load is parallel to the print layers and vice versa.

Chuang et al. [85] presented a reverse engineering procedure for generating interference-free tool paths in 3-axis machining from data of physical models acquired with a 3D laser scanner. Furthermore, using a shortest-distance method, they determined the connecting sequence of the neighboring points between two adjacent scan lines, such that the scanned data are converted into triangular polygons. They then generated Tool paths from the tessellated surfaces.

Yanamandra et al. [86] proposed a reverse engineered approach for an FDM part made of glass fiber reinforced ABS filament. Using μ CT scan and SEM images of the model, they captured the tool-path of 3D printing information by identifying the fiber orientation in each layer with the help of Recurrent Neural Network with LSTM architecture.

Rupal et al. [87] created a Reverse CAD algorithm, which reconstructs a CAD model from the g code containing the sliced file. The Reverse CAD model created by the team is the virtual replica of the part to be printed with specific printer and machine parameters like layer thickness, infill density, and so on. They concluded that the algorithm facilitates accurate modeling and analysis of the FDM printed part behavior. They validated the efficiency of the algorithm by geometric comparison, mass comparison, deviation analysis, and mechanical behavior analysis using different process parameters and printers.

The previous review shows that different process parameters will result in different final geometries that will differ from the CAD model in distinct ways. Furthermore, Some process parameters will directly change the slicing geometry [81] [82] [83]

- Layer thickness
- Object orientation
- Infill density
- Infill pattern
- Nuzzle size

While other process parameters will indirectly change the final part geometry [81] [83]:

- Extruder temperature
- Print speed
- Material

2.2 Inspection devices

The SEM machine consists of the following components [88]:

- A source to generate electrons of high energy is called an electron gun.
- Column down for traveling the electrons through two or more electromagnetic lenses.
- The deflection system consists of scan coils.
- Electron detector for backscattered and secondary electron.
- A chamber for the sample.
- The computer system consists of a viewing screen to display the scanned images and a keyboard to control the electron beam.

SEM is used in the Manufacturing & Assembly Industry for quality control, failure analysis, cleanliness inspection, and morphological and chemical analysis of particles. All samples were coated with gold using the Q150R-ES Rotary Pumped Coater from Quorum

CT scanning hardware consists of the following units [89]:

- The generator
- The scanning unit (gantry), which includes one or more
 - X-ray tubes
 - Photon detectors
 - Shielding elements

2.3 Methodology

Slicing programs are the programs that create part build-up instructions. These apps divide (slice) CAD models into layers using STL files from Computer Aided Software designs. For each layer, material deposition trajectories (rasters) are subsequently produced [90, 90]. In most cases, the application takes care of everything. The user's responsibility is extremely limited: they must submit CAD geometry, define part orientation in relation to the printing head, and choose part density and raster patterns from a menu. Some production aspects are outside the user's direct control. The user, in particular, does not influence the material deposition strategy. These pathways are automatically defined by programs using criteria that are unknown to the user (reduce material use or cycle time). Part build characteristics that are not controlled and have an effect on part strength are [91, 91]:

- Raster width: diameter of the raster depends on nozzle size.
- Raster angle: angle between the path of the nozzle and a reference axis.
- Raster gap: space between deposited filaments.
- Number of contours: paths along the periphery of the layer.

2.3.1 Large isogrid specimens

To explore the problems that emerge from part constructions strategies, a block measuring 58.8 by 37.4 by 25.4 mm, with an internal isogrid structure, was created and printed on a Marktwo using onyx with solid infill, 0.1mm print layer, 0.4mm nozzle, and two walls and floors. Different internal wall thicknesses (IWT) were used (0.5, 0.6, 0.8, 1.0, and 1.5mm.)The design is presented in Figure 9.

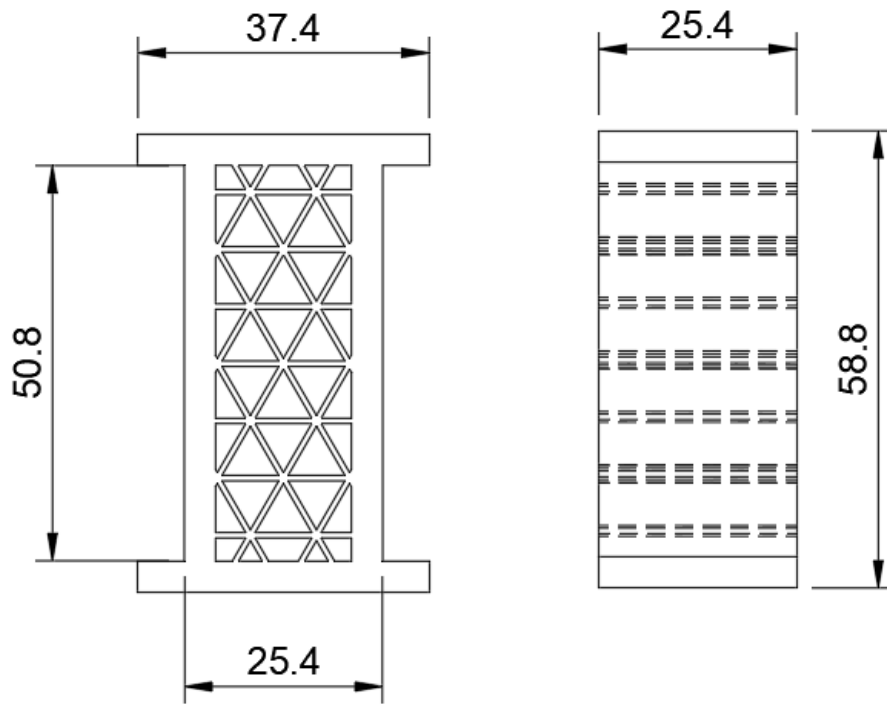


Figure 9. IWT specimen measurements

IWT 1.0 raster
gap and void

IWT 1.5 raster
gap and void

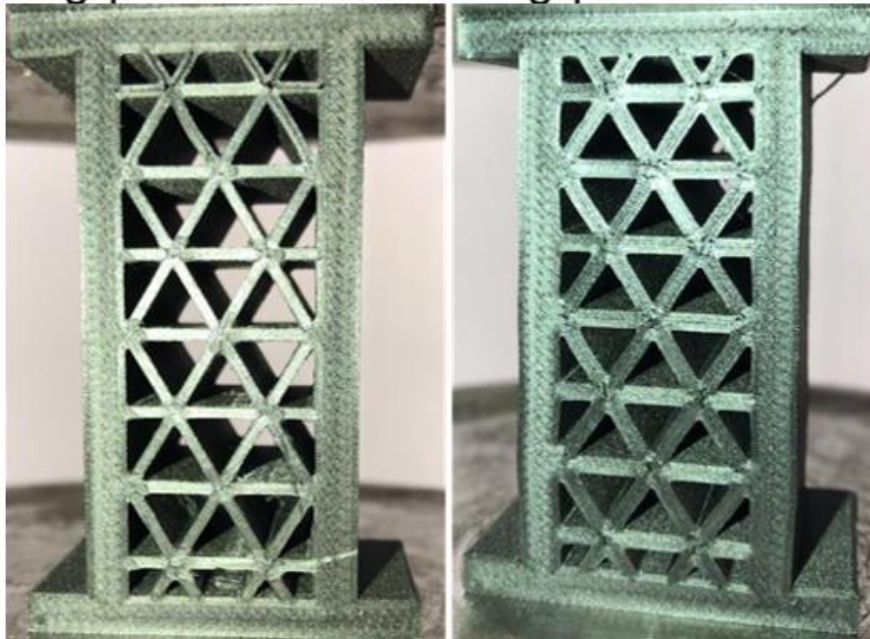


Figure 10. Deposition paths for the parts with IWT of 0.5 mm and IWT 0.8 in three different slicing software.

As seen in Figure 10, the path planning changes substantially in response to changes in internal wall thickness (IWT) of the same geometry. To produce a 0.5 mm IWT with a 0.4 mm nozzle, the slicer performs two 0.4 mm raster paths that overlap (“negative” raster gap). In theory, in the case of IWT, 0.8 mm no overlap is necessary, as two raster paths of 0.4 mm can be laid out side by side. In practice, these two paths are subject to poor binding of the deposited material, which results in a gap that negatively impacts part strength. Figure 2 shows these fabrication defects for different specimens.

Figure 11. Images of the actual experimental specimens and their manufacturing defects.



Figure 12. Details of defects in the reticle of the specimens.

In some cases, raster paths were insufficient to produce solid grid walls in a certain region of the part in IWT 1.0, and while paths result in a better fill for IWT 1.5, gaps and voids are visible. All specimens' deformations occurred on the plane.

2.3.2 Thin isogrid specimens

To take measurements of the internal structure on a SEM microscope, thin Isogrid specimens measuring 37.4x15.7x2mm were fabricated on a Marktwo using onyx with solid infill, 0.1mm print layer, 0.4mm nozzle, and two walls and floors. The specimens were frozen with liquid nitrogen and cut so as to not damage the internal structure.

The specimens were gold coated using the Q150R-ES Rotary Pumped Coater from Quorum, and inspection was performed with a SEM EVO MA 25 by Zeiss; the machine has a Maximum specimen height of 210 mm, Maximum specimen diameter of 300 mm, Motorized stage travel XYZ of 130x130x80mm

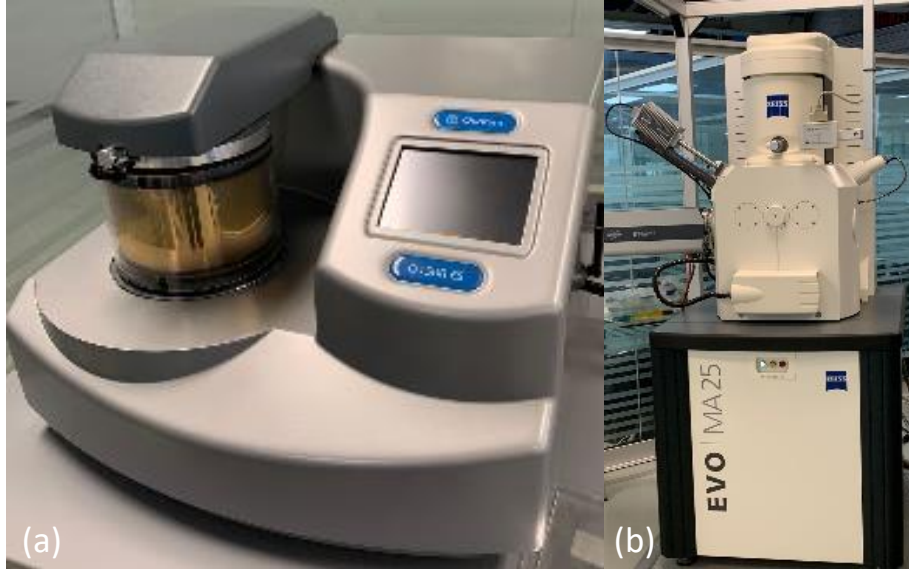


Figure 13. (a) Q150R-ES Rotary Pumped Coater from Quorum (b) SEM EVO MA 25 by Zeiss

To take scans of the internal cavities of the specimens the CT-scan Metrotom 800 by Zeiss was used, the voxel size was set to 36 microns, the voltage to 100-kilo Volts, and the current to 80 micro-amps.



Figure 14. Specimen mounted on Metrotom 800 CT-Scan

2.4 Results

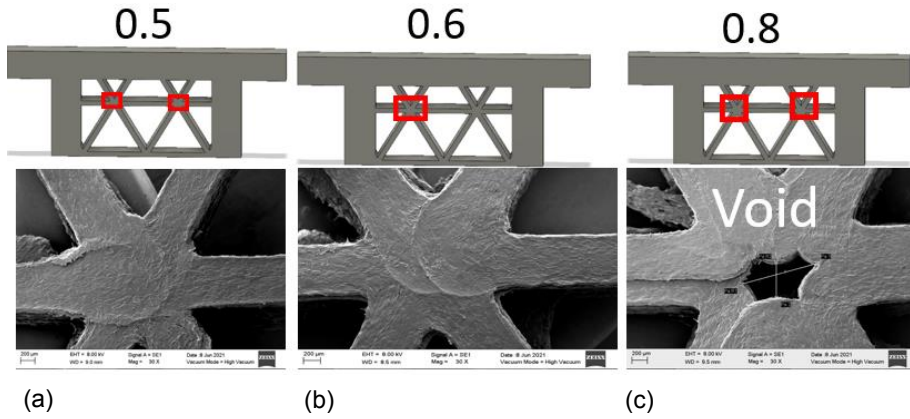


Figure 15. Comparison of reticle center. (a) Thin 0.5, (b) Thin 0.6, (c) Thin 0.8

As seen in Figure 15 (a) and (b), the raster passes through the center of the reticles, filling them. While as seen in Figure 15 (c), the rasters leave a void in the middle of the reticle

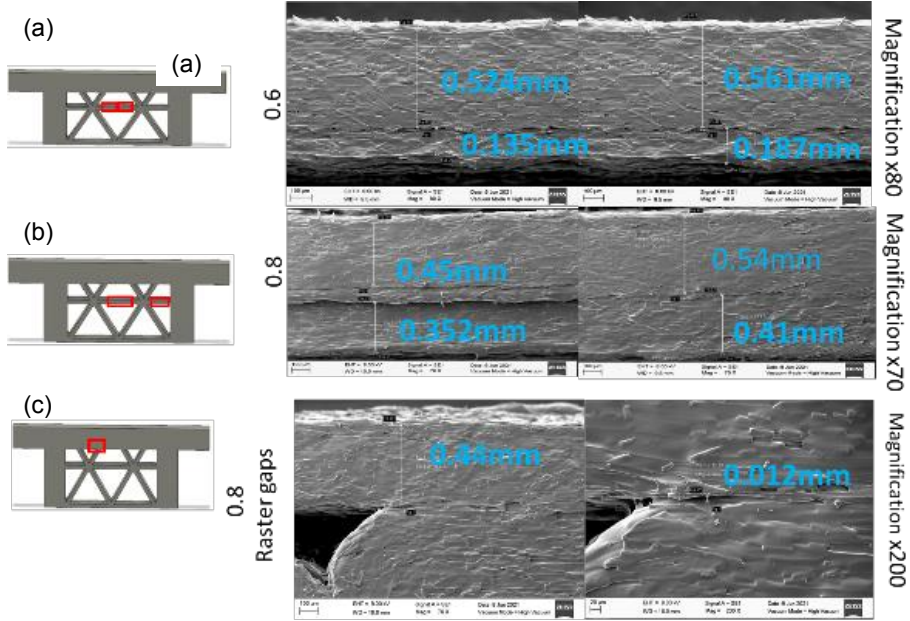


Figure 16. Comparison of raster width. (a) Thin 0.5, (b) Thin 0.8, (c) Thin 0.8

As seen in Figure 16 (a), raster overlap is apparently identified as the raster should be 0.4mm; however, as the thickness of the stub is 0.6mm, the geometry could not be created with 0.5mm rasters without overlapping. While in Figure 16 (b), no overlap is necessary as there is enough space for the 2 0.4mm rasters.

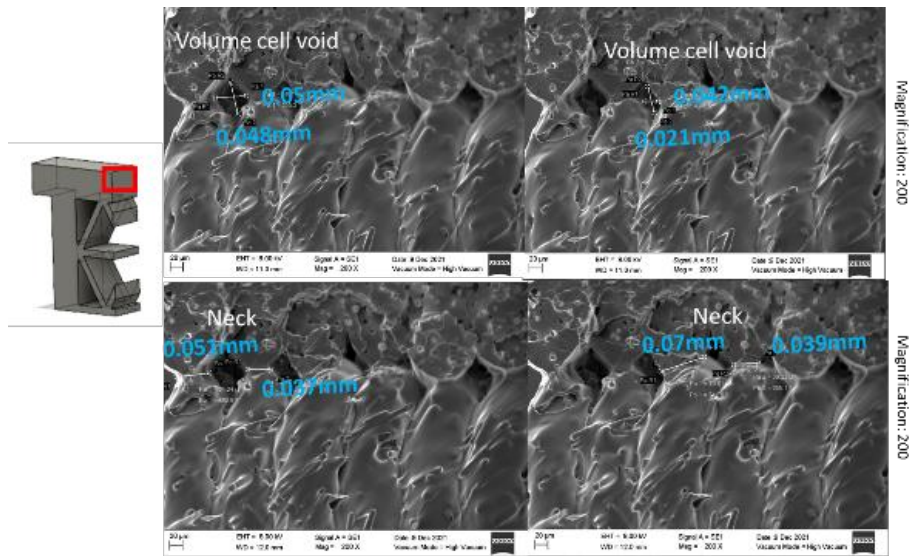


Figure 17. SEM images of the boundary between rasters.

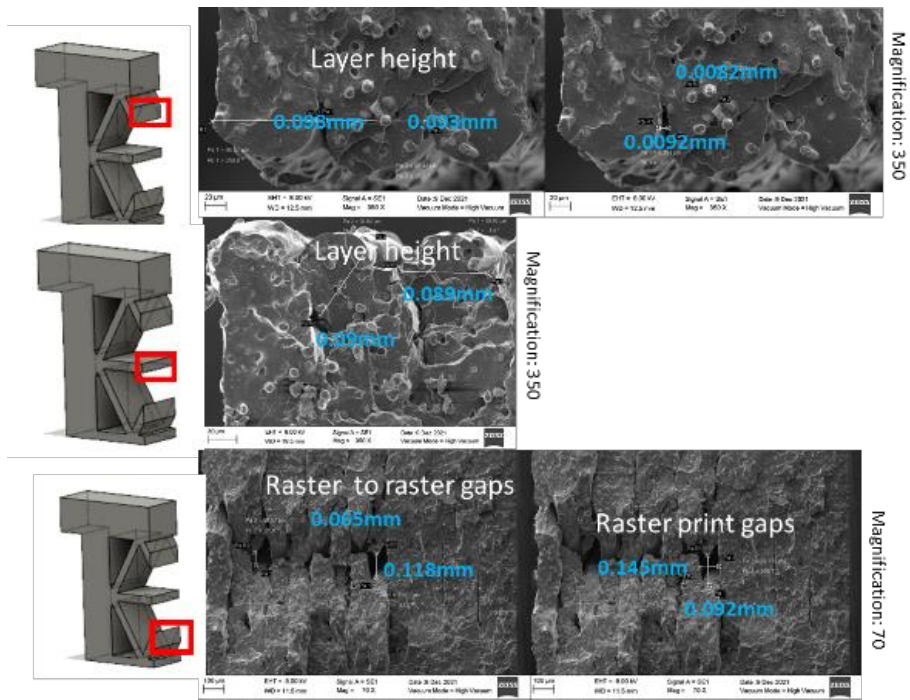


Figure 18. SEM images of layer and raster gaps

As seen in Figure 17, voids are present between rasters and layers, and these voids are not modeled in the slicer and deviate from the geometry.

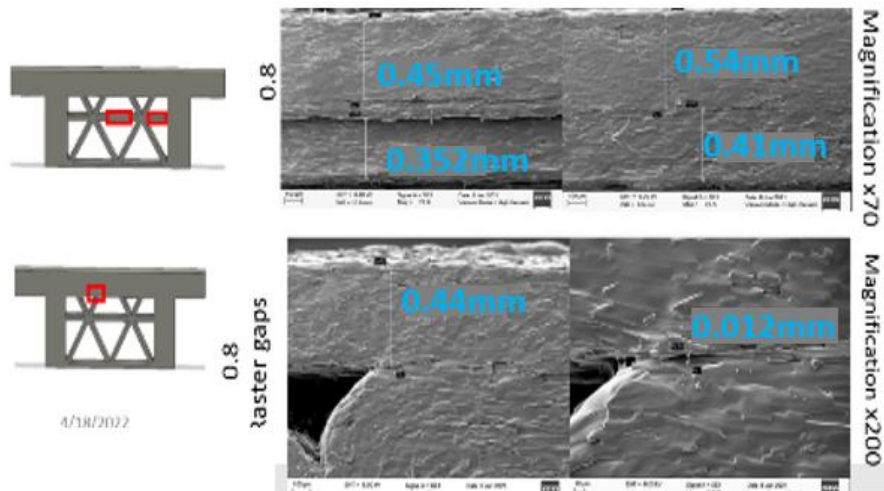


Figure 19 SEM images of rasters and volume cells

Figure 19 shows images of raster path measurements that were used to compare to the slicer geometry; as it can be seen, the measurements deviate from the intended 0.4mm width.

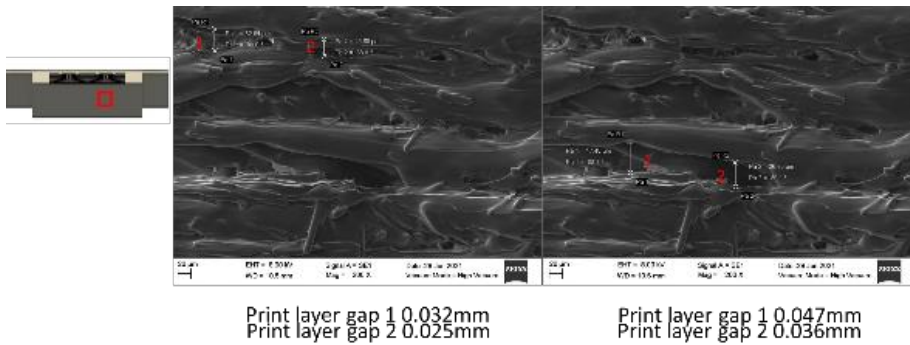


Figure 20. SEM images of print layers sliding

Figure 20 shows print layers curving and sliding in place, and this could have been a deposition defect or an effect of the thermomechanical profile of the part during fabrication.

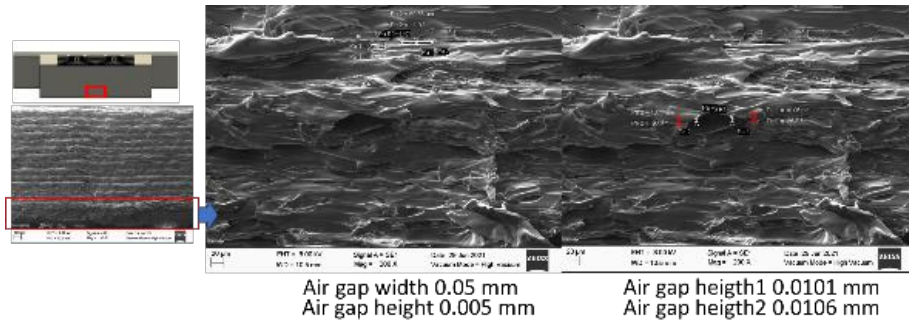


Figure 21 SEM images of air gaps

As seen in Figure 21, there is a zone in which the layer is thinner, and this could have been the cause of an air bubble or an extrusion problem.

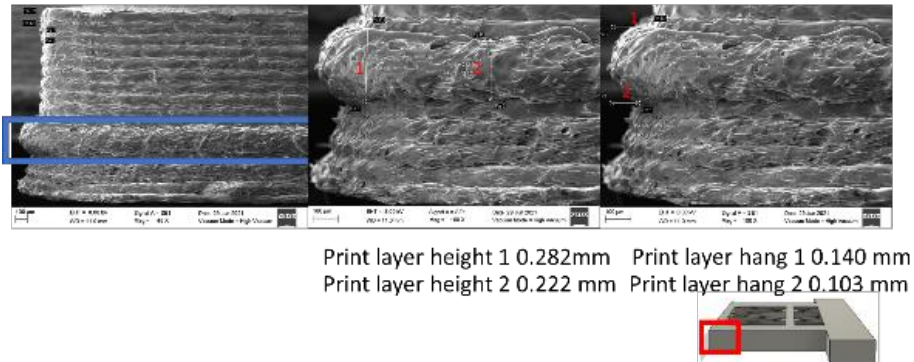
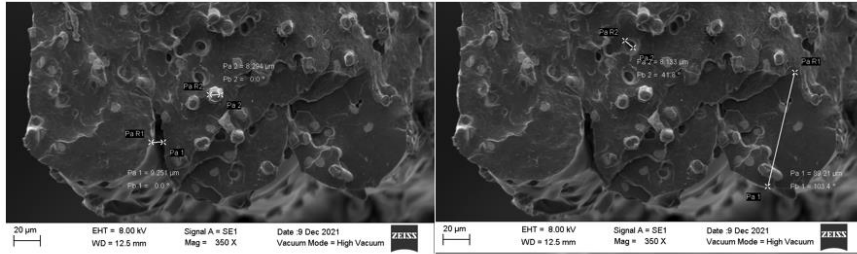


Figure 22. SEM images of print layer defect

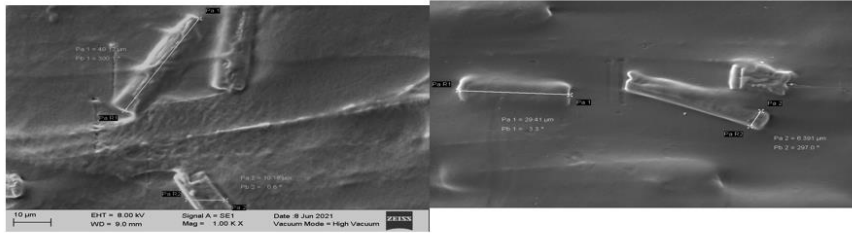
As seen in Figure 22, the highlighted print layer is more than twice as big as the other print layers, and this could have been the effect of the motor skipping a step or 2print layers merging.



Magnification X3350

Diameter 0.0082

Diameter 0.0081



Magnification X1000

Length:0.04mm
Width: 0.01mm

Length:0.029mm
Width: 0.006mm

Figure 23. SEM images of discontinuous carbon fiber strands

Figure 23 presents the measurements of the carbon fiber strands inside the Onyx mixture; as seen from the measurements, the strands are not uniform.

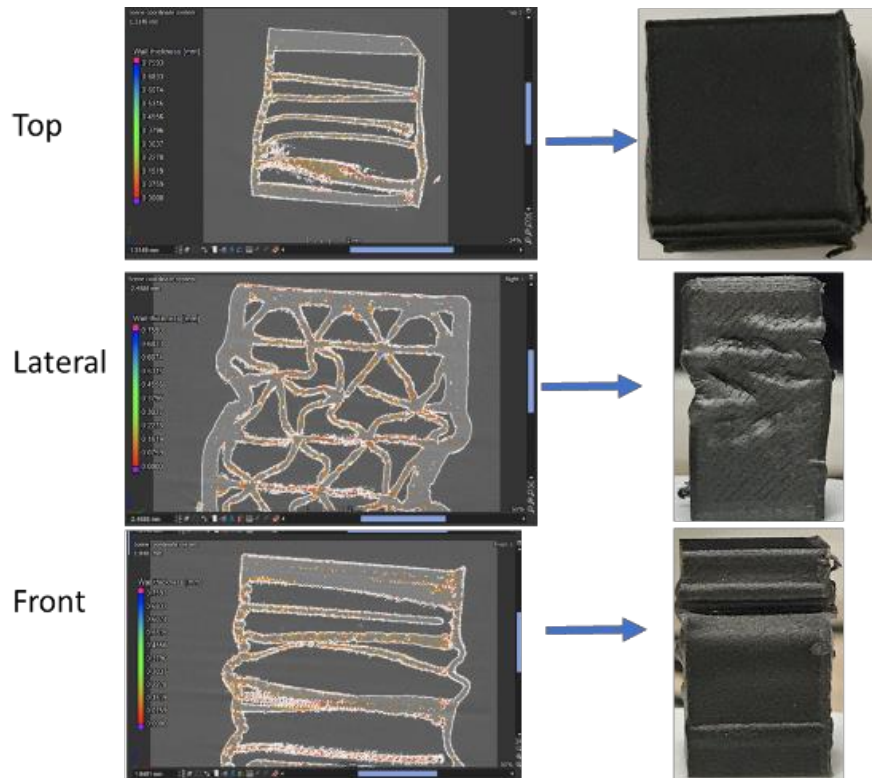


Figure 24. Post mortem CT scan of ASTM d695 specimen. (a) top view, (b) Lateral view, (c) front view

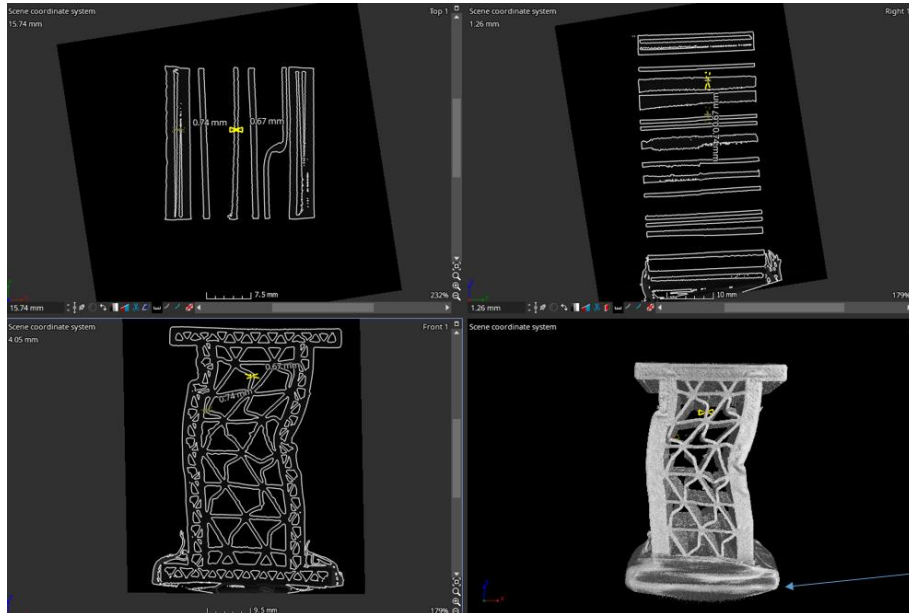


Figure 25 Post mortem CT scan of isogrid specimen. (a) top view, (b) Lateral view, (c) front view (d) STL

2.5 Discussion

As seen in Figure 10, IWT 0.5 and 0.6 specimens were built with overlapping 0.4 thick raster paths. Raster paths for IWT 0.8, 1.0, and 1.5 did not necessarily overlap as internal walls were built. The limiting case was IWT 0.8, in which raster paths are side by side.

As illustrated in Figure 12 for specimens IWT 1.0 and 1.5, the thicker studs caused the deposition architecture to avoid placing material in the middle of the reticle resulting in voids; also, an unknown deposition mistake caused the printer to omit to set the material between the raster resulting in gaps between the rasters

In Figure 16, the raster thickness was shown to deviate from the intended toolpath. From the 11 measurements performed on IWT 0.8, an error of 19.06 % was calculated.

Phase	Surface deviations average (mm)	Raster path width (mm)	Print Layer height (mm)	Raster to raster gaps (mm)	Print layer gaps (mm)	Print layer (merge) (mm)	Raster overlap (mm)
CAD Model	0	Solid model					No overlap needed
Slicer	0	0.4	0.1	No gaps		No merge	0.6
Printed Part	0.357	0.4599	0.0871	0.0433	0.023	0.252	0.703
% difference		14.975%	-12.9%				17.167%
n	40	15	39	15	14	1	2
SD	0.1140	0.0364	0.0304	0.0364	0.0167	-	0.0629

Table 2. Deviation result summary

The deviations result from Table 1 shows how each phase introduces more deviations from the CAD model as the CAD model has no deviation or internal structures, the slicer has no deviations but introduces internal structures, and finally, printed parts have deviations and internal structures

2.6 Conclusions

In this chapter, the deviation between the CAD model and the final part was studied, and slicing architecture, effects of process parameters, and defects in the fabrication of FDM parts were discussed and analyzed.

The fabrication of FDM parts may exhibit flaws like internal voids and raster gaps; the slicing software architecture causes the creation of print layers and raster paths, which, as seen on the SEM images, deviate from the toolpath strategy, they differ in thickness and geometry, and the rasters may even overlap based on the fabrication conditions.

Chapter 3

3.1 Introduction

As seen in the previous chapter, the complex effects of process parameters in the fabrication process deviate from the final part with respect to the CAD model. Deviations in the geometry of the CAD model may cause fabricated parts to not meet the required tolerances for the designed application. Furthermore, they may also negatively affect the structural integrity of the FDM. These deviations are caused by multiple factors, such as the accumulated stress during the thermo-mechanical job, machine error during production, and rheological issues during the deposition. To study in-depth the divergence between the expected behavior of the printing process and the actual fabrication of the part, in this chapter, the FEA simulations of the deposition process were performed, and the deviations predicted by the software were compared with those of the results of scanned printed parts.

FDM is hindered by the lack of processing knowledge [92], and their performance is judged by the dimensional and geometric precision of the parts produced [93]. It demands the ability to produce goods with acceptable dimensional accuracy [94]. Before additive manufacturing technology become the norm in the manufacturing sector, there is still a lot of effort and research to be done. Not all regularly used manufacturing materials can be handled, and the precision needs to be improved to do away with the requirement for a finishing process [95]. These new materials must meet particular 3DP specifications, and they must undergo extensive testing to ascertain their mechanical characteristics and ultimate geometry [62].

FDM is not suitable for complex parts since it has the lowest dimensional accuracy and resolution of the conventional 3DP processes [96] [78]. Component tolerance, which is a commonly used parameter for traditional manufacturing that helps assure part fit, can be thought of as how closely the 3D printed part matches the original CAD design in terms of dimensions [97]. Major print failures can originate from a variety of error sources; therefore, identifying only individual root causes may lead to the acceptance of faulty components [98].

The following four main elements can be summed up as affecting the accuracy of FDM parts [99]:

- Machine error: caused by the printer movement.
- Software error: caused during the slicing process by geometric. Approximation.
- Thermomechanical extrusion errors: caused during the material extrusion by nozzle and filament diameter, and extrusion speed.
- Thermomechanical deposition errors: caused during the deposition and rest by material and environment.

The accumulation of the defects that occur throughout the manufacturing process has an impact on the accuracy of an anatomical 3D model [100]. Process parameters have an important effect on the final geometry of the part. The main FDM process parameters are [101]:

- Slicing parameters
 - nozzle diameter
 - road width
 - flow rate
 - print speed
 - infill pattern
 - infill density
 - raster orientation
 - air gaps
 - number of contours
 - roof thickness
 - floor thickness
 - layer thickness
 - building orientation

- Temperature parameters:
 - environment temperature,
 - extrusion temperature,
 - print-bed temperature.

Tolerances for 3D printing using fused filament fabrication (FFF) range from 0.15 mm for industrial printers used in manufacturing settings to 0.5 mm for desktop printers used by hobbyists [97]. Given the lower production rates that additive manufacturing processes achieve compared to conventional manufacturing, it becomes necessary to continuously monitor the entire process and make the necessary adjustments to increase the number of acceptable parts, thereby raising the process' overall quality.

Creating geometries with higher component precision can be achieved by modifying the design to account for anticipated deviations produced during the part's manufacture [102]. However, distortion detection currently requires computationally intensive simulation and analysis of sensing data [98].

Successful realization of a specific 3DP process involves the printing process along with process details for printing and post-processing, both of which play a major role in determining the mechanical properties of the parts produced [103]

Iterative processes are typical of 3D printing. The steps listed below are used to carry out 3D printing [104]:

- Conceptualize the geometry.
- Design a virtual CAD model.
- Convert the CAD model into an STL.

- Convert the STL dataset into a toolpath.
- Export the machine instructions to a 3D printer and execute the printing process.
- Carry out finishing operations.

Typically, the workflow has to start over if a printed component doesn't comply with the anticipated usage, whether it be due to parameter errors or fabrication faults. This leads to longer lead times, lost material, and perhaps even geometric restrictions for the component.

A major barrier to AM's widespread use in the industry is the lack of process robustness, stability, and repeatability brought on by the complicated, unresolved interactions between material properties, product design, process parameters, process signatures, post operations, and product quality [24]. Due to the nature of additive manufacturing (AM) processes, it is necessary to identify manufacturing flaws early in the production phase in order to prevent the creation of defective parts [105]. By identifying part distortion quickly, significant print errors can be prevented.

Molten fibers are extruded and placed over the previously printed layer in FDM, forming bonds with contiguous fibers [106]. Diverse thermo-mechanical profiles are applied to FDM parts, which results in residual stresses and geometry deformation [107]. Warpage and shrinkage occur when the material cools by a high thermal gradient [108]. That occurs since cooling induces residual stresses to build [109]. One of the most extreme conditions is residual stress-induced distortion [110].

Through comparison of the measurement results of several tolerance values, such as flatness and symmetry, Mahes et al. [111] discovered that warpage and delamination, which influenced flatness, were produced by residual stresses. These print flaws are common in AM. Rapid cooling of the melted fibers may result in solidification before full fusion with other fibers, leaving gaps between the fibers and bonds with inadequate mechanical properties [112] [106]. The thermal gradient influences fiber adhesion [106]. All through the fabrication process, FDM parts suffer a constant time-varying temperature profile [113]. This makes it difficult to accurately simulate the deposition process.

Using FDM for practical engineering components requires having improved mechanical qualities, surface polish, dimensional control, and tolerances [114]. A deeper comprehension of the deposition process is required for these advancements to be feasible. Typically, for a given set of materials, process parameters are set and optimized experimentally. Generally, process parameters are set and optimized experimentally for specific materials. Nevertheless, the procedure is time-consuming and expensive. As an alternative solution, numerical techniques are used to investigate the effect of process parameters on the thermo-mechanical behavior of 3D printed composite parts [115]. Simulations based on DTs can collaborate in real-time with their physical counterparts to verify, validate, and optimize the process [32]. Digital Twin simulation, as opposed to traditional

simulation, is used to optimize solutions [31]. Simulations of fabrication processes are widely used in design and production to achieve high geometrical accuracy [116].

Abaqus' Additive Manufacturing framework includes technologies to address a variety of simulation challenges [113]:

- Finite element mesh with varying mesh density.
- The input of process parameters and specifics for various AM processes such as deposition head dimension and moving speed, stack direction.
- Supporting progressive heating computation using actual tool path data.
- Supporting progressive cooling computation using evolving heat transfer surfaces during the printing process.

FDM thermal simulation is complicated for at least two main reasons. The first is the manufacturing process's inherent geometric complexity, which discretizes the design model and results in numerous artifacts such as "stair-stepping" on the surface, voids between roads, and under-fill. The second challenge is the high computational complexity of the transient thermal simulation, which necessitates a numerical solution at each time increment of the process. [117].

Voxel mesh is used in streamlined thermal simulation techniques, which decreases the size of the finite element mesh and, as a result, the amount of time needed to model intricate additive designs [118]. Nevertheless, this approach is neither precise nor efficient since the design geometry greatly differs from the produced shape [117]. The geometric change during the deposition process is not taken into account by two-dimensional models for FEA analyses of AM processes [110]. Making the models less accurate, as in FDM, the primary heat transfer modes are convection and conduction [94] [110]. The prediction of the grinding temperature (background temperature) can be improved by using the finite difference method and more precise convective heat transfer information [119].

An effective way to validate computer simulations is through experimental testing. Real-time three-dimensional form measurement techniques are becoming more and more crucial as artificial intelligence and robotics grow quickly [80]. The present unsolved issues in layer imaging relate to the trade-off between imaging resolution and extension of covered area, as well as to the complexity of picture interpretation, which is made worse by optically challenging materials, intricate filament patterns, and non-uniform environmental circumstances [25]. The life cycle of any asset, starting with design, manufacture, distribution, maintenance, and ending with recycling, is being improved through sensors and intelligent data collecting [79].

The following Literature review briefly shows the work done in deposition simulation for additive manufacturing.

Using ANSYS software, Zhou et al. [120] created a thermal model for FDM that took into account the nonlinear behavior of thermal conductivity and specific heat due to temperature changes and phase transformations. Using a finite element analysis technique based on the continuous media theory, they looked at the temperature evolution and how the modeled component formed. They came to the conclusion that the impacts of modeling have a significant impact on the thermal evolution when the material's thermal properties are changed.

Cattenone et al. [121] developed an FEA framework to simulate the Fused Deposition Modeling process using the Abaqus software to study the effect that simulation parameters such as time step and the mesh size have on strength. They concluded that:

- While it has little effect on the outcomes of the mechanical analysis results, the time step has a significant impact on the local temperature distribution during printing.
- The meshing method is crucial for simulating the actual printing process. For small models to examine local impacts, a finer meshing method is recommended; however, for large models where the local effects are minimal, a coarser meshing strategy is advised.
- Accurate calibration is required for the constitutive model to get findings that are physically feasible, and it's essential to consider the temperature dependence of Young's modulus and the yield stress limit.

They discovered that, in conjunction with other printing factors like extrusion temperature, chamber temperature, nozzle velocity, and extruded filament diameters, thermal gradients have a significant impact on the quality of the things that are generated. The adhesion model between the first layer and the constructing plate was the study's biggest flaw. To evaluate the adhesion force between the plate and the filament, complicated experimental experiments must be carried out at various temperatures before any form of adhesion model can be introduced.

Croccolo et al. [122] developed and experimentally validated an analytical model that can be easily implemented in a calculation sheet and is able to predict the strength and stiffness of FDM parts based on the print setting such as raster pattern, number of contours, and raster angle. The developed method can forecast the failure of the entire part by modeling the rupture event of each individual bead.

Courter et al. [113] developed an open user customizable subroutine interface framework in Abaqus aiming at providing accurate and scalable predictions for Additive Manufacturing processes like FDM, SLM, DLM, and Polyjet. Following an experimental validation, they came to the conclusion that the finite element simulations accurately depict how the tool path and thermomechanical physical processes interact with one another and how this affects the final state of the printed part. In comparison to the physically printed samples, the temperature history and distortion forecasts are qualitatively accurate

Zhang et al. [117] proposed an approach to thermal simulation for FDM using an explicit finite difference method that is applied directly to an as-manufactured model described by a typical manufacturing process plan. The thermal model takes into account the majority of significant thermal impacts, such as heat radiation and convection to the environment, heat conduction with the build platform, and heat conduction with nearby roads (and adjacent layers). Conduction and convection are the primary heat transport modes in FDM [110]. They demonstrated, both conceptually and numerically, that the suggested simulation technique achieves linear time complexity.

Zhang et al. [110] developed a finite element analysis model with simplified material properties and boundary conditions. The stress accumulations during the deposition and subsequent part deformation are examined using simulations. They also looked at how the tool route affected the part's residual stresses and distortion pattern.

They came to the conclusion that residual stresses built up during the deposition caused tool-path patterns to alter the deflection of the part as well noticeably. It can therefore be inferred that the process factors, such as the tool-path pattern and others, have an impact on the FDM parts.

Sonmez et al. [123] studied the relationship between process parameters, temperature, and stress distributions during fabrications. They developed models for the thermomechanical laminated object manufacturing process.

Baronio et al. [124] proposed a methodology for the production of a printable orthosis made with FDM. They used a 3D scanner for the precise recording of a person's forearm geometry. They emphasized the value of submillimeter accuracy in acquiring the anatomy of the hand and fingers since it enabled the design and manufacture of orthoses that were incredibly comfortable and tolerable.

Chen et al. [125] inspected The 3-dimensional surface data of FDM parts with hand scanners to evaluate the accuracy of printed parts. They analyzed the difference between the CAD model and the fabricated parts, and concluded that by improving this system, the production process will become more accurate and efficient overall while also saving time in the clinic.

Henson et al. [98] proposed a Digital Twin strategy approach for the detection of catastrophic failures during printing. The methodology described starts with the simulation of ground truth images prior to printing, is followed by the processing of print images that are captured during printing, and is concluded with a real-time comparison of the ground truth images and captured images to determine whether or not the print should be stopped. They emphasized that a drawback of this method has to do with part concavity; any part geometry that is hidden from camera view cannot be monitored using this method, which could result in the part deforming without being seen.

The literature is deficient in explaining how changes in the process parameter may impact the dimension and geometric accuracy [78] [126]. Additionally, how do they differ between a proprietary AM system and an open-source AM system [127] [128]. The increased accuracy and shortened inspection time of hand scanners is beginning to allow the in situ inspection of FDM prints; based on GD&T standards, its implementation could ease the adoption of FDM as a true manufacturing option for engineering parts. Furthermore, currently, there are no models that have been capable of predicting all the complexities of the FDM process [112].

3.2 Creation of FDM specimens for tolerance performance inspection

To study the geometrical accuracy of parts created through FDM, two kinds of specimens, one wall (1W) and two walls (2W), were created. The model included specific geometry to evaluate and compare the performance in terms of GD&T dimensional accuracy of 2 different machines, machine 1 and machine 2, with different filaments. For example, the model included cylindrical bosses and thin-walled structures. Annotated Computer-aided Design (CAD) drawings of the models along with the associated measurements for the identified features are shown in Figure 26 and Figure 27.

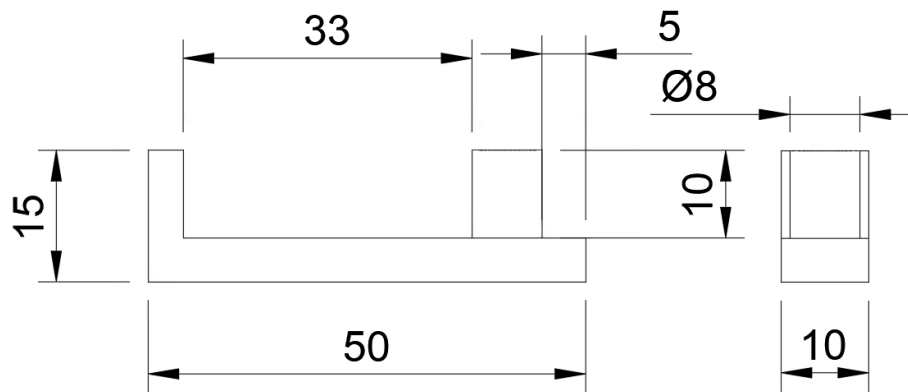


Figure 26. 1W geometry, all dimensions are in mm.

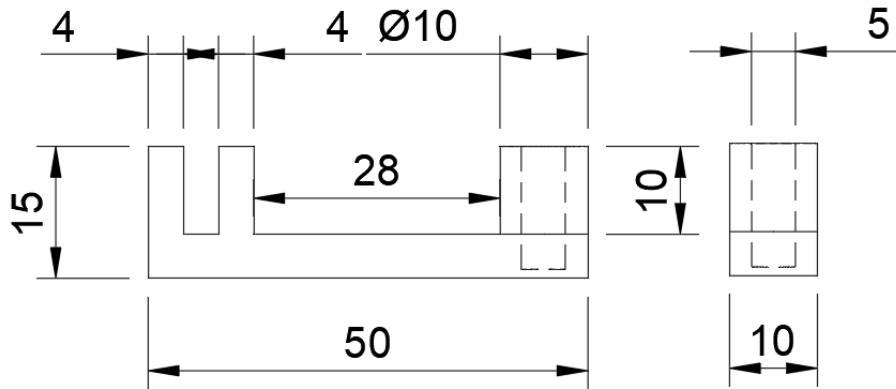


Figure 27. 2W geometry, all dimensions are in mm.

To analyze the effects of build orientation, both machine 1 and machine 2 1W and 2W specimens were printed each on two different orientations, as seen in Figure 28, since the structural properties of the built object and geometry are affected by the orientation [129].

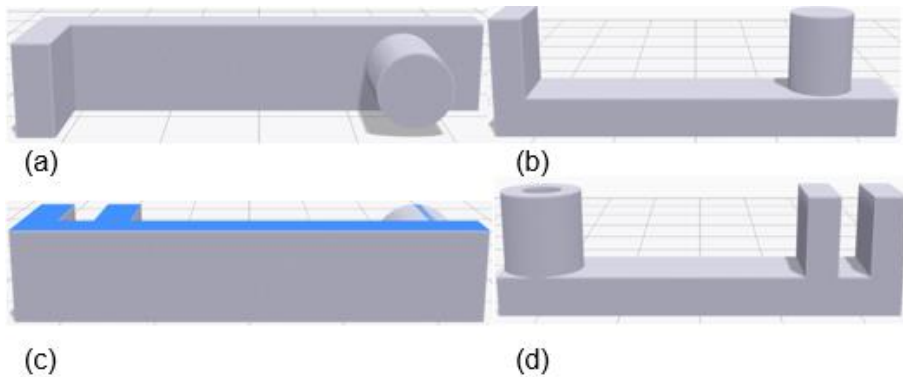


Figure 28. Printing orientations (a) 1W Horizontal. (b) 1W Vertical. (c) 2W Horizontal. (d) 2W Vertical.

For machine 1 specimens, the parts were printed using a Marktwo by Markforge, the toolpath was generated in Eiger by Markforge, 37% triangular infill was selected as it is the default setting, and 0.1mm was set as the layer height. Roof and layers were set to 4 (0.4mm total), and walls at 2 (0.8mm total)

For machines 2 specimens, the parts were printed on an in-house FFF machine, and the toolpath obtained in Cura, 20% triangular infill was selected, and 0.2mm was

set as the layer height. The roof and layers were set to 4 (0.4mm total), and the walls at 2 (0.8mm total).

On each of the two machines, five 1W specimens were printed vertically and five horizontally; also, five 2W specimens were printed horizontally and five vertically. Forty total specimens were created.

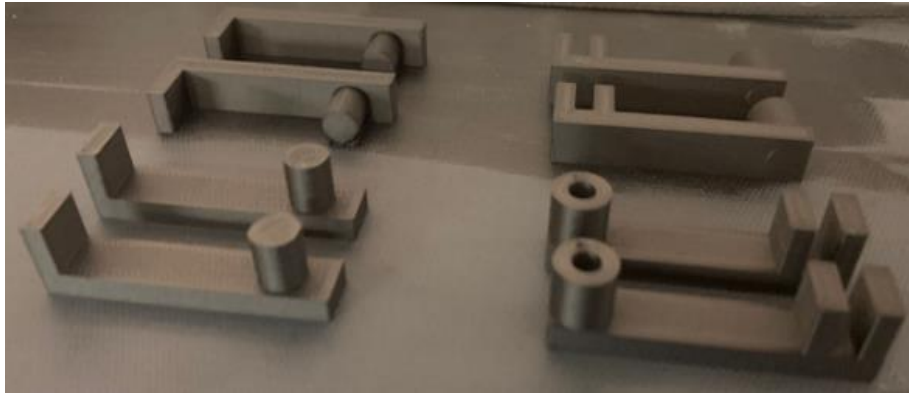


Figure 29. Specimens on the print bed

3.3 Surface inspection of printed specimens

To digitally inspect the surface geometry of the printed specimens, the fabricated parts were scanned by a 3D laser scanning system, HandyScan Black Elite from Creaform, which has 11 blue laser crosses that enable it to have measurement rates of up to 1,300,000 measurements/s and an accuracy of 0.025 mm according to ISO 17025.



Figure 30. HandyScan Black Elite from Creaform

The specimens' surface geometries were captured using VXelements (a software program for 3D scanning and post-processing). A laser scanning approach is uniquely suited for the inspection of parts fabricated using AM, considering the possibility of layer-wise deviations [127]. Using the Vxelements analysis tool, the GD&T range of variations in the tolerances were calculated on the surfaces shown in Figure 31 and Figure 32. GD&T communicates acceptable 3D variations of geometric elements, and it is based on mathematical representations of the variation of geometric elements [130].

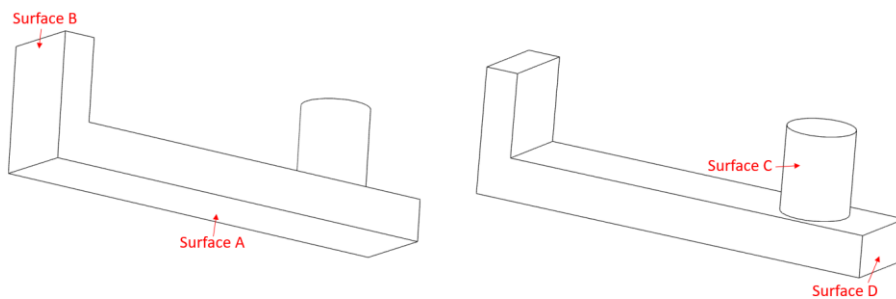


Figure 31. Locations of inspected surfaces for 1W

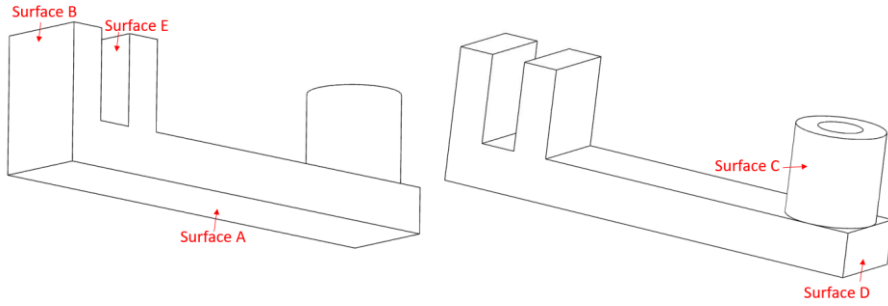


Figure 32. Locations of inspected surfaces for 2W

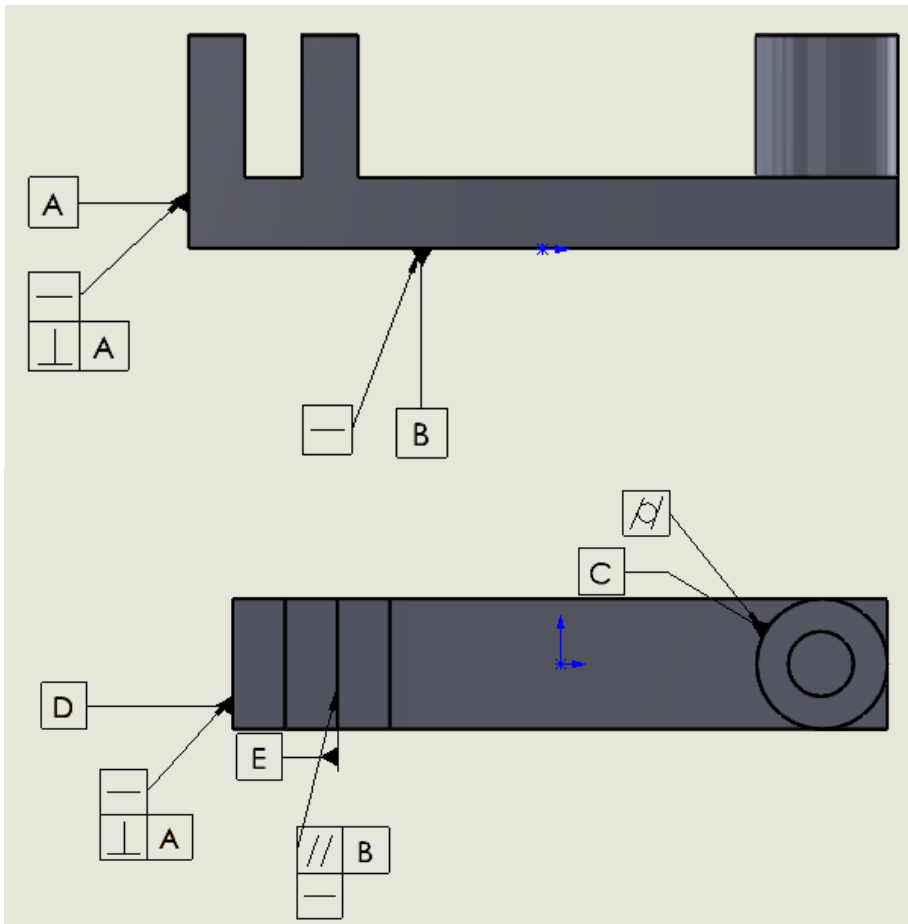


Figure 33. Location of future tolerances for specimens

Figure 33 shows the locations of feature tolerances for specimen 2W, specimen 1W has no Datum E and their respective tolerances, and no other difference in feature tolerances exists.

3.4 Thermo-mechanical simulation

To study the prediction accuracy of FEA deposition simulation software of parts created through FDM, Digimat-AM was used to simulate the thermomechanical behavior of the fabrication process of the 1W and 2W specimens, in vertical and horizontal orientations, with two different materials.

Digmat-AM provides thermal and thermomechanical simulations to inspect the deposition process, minimizing warpage and part deviation. Digimat-AM uses the Mark solver, which is a general purpose, nonlinear finite element analysis solver.

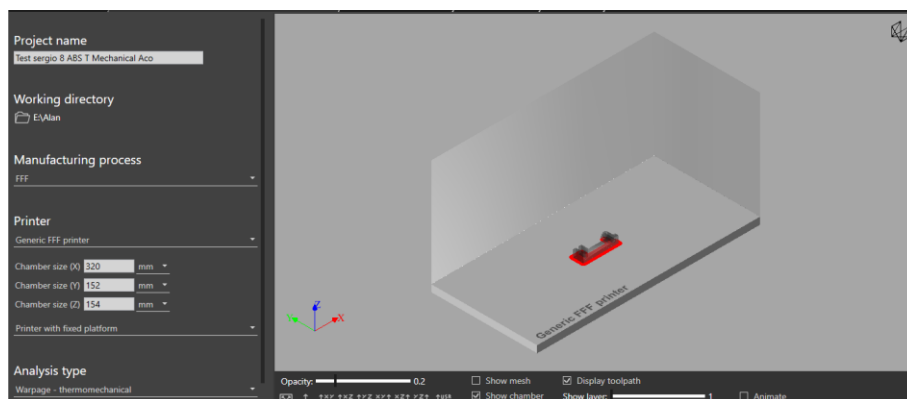


Figure 34. Digimat-AM printer setup

FFF was selected for the manufacturing process, along with a generic printer with a Chamber of 320x152x154 to represent the Marktwo. The chamber temperature was set at 240C, bed with at 0.4, discretization by filament, voxel size 0.1mm. The CAD model was created in Fusion 360. the toolpath created in Markforge's Eiger software for Machine 1 and Cura for machine 2. PA6 with 0.2 carbon fiber bead was used as the material representing Markforge's Onyx and ABS for machine 2, as PLA is not available in the material database.

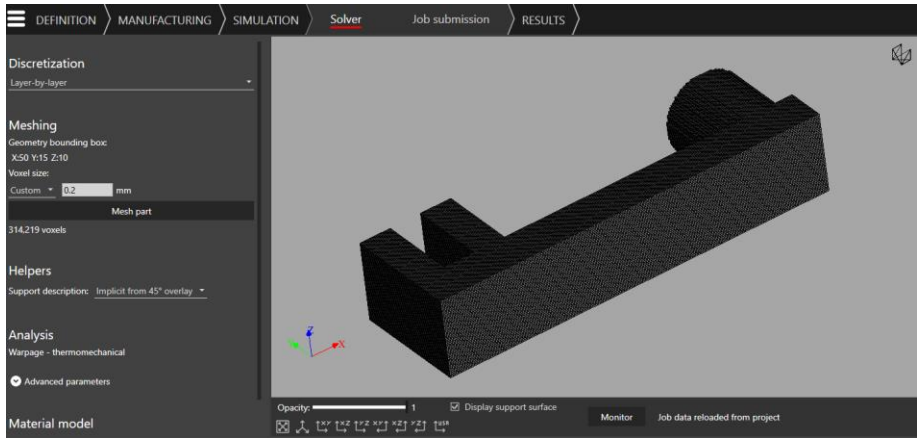


Figure 35. Digimat-AM fabrication setup

The mesh of the expected deformed geometry created by Digimat-AM was exported into VXelements for feature measurements to compare to the printed parts surface inspection



Figure 36. Simulation 2W deformed geometry exported as STL

The deformed geometry was compared against the CAD model to quantify the point deviation by superimposing both geometries in the Digimat-AM software.

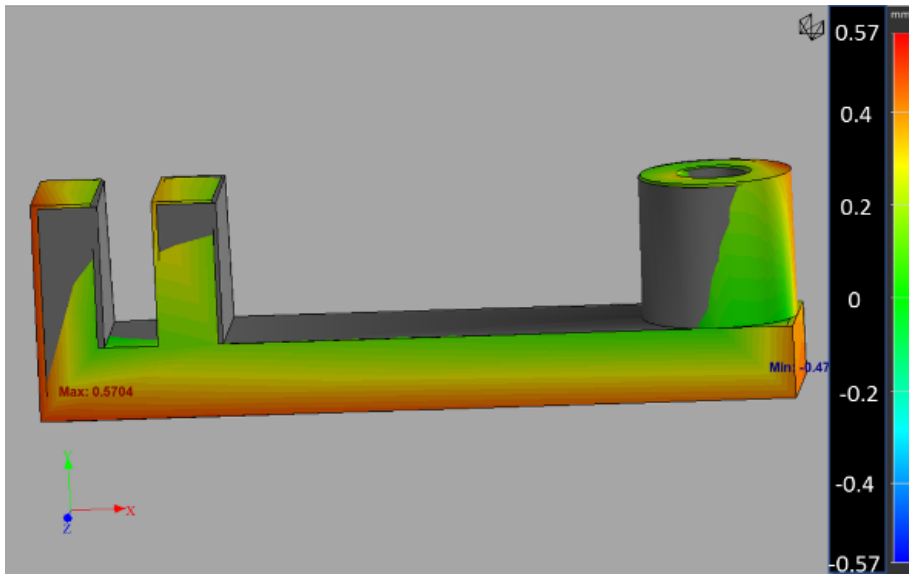


Figure 37. Deformed geometry superimposed in CAD model

Figure 37 shows the predicted deformed geometry the software calculated, superimposed over the original CAD model. The thermometer on the right indicates the amount of deviation in millimeters, with red indicating the highest deviation and blue the lowest.

3.4.1 Results

The predicted deformation from the fabrication is shown in Figure 38

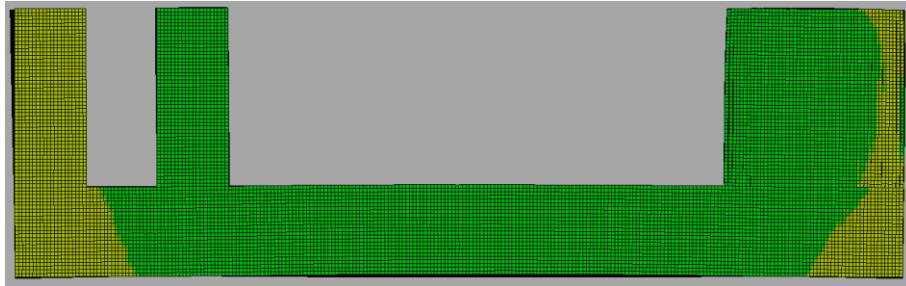


Figure 38. Result of simulated deformed 2W horizontal from Digimat-AM

As seen in Figure 37 and Figure 38, the software predicted that the part would have deformations mainly in the base, walls, and cylinder, as seen from the red shading in Figure 37 and yellow in Figure 38

The dimensional accuracy of the compared FDM parts is reported in terms of variation of individual feature tolerance associated with the GD&T form tolerances, as seen in Table 3, Table 4, Table 5, and Table 6

Table 3 2W machine 1 geometrical tolerance deviation based on GD&T

Specimen name	Surface A	Surface B		Surface C	Surface D		Surface E
	Flatness (mm)	Perpendicularity with A (mm)	Flatness (mm)	Cylindricity (mm)	Perpendicularity with A (mm)	Flatness (mm)	Parallelism with B (mm)
2W Vertical sim	0.005	0.069	0.002	0.126	0.076	0.070	0.010
2W Vertical scan 1	0.615	0.463	0.439	0.227	0.463	0.313	0.535
2W Vertical scan 2	0.363	0.170	0.099	0.130	0.185	0.153	0.078
2W Vertical scan 3	0.274	0.201	0.196	0.132	0.304	0.273	0.239

2W Vertica l scan 4	0.187	0.210	0.206	0.201	0.132	0.131	0.213
2W Vertica l° scan 5	0.438	0.162	0.157	0.319	0.173	0.121	0.276
2W Horizo ntal sim	0.047	0.260	0.204	0.483	0.092	0.086	0.553
2W Horizo ntal scan 1	0.341	0.245	0.237	0.440	0.110	0.096	0.506
2W Horizo ntal scan 2	0.222	0.118	0.106	0.342	0.251	0.181	0.153
2W Horizo ntal scan 3	0.208	0.144	0.107	0.479	0.172	0.123	0.111
2W Horizo ntal scan 4	0.202	0.170	0.154	0.361	0.173	0.163	0.465
2W Horizo ntal scan 5	0.327	0.148	0.127	0.416	0.126	0.149	0.116

Table 3 presents the results from the tolerance deviation inspection of specimens 2W on machine 1 on both vertical and horizontal orientations, and the tolerance deviation results from the deposition simulation on both vertical and horizontal orientations as well. Surfaces A, B, C, D, and E with their corresponding feature tolerance are presented for each case.

As appreciated in Table 3, both thermo-mechanical simulations underpredict the actual flatness deviation seen on the printed specimens, while the 1W simulation underpredicts the flatness deviation of surface B when compared to the results of the 1W specimens.

Table 4 1W machine 1 geometrical tolerance deviation based on GD&T

Specimen name	Surface A	Surface B		Surface C	Surface D	
	Flatness (mm)	Perpendicularity with A (mm)	Flatness (mm)	Cylindricity (mm)	Perpendicularity with A (mm)	Flatness (mm)
1W Vertical sim	0.000	0.043	0.010	0.024	0.039	0.009
1W Vertical scan 1	0.239	0.228	0.439	0.627	0.176	0.158
1W Vertical scan 2	0.098	0.209,	0.173	0.153	0.461	0.461
1W Vertical scan 3	0.113	0.113,	0.087	0.110	0.127	0.124
1W Vertical scan 4	0.234	0.204	0.180	0.405	0.227	0.222
1W Vertical scan 5	0.322	0.199	0.172	0.427	0.264	0.198
1W Horizontal sim	0.093	0.279	0.152	0.470	0.067	0.065
1W Horizontal scan 1	0.726	0.380	0.285	0.805	0.508	0.508
1W Horizontal scan 2	0.182	0.219	0.157	0.873	0.079	0.076
1W Horizontal scan 3	0.071	0.133	0.076	0.830	0.228	0.208
1W Horizontal scan 4	0.197	0.264	0.244	0.997	0.255	0.202
1W Horizontal	0.178	0.280	0.130	0.853	0.112	0.098

tal scan 5						
---------------	--	--	--	--	--	--

Table 4. presents the results from the tolerance deviation inspection of specimens 1W on machine 1 on both vertical and horizontal orientations, and the tolerance deviation results from the deposition simulation on both vertical and horizontal orientations as well. Surfaces A, B, C, and D with their corresponding feature tolerance are presented for each case.

As seen in Table 4, the thermo-mechanical simulation of 1W underpredicts the deviation of all features when compared to the results of the 1W specimen, especially since the software under-predicts the flatness deviation of Surface A, as it predicted the deviation was 0mm.

Table 5 2W machine 2 geometrical tolerance deviation based on GD&T

Specimen name	Surface A	Surface B		Surface C	Surface D		Surface E
	Flatness (mm)	Perpendicularity with A (mm)	Flatness (mm)	Cylindricity (mm)	Perpendicularity with A (mm)	Flatness (mm)	Parallelism with B (mm)
2W Vertical sim	0.006	0.045	0.001	0.034	0.038	0.038	0.013
2W Vertical scan 1	0.416	0.366	0.376	0.322	0.214	0.195	0.303
2W Vertical scan 2	0.694	0.248	0.156	0.350	0.352	0.350	0.552
2W Vertical scan 3	0.853	0.167	0.152	1.195	0.193	0.193	0.666
2W Vertical scan 4	0.357	0.160	0.132	1.081	0.380	0.379	0.398
2W Vertical scan 5	0.408	0.260	0.138	0.407	0.575	0.574	0.287

2W Horizo ntal sim	0.004	0.179	0.124	0.247	0.049	0.032	0.295
2W Horizo ntal scan 1	0.400	0.122	0.009	0.247	0.530	0.471	0.148
2W Horizo ntal scan 2	0.221	0.473	0.465	0.869	0.513	0.459	1.077
2W Horizo ntal scan 3	0.388	0.459	0.425	1.459	0.724	0.694	0.884
2W Horizo ntal scan 4	0.284	0.256	0.252	1.129	0.385	0.404	0.546
2W Horizo ntal scan 5	0.510	0.532	0.536	1.090	0.815	0.373	0.403

Table 5 shows the results from the tolerance deviation inspection of specimens 2W on machine 2 on both vertical and horizontal orientations, and the tolerance deviation results from the deposition simulation on both vertical and horizontal orientations as well. Surfaces A, B, C, D, and E with their corresponding feature tolerance are presented for each case.

Table 5 continues the trend of the thermo-mechanical simulation of both specimens under predicting the actual flatness deviation of surface A seen on the printed specimens, while again, as in Table 3, the flatness deviation of the 1W specimen was under predicted in surface B as well.

Table 6 1W machine 2 geometrical tolerance deviation based on GD&T

Specimen name	Surface A	Surface B		Surface C	Surface D	
	Flatness (mm)	Perpendicularity with A (mm)	Flatness (mm)	Cylindricity (mm)	Perpendicularity with A (mm)	Flatness (mm)

1W Vertical sim	0.006	0.104	0.002	0.022	0.011	0.000
1W Vertical scan 1	0.369	0.657	0.435	0.582	0.306	0.248
1W Vertical scan 2	0.480	0.269	0.230	0.906	0.629	0.613
1W Vertical scan 3	0.855	0.574	0.557	1.033	0.208	0.177
1W Vertical scan 4	0.480	0.348	0.290	0.869	0.277	0.277
1W Vertical scan 5	0.343	0.512	0.468	0.748	0.377	0.285
1W Horizont al sim	0.057	0.139	0.089	0.221	0.061	0.054
1W Horizont al scan 1	0.532	0.483	0.264	0.986	0.334	0.334
1W Horizont al scan 2	0.330	0.382	0.346	1.107	0.355	0.325
1W Horizont al scan 3	0.278	0.263	0.254	1.19	0.112	0.109
1W Horizont al scan 4	0.321	0.300	0.282	0.933	0.242	0.224
1W Horizont al scan 5	0.533	0.204	0.201	0.795	0.252	0.197

Table 6 presents the results from the tolerance deviation inspection of specimens 1W on machine 2 on both vertical and horizontal orientations, and the tolerance deviation results from the deposition simulation on both vertical and horizontal

orientations as well. Surfaces A, B, C, and D with their corresponding feature tolerance are presented for each case.

Table 6 finishes the trend of the thermo-mechanical simulation of both specimens under predicting the actual flatness deviation of surface A seen on the printed specimens, while again, as in Table 3 and Table 5, the flatness deviation of 1W specimen was under predicted in surface B as well.

From the results, it can be concluded that the simulations mostly under-predict the actual deviations seen on the printed specimens, especially the flatness deviation. It can also be concluded that the software under-predicts the actual flatness deviation of surface B more in vertical orientation than in horizontal.

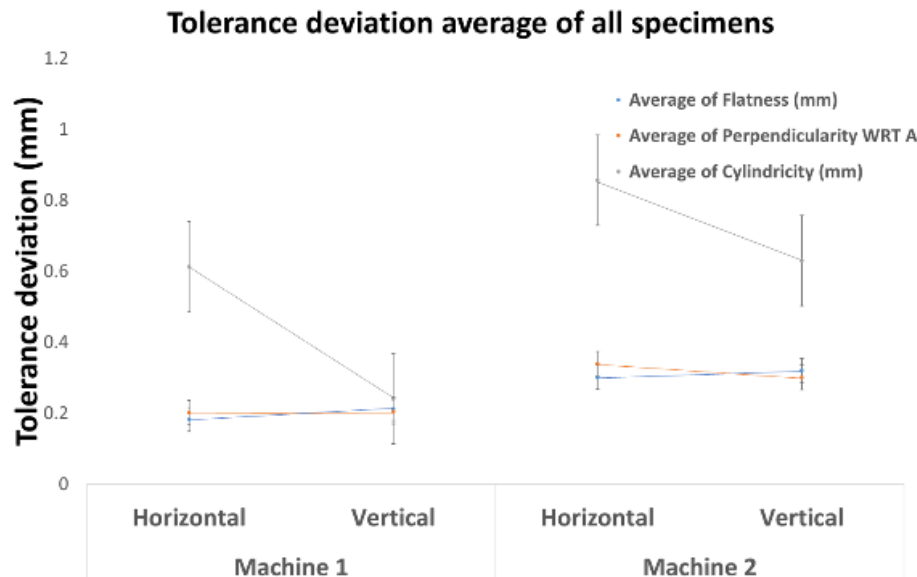


Figure 39. Tolerance deviation results based on GD&T

Figure 39 shows the tolerance deviation average of flatness, perpendicularity, and cylindricity on both orientations and both machines. Cylindricity tolerance has the highest deviation among all configurations, with the horizontal orientation showing the highest effect on deviation. Cylindricity has 125% more deviation than perpendicularity and 122% more than flatness,

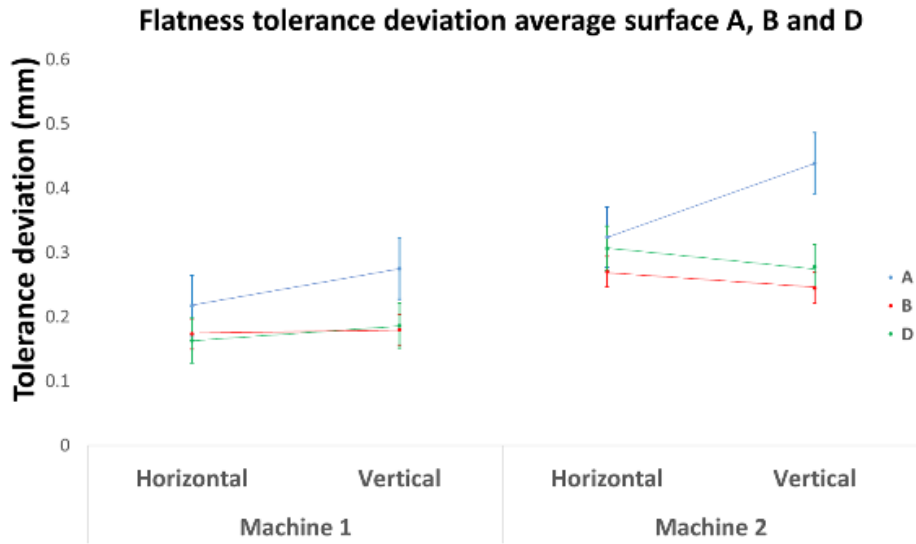


Figure 40. Flatness tolerance deviation results based on GD&T

Figure 40 shows the tolerance deviation average of flatness in both orientations and both machines. The results demonstrate that surface A has 50% more flatness deviation with respect to B and 14% with respect to D.

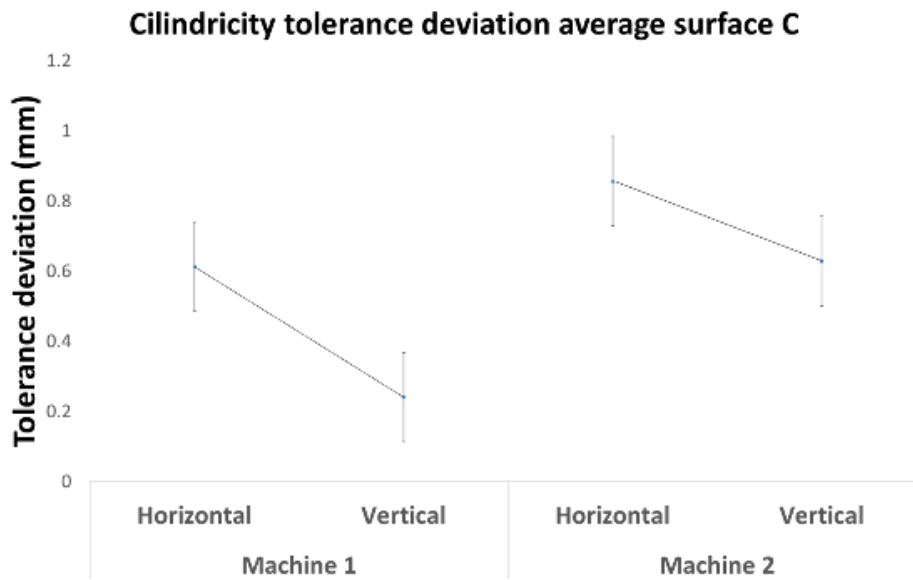


Figure 41. Cylindricity tolerance deviation results based on GD&T

Figure 41 shows the tolerance deviation average of cylindricity in both orientations and both machines. Horizontal orientation has 38% more deviation than vertical. Thus it would be recommended to print cylinders in the vertical orientation, if allowed by design, to have better surface accuracy.

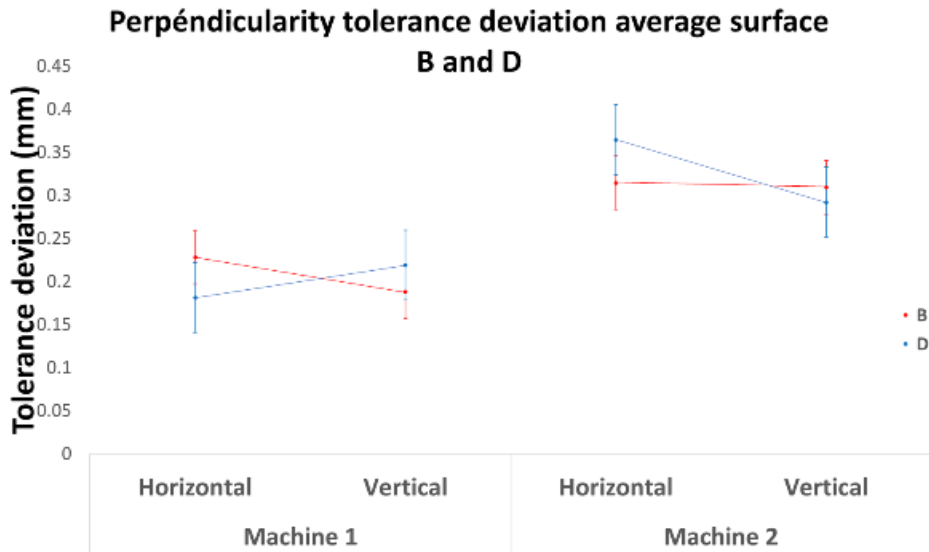


Figure 42. Perpendicularity tolerance deviation results based on GD&T

Figure 42 shows the tolerance deviation average of Perpendicularity on both orientations and both machines. Orientation and surface don't seem to have an effect on perpendicularity deviation.

Table 7 Machine1 2W point cloud differences.

Specimen name	Min deviation (mm)	Maximum deviation (mm)	+/- deviation (mm)	SD (-)	Error distribution between -0.25-+0.25mm (%)
2W Vertical scan 1	-0.196	0.402	0.597	0.040	99.95
2W Vertical scan 2	-0.542	0.204	0.745	0.065	99.75
2W Vertical scan 3	-0.278	0.216	0.494	0.055	100
2W Vertical scan 4	-0.326	0.721	1.047	0.073	99.18

2W Vertical scan 5	-2.000	0.537	2.537	0.432	86.97
2W Horizontal scan 1	-0.290	1.059	1.349	0.087	98.51
2W Horizontal scan 2	-0.442	1.844	2.287	0.095	99.12
2W Horizontal scan 3	-0.270	0.943	1.213	0.100	98.13
2W Horizontal scan 4	-0.638	0.995	1.634	0.116	94.97
2W Horizontal scan 5	-1.171	0.781	1.952	0.088	98.52

Table 7 Shows the point cloud difference of 1W machine 1 specimens with respect to the CAD model.

Table 8 Machine 1 1W point cloud differences.

Specimen name	Min deviation (mm)	Maximum deviation (mm)	+ - deviation (mm)	SD (-)	Error distribution between - 0.25- +0.25mm (%)
1W Vertical scan 1	-0.196	0.402	0.597	0.040	99.95
1W Vertical scan 2	-0.208	1.785	1.993	0.092	99.58
1W Vertical scan 3	-0.231	0.155	0.386	0.054	100
1W Vertical scan 4	-0.338	0.773	1.111	0.114	95.70
1W Vertical scan 5	-0.632	0.491	1.123	0.132	94.00
1W Horizontal scan 1	-0.349	0.714	1.063	0.062	99.27
1W Horizontal scan 2	-0.216	0.775	0.991	0.068	99.43
1W Horizontal scan 3	-0.239	0.761	1.000	0.071	99.34
1W Horizontal scan 4	-0.414	0.906	1.320	0.099	98.00
1W Horizontal scan 5	-0.392	0.957	1.348	0.117	96.17

Table 8 Shows the point cloud difference of 1W machine 1 specimens with respect to the CAD model.

Table 9 Machine 2 2W point cloud differences.

Specimen name	Min deviation (mm)	Maximum deviation (mm)	+ - deviation (mm)	SD (-)	Error distribution between - 0.25- +0.25mm (%)
2W Vertical scan 1	-1.968	0.560	2.528	0.100	94.82
2W Vertical scan 2	-1.523	0.345	1.869	0.097	98.16
2W Vertical scan 3	-1.839	0.653	2.492	0.127	96.42
2W Vertical scan 4	-0.743	1.859	2.602	0.197	79.70
2W Vertical° scan 5	-4.998	4.973	9.971	0.893	75.70
2W Horizontal scan 1	-1.449	0.845	2.295	0.197	76.70
2W Horizontal scan 2	-1.705	0.651	2.356	0.167	82.18
2W Horizontal scan 3	-1.722	0.760	2.482	0.185	83.26
2W Horizontal scan 4	-1.856	1.884	3.740	0.184	82.63
2W Horizontal scan 5	-1.796	1.997	3.794	0.231	65.89

Table 9 Shows the point cloud difference of 2W machine 2 specimens in relation to the CAD model.

Table 10. Machine 2 1W point cloud differences.

Specimen name	Min deviation (mm)	Maximum deviation (mm)	+ - deviation (mm)	SD (-)	Error distribution between - 0.25- +0.25mm (%)
1W Vertical scan 1	-0.933	0.768	1.700	0.135	89.46
1W Vertical scan 2	-1.942	0.624	2.566	0.103	89.21
1W Vertical scan 3	-0.583	0.871	1.454	0.122	97.05

1W Vertical scan 4	-1.951	1.052	3.003	0.226	79.87
1W Vertical scan 5	-0.621	0.592	1.213	0.102	94.05
1W Horizontal scan 1	-0.790	0.702	1.492	0.204	76.58
1W Horizontal scan 2	-1.752	0.694	2.445	0.131	87.37
1W Horizontal scan 3	-0.740	0.883	1.622	0.177	84.09
1W Horizontal scan 4	-1.622	0.699	2.322	0.147	85.27
1W Horizontal scan 5	-0.739	1.080	1.819	0.149	91.27

Table 10 Shows the point cloud difference of 1W machine 2 specimens with respect to the CAD model.

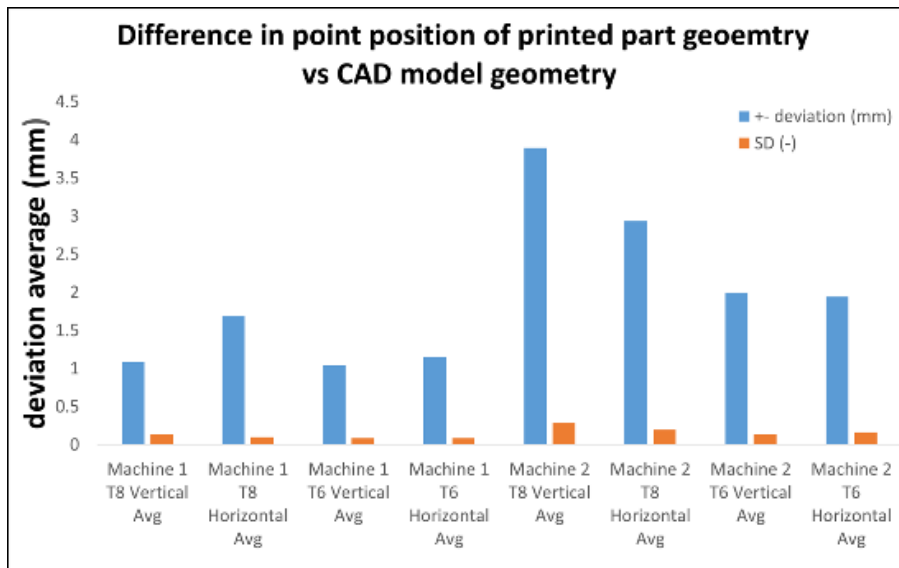


Figure 43. Point cloud differences result in the average of printed parts against CAD models for all specimens

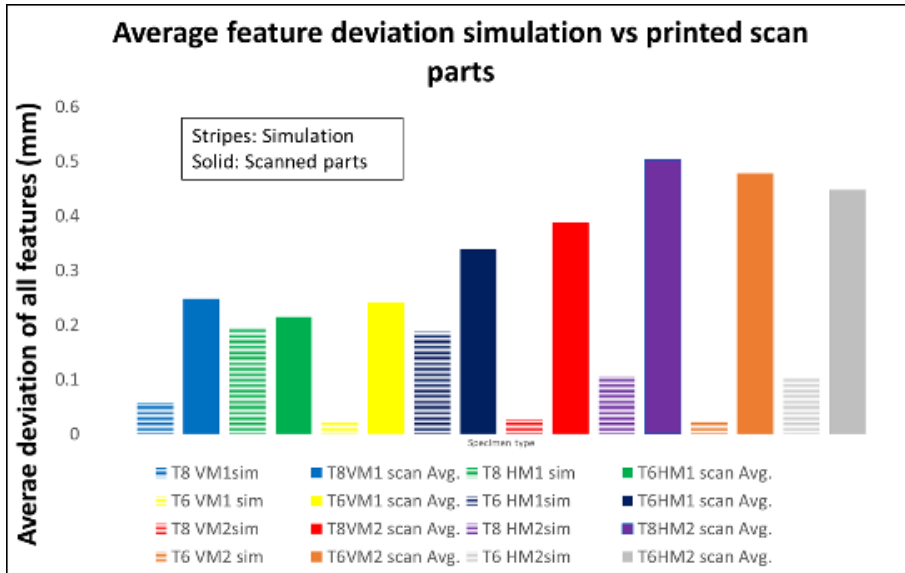


Figure 44. Results of average feature deviation between simulations and scanned parts. H: Horizontal, V: Vertical, M: Machine.

The graph shows the point cloud difference in mm between the average of each specimen type, including simulation, and the CAD model. The simulations predict 46-94% less deviation than the final parts.

3.5 Thermal simulation

To study the relation between the thermal gradients and the surface deviation of parts fabricated through FDM, Digimat-AM was used to simulate the thermal behavior of the fabrication process, and the results were compared to thermal images of the actual deposition of the printed parts.

Digmat-AM was used for the thermal simulation, FFF was selected as the manufacturing process, and a generic printer with a Chamber of 320x152x154 to represent the Marktvo was used. The chamber temperature was set at 24°C, bed width at 0.4, discretization by filament, and voxel size 0.1mm. The CAD model was created in Fusion 360. the toolpath created in Cura, ABS was used for the simulation as PLA is not available in the material database

3.5.1 Results

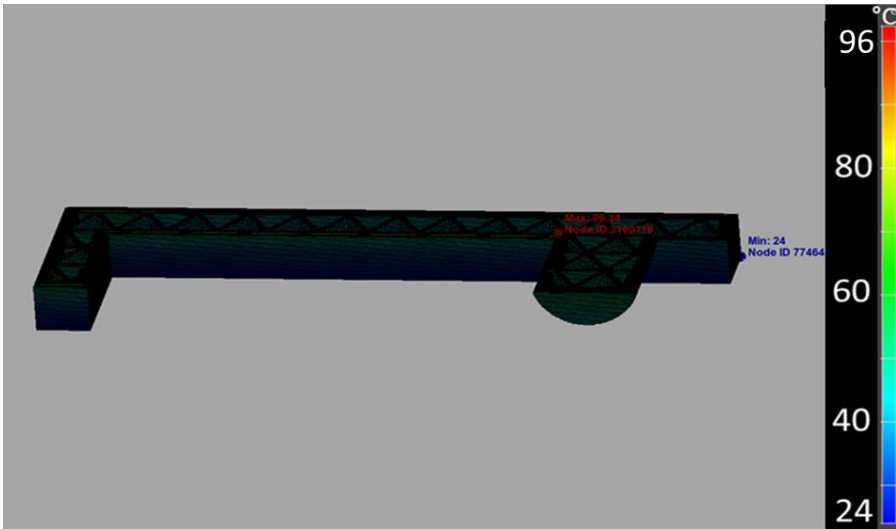


Figure 45. Temperature prediction from thermal simulation of 1W specimen

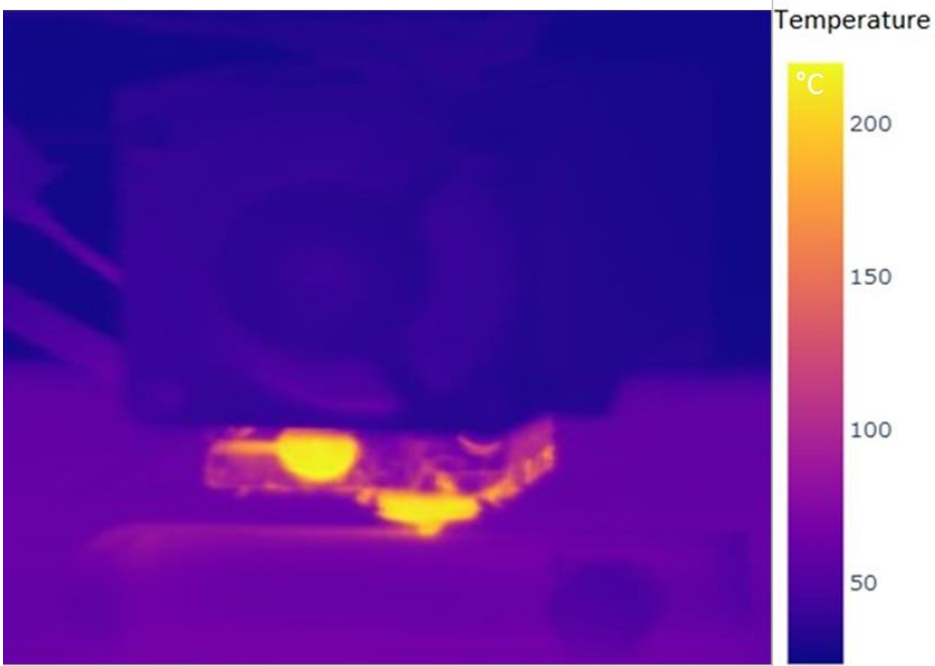


Figure 46. Thermal image from the deposition of 1W specimen

Figure 45 shows the predicted temperature from the deposition process of specimen 1W. At the current fabrication moment, the maximum temperature is 96°C.

Figure 46 shows a thermal image from the deposition of specimen 1W, the maximum temperature at the time of recording was 200°C.

As seen in Figure 45 and Figure 46, the thermal simulation could be under predicting the deposition temperature by half what we see on the thermal camera. This trend was observed in all observed instances of the simulation. Because of this, the thermal simulation was concluded to be unreliable and inaccurate.

3.6 Discussion

As seen in Figure 43, the PLA samples of machine 2 have more deviation compared to the Onyx samples of machine 1 Tanoto et al. [84] noted PLA to have good dimensional accuracy. Zharylkassyn et al. [131] reported in an extensive review that the layer thickness levels between 0.1 mm and 0.2 mm are more likely to be optimal for the dimensional accuracy of FDM parts that uses ABS or PLA resins, whereas for Nylon, about 0.3 mm are preferable. Therefore, the print settings for Machine 2 (0.125 mm layer height) that uses PLA were better aligned with what the literature has reported for better accuracy than those of machine 2 (0.1mm layer height) that uses Onyx which has a Nylon matrix. The lower tolerance deviation of machine 1 could be attributed to the better mechanical solutions of the Marktwo printer.

Cylindricity has the highest overall deviation in the case of the vertical specimens, and this is probably due to the complexity of using two motors for simultaneously moving in 2 axes to create a circle, compared to the other tolerances, which only move in a straight line. In the case of the horizontal specimens, the staircase effects may be involved.

Horizontal orientation seems to have higher cylindricity deviation due to gravity deforming the polymer, while 2W seems to have lower cylindricity deviation, possibly due to the lack of material in the inner hole resulting in less thermal gradient, which causes less thermal stresses, therefore less thermal induced deviations.

As shown in Figure 44, the average error ranged from 46-94% less deviation in the simulation than in the scanned parts. Therefore, the simulation isn't accurate enough under the studied conditions.

3.7 Conclusion

In this chapter, deposition simulations were performed to predict the expected geometry of parts fabricated by FDM. The simulations were compared to experimental tests to validate the predicted geometry. From the results, it can be concluded that the thermos-mechanical deposition simulations failed to accurately predict the geometric deviations seen in the physical parts due to the complexities of the thermomechanical process and the effects of process parameters. The thermal deposition simulation was concluded to be unreliable and inaccurate based on the results of the thermal images.

Chapter 4

4.1 Introduction

As seen in chapter 2, defects in the fabrication process and the slicing process deviate the final part with respect to the CAD model, which is used in FEA static simulations. Anisotropy caused by the layered process, surface deviation, and internal structures are not considered when simulating the original CAD model. This deviation between the CAD model and the final part geometry can affect the performance prediction accuracy of typical FEA static simulations, as geometry and mechanical properties have a direct effect on stiffness. Furthermore, as seen in Chapter 3, the selection of process parameters may also change the sliced geometry, and other parameters that affect the fabrication process may indirectly affect the final parts' geometry. This chapter seeks to analyze the effects that process induce defects have on the strength of FDM parts

For a Digital Twin to accurately represent an FDM part, not only the geometry needs to be mimicked, but the physical behavior as well. This includes the mechanical properties of the part. As the stiffness depends on the geometry as well as the mechanical properties of the material, the previously discussed geometrical deviations will cause the FDM parts to have different mechanical behavior than traditionally manufactured parts. This chapter studies the effects of process-induced deviations and defects in the mechanical strength of FDM parts.

FDM parts are already generally weaker than their traditional manufacturing counterpart as the inherent printing process creates print layers and raster. These structures adhere to one another through the melting process. However, this bond is normally weaker than the bulk material; because of this, the structure becomes anisotropic and weaker when a force is applied in a certain direction.

Process induce defects affect the geometrical accuracy of the part. However, this is not the only problem they cause. By altering the intended internal structure, the toolpath attempts to construct, voids and gaps may be created that hinder the part's stiffness

When designing a new component, verifying if the mechanical requirements fulfill the specific needs of the applications for which they are manufactured is important. Designers usually employ computer-aided simulation and engineering tools to predict the performance of various designs earlier in the life cycle, reduce reliance on expensive and various physical testing, optimize the design for maximum performance, and cut-down design time and cost [33]. Experimental testing is time-consuming and costly. Finite Element Analysis was developed to solve complex elastic and structural analysis problems in aerospace and civil engineering [132] FEA can reduce material and experimental testing costs [133]. FEA is a method for converting approximate partial differential equation solutions into a linear combination of polynomial trial functions specified over elements [133].

FEA reduces complicated problems to a small number of variables. FEA is commonly used to simulate constrained parts with various materials, restrictions, and loads under various boundary conditions [134] [135]. Following the analysis of the simulation results, adjustments to the current design can be made and re-simulated for compliance. For structural analysis, thermomechanical simulations, and thermal analysis, FEA is commonly employed [133]. By modeling the existing model, FEA can be utilized to forecast stress distribution and deformations [135]. However, existing FEA simulations have a number of drawbacks, particularly when it comes to FDM parts.

CAD software creates designs with the assumption that the internals of the parts is geometrically and materially homogenous. The tensile behavior of an FDM sample constructed with various layer thicknesses and/or raster orientation differs from that of solid material [136]. A reliable AM CAD tool should give you the flexibility to customize the material distribution and composition inside the part [137].

When using FEA, it's critical to be able to check whether the analysis' conclusions converge with the actual testing of a part, resulting in accurate and useful results. As a consequence, experimental validation is essential [138]. Most FEA material databases contain isotropic materials that have been developed using typical manufacturing methods, and they are unable to represent layered manufactured anisotropic materials effectively [134]. With FEA techniques, parts are intended to be operational when fabricated from molded or machined stock material [139]. The current restriction in material properties is that they are not well understood, rather than that they are inadequate [140] [139].

Due to substantial deformation, thermoplastic properties are difficult to identify, and they have less strength and stiffness than metal [141]. The strength and stiffness of the part are determined by the strength of the material and bonding between the extruded infill and the air gaps that separate them, making the FEA simulation of FDM products difficult [137].

Understanding the interplay of process parameters, material properties, and mechanical behavior of FDM specimens and parts is critical for determining whether the objects can meet the mechanical requirements of the applications for which they are made [101]. More realistic simulations that account for all the intricacies of the FDM process are required in order to pick the best printing parameters. Modeling and simulation are the basis of implementing DT [142]

The following review shows the work done in simulation and experimental validation of AM parts.

Hambali et al. [138] performed numerical simulations to compare the stress-deformation failure differences between a solid component model and a model that included each layer as a solid and union forces between layers. They concluded that, given the identical charge conditions, the layer-based model achieves larger

elastic values than the solid case, implying that the second case is more restricted than the first. They highlighted that when a ply fails, its stresses could be redistributed and carried by the rest of the plies.

Garg et al. [136] performed simulation and modeling of realistic models that consider layers of different thicknesses and rasters at different angles maintaining the inter-layer and intra-layer bonded region. They experimentally validated by comparing them with observations. Fractographic studies are also carried out to analyze the mode of failure of the FDM samples. They highlighted that compared to solid simulation, the 0.178 and 0.254 mm layer thickness specimens had the stress more concentrated towards the end of the gage length, where the area starts decreasing. They also concluded that for 90° raster angles, since layers are laid perpendicular to the loading direction, fewer stresses are generated, and failure of specimen mainly depends upon adhesion between successive layers

Baikerikar et al. [140] carried out FEA simulations of FDM dogbone parts with bulk material properties and derived material properties. To experimentally validate the simulation results four different infill patterns were printed and tensile tested. Bulk isotropic properties resulted in up to 70% error in normal stress values as compared to the experimental results. FEA results using derived material properties resulted in up to 45% error in normal stress values.

The team concludes that the Finite Element Analysis using isotropic models is not a reliable tool for analyzing FDM parts. They also noted that as the geometries get finer, FEA predictions become worse. And for FDM were fine, complex shapes are an advantage over traditional methods. This is a downside.

Abbas et al. [143] performed an experimental analysis on the influence of infill density on the compressive strength in FFF specimens. The compressive strength of the additively built polylactic acid (PLA) samples increased almost linearly with the increase in infill density, according to the researchers. The study also discovered that the maximum compressive strength for PLA pieces (30 MPa) is obtained at an infill density of 80%, advocating for the employment of internal structures.

Naranjo et al. [144] studied the effects of several deposition techniques on the tensile characteristics of FFF composites. They discovered that Nylon samples fail macroscopically ductile, whereas Onyx (Nylon fibers containing chopped carbon fibers) fails macroscopically brittle. Furthermore, the fiber deposition arrangement has an impact on tensile strength, with discontinuities and bends acting as failure initiation points.

Forcellese et al. [145] studied the buckling behavior of composite isogrid structures in compression. FFF of polyamide reinforced with chopped carbon fiber was used to produce these constructions. They experimented with buckling loads for various geometric parameters. Outside the plane of loads, specimens buckled. During compression tests, the load applied to isogrid structures increases with displacement until it reaches a maximum value at the commencement of buckling.

Parts can buckle locally (internally) or globally (globally) depending on the values of geometrical parameters. They discovered that increasing rib thickness helped them to carry heavier burdens. Their internal architecture is geometrically similar to the test specimens used in this study.

Block et al. [146] found that continuous fibers embedded in a thermoplastic matrix help improve the mechanical properties of products. However, because continuous fibers cannot be added in sharp radius and angles, design flexibility is limited. They also found that embedding carbon microfibers in a thermoplastic fiber has no additional design limits but that the mechanical qualities are only marginally better than the material without fibers. These findings are in line with those of Naranjo.

To avoid low-quality prints, Günaydn et al. [147] examined the sources of faults in AM and found that slicing software options and FDM machine work principles should be thoroughly understood to make production plans. This emphasizes the significance of slicing software in the printing process.

The impact of gaps on tensile strength, modulus, and failure strain on 3D printed parts was investigated by Fayazbakhsh et al. [148], who found that defects transverse to the loading direction have a more severe impact than defects along the loading direction.

The previous review shows that the mechanical properties of FFF fiber reinforced parts are affected by the material deposition process and that the study of the response to compression is a field of recent interest.

This article shows that path planning programs follow strategies that do not favor part strength. The objective of this work is to evaluate the effects that internal voids and raster gaps have on the mechanical strength of the part, specifically the compressive strength of FDM parts made out of Onyx. The effects of internal structure thickness and part geometry on FFF composites' compressive properties are also analyzed. Experimental results are compared to that of Finite Element model simulations.

4.2 Methodology

Exploratory tests were specifically built to evaluate the compressive behavior of a composite structure and to determine its maximum compressive strength. Specimens were fabricated with Onyx filament in a Markforged Mark two. The printing layers in all specimens ended up in planes parallel to the direction of load application in the compressive test. The internal structure's wall thickness varied between 0.5 mm and 1.5 mm. All other variables were maintained constant (layer thickness, print speed, infill density, material, nozzle size, and geometry). For each case, five specimens were made, and compressive tests were done at 1.3 mm/s using a Shimadzu 250 KN Universal Machine.

Linear static exploratory FEA simulations for all specimens were run in 1 KN increments from 1 to 10 Kilo-Neutons (KN). The results of the stress-displacement tests were graphed alongside the results of the experimental testing. Non-linear static large deformation and buckling simulations for specimens were also done to model the effect of printing flaws on part strength for three cases: entirely solid structure, structure with raster gaps on walls, and structure with raster gaps and voids. Figure 47 summarizes the cases that were modeled and examples of the specimens that were tested. Simulations were performed in Fusion 360. Linear and buckling static models assumed a constant Elastic Modulus (E) of 1.0 GPa and a yield strength of 32 MPa [146]. For non-linear static analysis, a function of the Elastic Modulus (E) was prepared based on the work of Block [146]. Non-linear static simulations for solid models and models with raster gaps and voids were performed. The average mesh element size was 4% of the model, the element was set at parabolic, curved mesh elements were enabled, and max turn angle was set at 60°

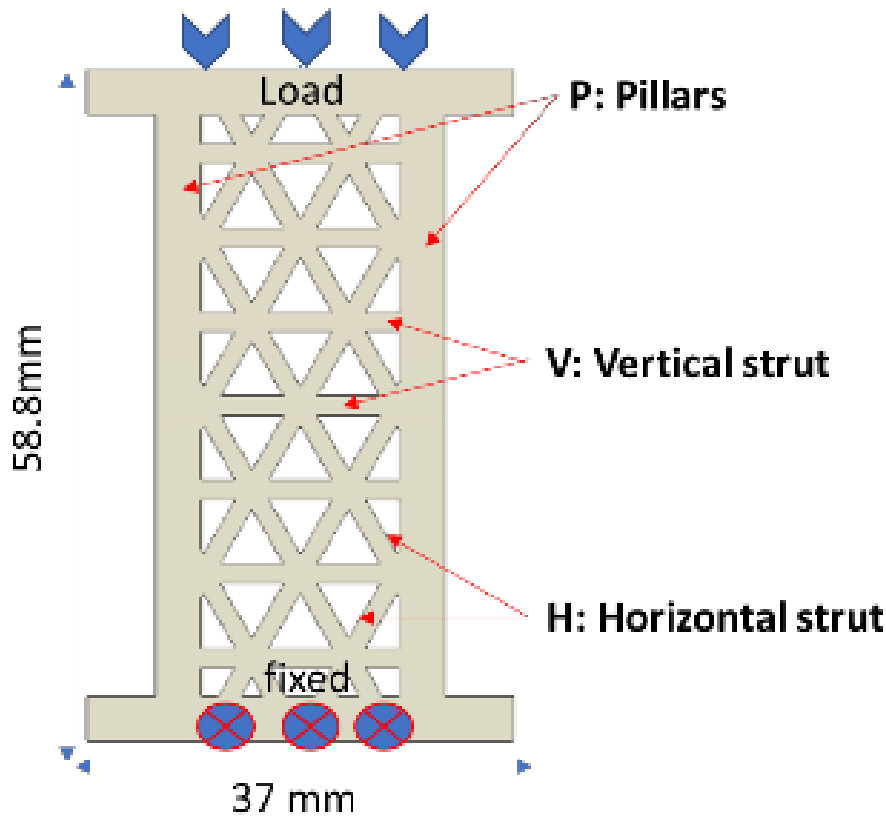


Figure 47. Basic model and simulation conditions, defect free (solid) case.

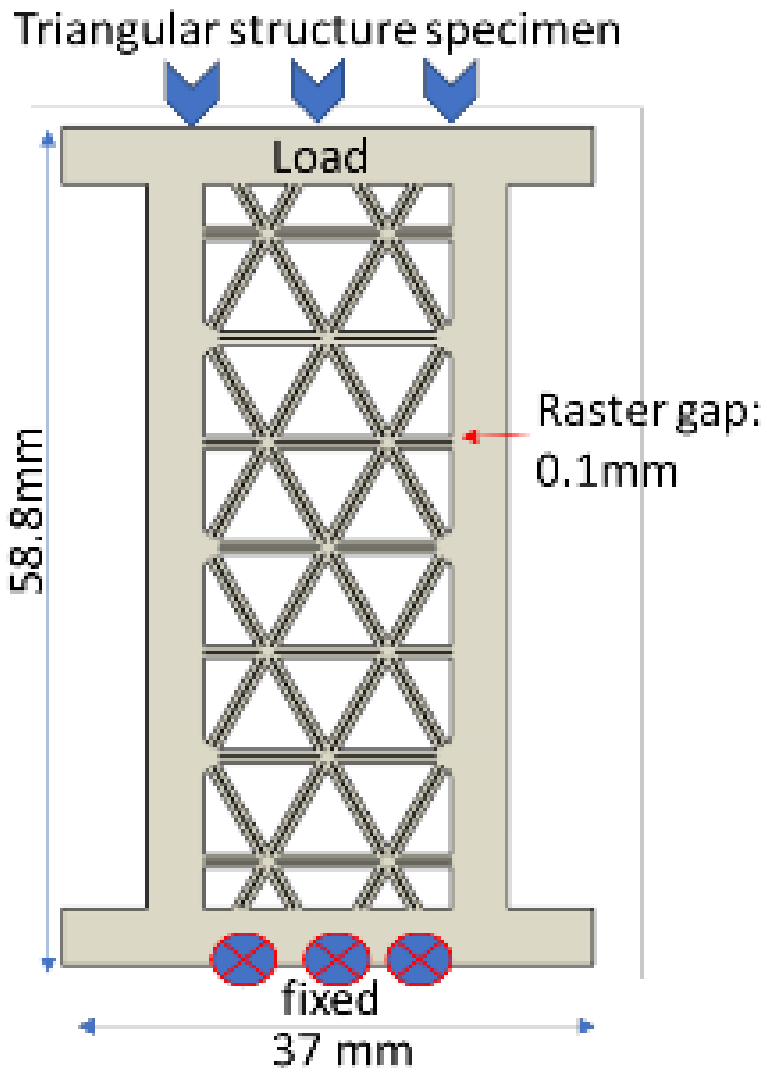


Figure 48. Model with raster gaps simulation conditions.

Non-linear and buckling static simulations were conducted with geometries that attempted to replicate the faults of the actual parts by using 0.1 mm raster gaps and 1 mm diameter voids, respectively. The total gap and void in all models were between 2% and 3% of the part volume.

4.3 Results

Table 11. Experimental tests and the simulation results

Specimen (IWT)	Experimental buckling load (N)	Simulation linear critical buckling load (N)	Displacement at buckling load experimental (mm)	Theoretical displacement with experimental buckling load (mm)	Displacement at buckling load theoretical (mm)
0.5 solid	3680.7	3761	0.73	0.7	0.65
0.6 Solid	4653.2	5604	1.19	0.85	1.065
0.8 gap and void	3858.9	3005	1.55	1.2	0.935
1.0 gap and void	3106.7	4072	1.07	1.01	0.935
1.5 gap and void	6008.7	5412	3.07	N/A	N/A

Table 11 shows the following results:

- Experimental buckling load.
- Theoretical critical buckling load (FEA).
- Displacement at experimental buckling load from the onset of buckling.
- Theoretical (FEA) displacement using experimental buckling load.
- Theoretical (FEA) displacement at critical buckling load.

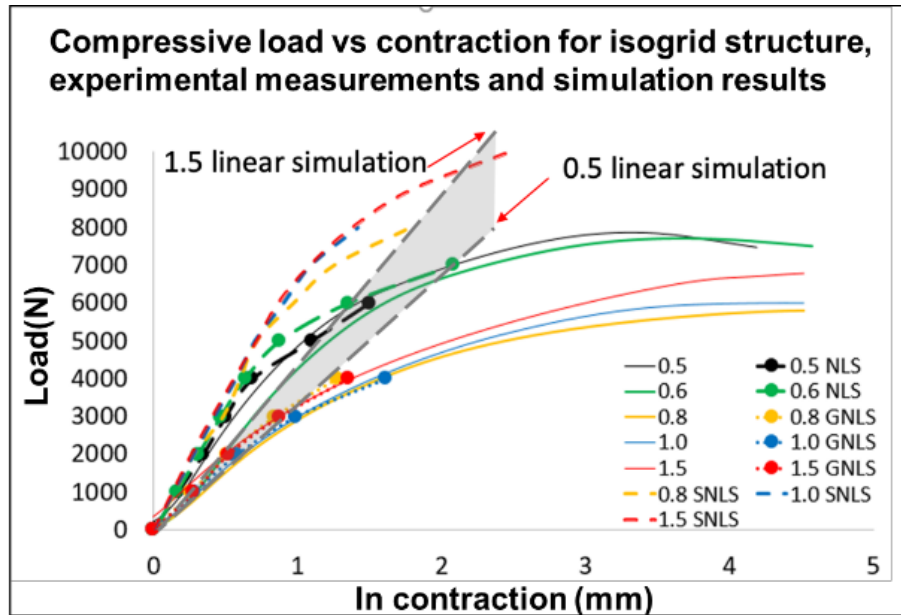


Figure 49. Compressive load vs contraction of the different IWT specimens (0.5, 0.6, 0.8, 1.0, 1.5). Solid lines show experimental results, dashed and dotted lines represent Nonlinear Static Simulations (NLS), with overlap represented as a solid structure

Figure 49 plots compressive loads vs. displacement of the top surface for all cases.

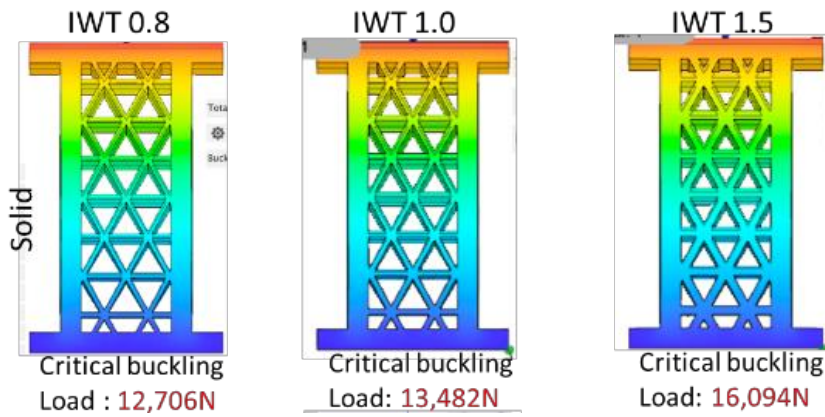


Figure 50. Buckling simulation results of solid models IWT 0.8, 1.0 and 1.5

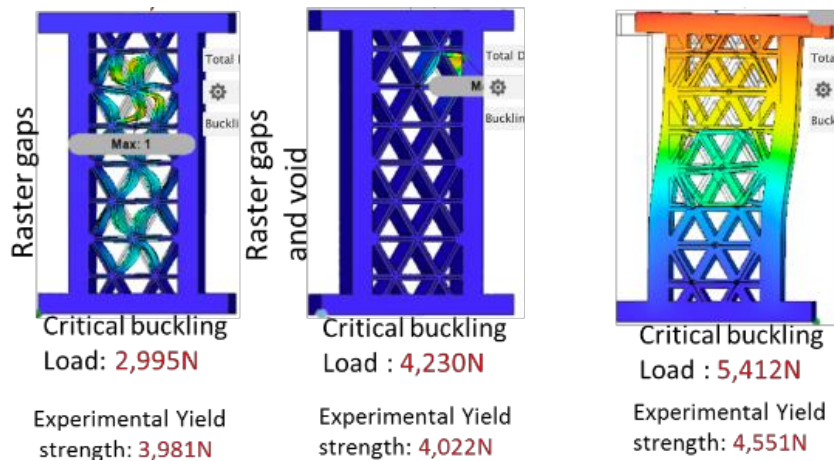


Figure 51. Buckling simulation results of models with raster gaps and voids IWT 0.8, 1.0 and 1.5

As seen from the results of Figure 50 and Figure 51, the simulation results of models with raster gaps and voids behave in a manner closer to that of the experimental tests, thus supporting the use of simulations with modeled raster gaps and voids.

4.4 Discussion

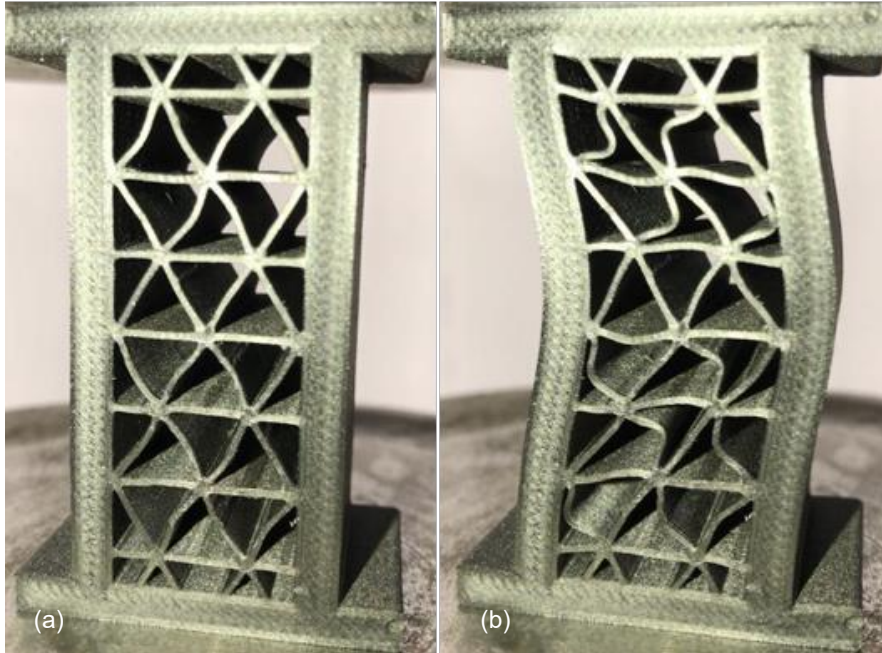


Figure 52. Experimental specimens during the test. (a) The onset of buckling occurs when the internal structure begins to collapse; (b) Buckling of the full structure.

At small loads (under 2000 KN), every part behaves linearly and shows similar strength, indicating that the side walls take most of the loads. The results of linear simulations shown in Figure 49 represent what would be intuitively expected: parts with thicker sections take larger loads for the same deflection. Experimental results, however, behave differently. The thinnest specimens (IWT 0.5 and 0.6) take heavier loads, while specimens with IWT 0.8, 1.0, and 1.5 suffer larger deformations.

Non-linear simulations of geometries that include gaps and voids behave in a similar pattern to the experimental results and provide a good representation of the behavior of the part. For the case of IWT 1.0, models with gaps and one void showed the best correlation with the experimental results, while for the 1.5 cases, models with voids in all intersections and gaps at selected locations (particularly on horizontal trusses) showed the best correlation. Buckling simulations provided a good representation of the mode shape for the onset of buckling of the isogrid. Theoretical buckling loads were used in non-linear simulations to predict the displacements at the onset of buckling. Simulation values for the displacement at buckling are reasonably close to the experimental values. Overall, the results of

experimental tests and the simulations indicate that the manufacturing defects generated during filament deposition have an important effect on part strength and cannot be ignored when parts are designed.

It is important to note that these simulation models are only approximations of the macroscopic behavior of the part, as they lack the detail to accurately model the failure mechanisms at a microscopic level. Nevertheless, they serve to illustrate the effects that the defects produced during part manufacture have on the strength of the part.

Static simulations should use CAD models that include raster roads, print layers, printing defects, and non-linear materials to accurately predict the part's performance.

4.5 Conclusions

This work has shown that different slicing programs use raster path definition strategies that are not represented in the CAD model. Experimental tests, supported by simulation results, show that gaps and voids produced by typical manufacturing processes significantly affect the load-bearing capabilities of parts in compression. And that by not modeling these defects in the CAD, the FEA static simulations fail to predict the part's performance accurately. This work also shows that slicing strategy defects, such as raster overlap, positively affect the load-bearing capabilities of the parts, which will also affect the simulation if not properly modeled.

AM processes inherently require that nozzle sizes and the material they deposit be smaller than the smallest walls they produce. As a consequence, decisions must be made about the strategies to deposit material to produce solid parts. The results of this work indicate that slicer programs need to allow the part designer to have better control of the raster paths. A highly desirable capability for slicers would be a diagnostics routine that could interact with the part (or process) designer to evaluate the quality of a proposed filling strategy and help identify and correct potential weaknesses in the structure. The slicer software could then allow the designer to eliminate gaps by programming overlapping rasters. Other parameters that affect part strength and that could be controlled by proper path deposition strategies are the location of discontinuities of the fiber strands and the temperature of the part at the deposition point, which affects interlayer bonding.

Chapter 5 Conclusion and future work

Many challenges for the creation of Digital Twins of FDM parts have been presented and analyzed in this work; CAD models don't fully represent the printed part, deposition simulation fails to predict the final part geometry, and static simulations don't accurately predict part performance.

A definition based on the literature and ISO 23247 was established. The elements and components that constitute a Digital Twin, as well as how they interact in a framework, was presented along with the advantages and limitations of Digital Twins in Additive manufacturing were presented in addition to the main challenges to overcome for the implementation of DT in AM.

It was presented how FDM parts are not an accurate replica of the designed CAD model as they incorporate inherent printing architecture, fabrication defects, and geometric deviations. It was discussed how the geometric deviation could be caused by the printing machine, the slicing software, the rheological extrusion of the material, or the thermomechanical deposition of the printed part. It was proposed how some process parameters change the sliced geometry from the CAD model while others indirectly deviate the final part geometry from the intended CAD model.

An analysis of how slicing architecture and the deposition process induce geometric deviations to the final part that are not present in the CAD model is presented with an in-depth Inspection of the FDM parts using various advanced equipment such as SEM microscope, light microscope, and CT-Scan.

First, it was presented how the slicing architecture introduced raster paths and print layers to the geometry, which, if not taken into account during the design stage, could result in raster gaps or raster overlaps.

By fabricating thin isogrid specimens and taking images with a SEM microscope, it was shown how the internal structure's geometry deviates from that of the slice model as the dimensions of the internal structure were not as intended by the slicing software, with raster paths being on average 14.975% larger and print layers being 12.9% smaller than those of the slice model.

By analyzing isogrid FDM parts with a light microscope, defects in the fabrication process resulted in the creation of voids on the reticle center, raster to raster gaps, and even a deposition failure which resulted in no raster being deposited between 2 adjacent rasters, leaving a bigger than usual gap.

CT-scans of post-mortem isogrid FDM specimens showed dislocations in the print layers and triangular structure, which are not taken into account in the CAD model, this dislocation in the internal structure could lead to yielding sooner than what would be expected from a solid plastic injection part

Varying thermo-mechanical induce stresses were stated to be a cause for geometric deformation, and the intricate geometries and complex time-varying thermal were proposed to make accurate deposition simulations of geometric deviations challenging.

Two different specimens in 2 orientations with two different materials were designed, and FDM deposition simulations of the specimens were performed to predict the expected geometric deviation caused by the printing process. The deformed geometry from the simulation was exported to analyze the GD&T tolerances of specific zones to compare the feature deviation to the deviation of actual printed parts.

As shown by the results from the deposition simulations, it is concluded that the deposition simulations fail to accurately predict to a full extent the geometric deviations caused by the printing process, possibly due to the complexities of the thermomechanical process.

Challenges in the implementation of FEA simulations for FDM parts like the absence of slicing architecture in the CAD model, the use of bulk material properties obtained through traditional manufacturing processes, and the idealized CAD geometry that lacks the deviations caused by the printing process exhibited in the actual printed parts was presented. By performing compression tests of isogrid FDM specimens, it was proven that process-induced defects like raster gaps, internal voids, and print gaps negatively affect the compressive strength of the part, while overlap benefited the stiffness of the specimens, as seen from the results of IWT 0.5 and IWT 0.6, which contrary to the simulations results handled higher compressive loads than the specimens with thicker internal walls (1.0 and 1.5).

Because of the recent increase in the adoption rate of both AM and DT in the industry, this becomes ever more important to address to take advantage of both technologies' benefits further.

Bibliography

- [1] Mabkhot, M. M., Al-Ahmari, A. M., Salah, B., & Alkhalefah, H. (2018). Requirements of the smart factory system: A survey and perspective. *Machines*, 6(2), 23.
- [2] Warke, V., Kumar, S., Bongale, A., & Kotecha, K. (2021). Sustainable Development of Smart Manufacturing Driven by the Digital Twin Framework: A Statistical Analysis. *Sustainability*, 13(18), 10139.
- [3] Jones, D., Snider, C., Nassehi, A., Yon, J., & Hicks, B. (2020). Characterising the Digital Twin: A systematic literature review. *CIRP Journal of Manufacturing Science and Technology*, 29, 36-52.
- [4] Hu, L., Nguyen, N. T., Tao, W., Leu, M. C., Liu, X. F., Shahriar, M. R., & Al Sunny, S. N. (2018). Modeling of cloud-based Digital Twins for smart manufacturing with MT connect. *Procedia manufacturing*, 26, 1193-1203.
- [5] Autiosalo, J., Vepsäläinen, J., Viitala, R., & Tammi, K. (2019). A feature-based framework for structuring industrial Digital Twins. *IEEE access*, 8, 1193-1208.
- [6] Kritzinger, W., Karner, M., Traar, G., Henjes, J., & Sihn, W. (2018). Digital Twin in manufacturing: A categorical literature review and classification. *IFAC-PapersOnLine*, 51(11), 1016-1022.
- [7] Tao, F., Cheng, J., Qi, Q., Zhang, M., Zhang, H., & Sui, F. (2018). Digital Twin-driven product design, manufacturing and service with big data. *The International Journal of Advanced Manufacturing Technology*, 94(9), 3563-3576.
- [8] Lee, J., Lapira, E., Bagheri, B., & Kao, H. A. (2013). Recent advances and trends in predictive manufacturing systems in big data environment. *Manufacturing letters*, 1(1), 38-41.
- [9] Zheng, Y., Yang, S., & Cheng, H. (2019). An application framework of Digital Twin and its case study. *Journal of Ambient Intelligence and Humanized Computing*, 10(3), 1141-1153
- [10] Bilberg, A., & Malik, A. A. (2019). Digital Twin driven human–robot collaborative assembly. *CIRP annals*, 68(1), 499-502.
- [12] VanDerHorn, E., & Mahadevan, S. (2021). Digital Twin: Generalization, characterization and implementation. *Decision support systems*, 145, 113524.
- [13] Haag, S., & Anderl, R. (2018). Digital Twin–Proof of concept. *Manufacturing letters*, 15, 64-66.

- [14] Boschert, S., & Rosen, R. (2016). Digital Twin—the simulation aspect. In *Mechatronic futures* (pp. 59-74). Springer, Cham.
- [15] Dembski, F., Wössner, U., & Yamu, C. (2019, July). Digital Twin. In *Virtual Reality and Space Syntax: Civic Engagement and Decision Support for Smart, Sustainable Cities: Proceedings of the 12th International Space Syntax Conference, Beijing, China* (pp. 8-13).
- [16] Boschert, S., Heinrich, C., & Rosen, R. (2018, May). Next generation Digital Twin. In *Proc. tmce* (Vol. 2018, pp. 7-11). Las Palmas de Gran Canaria, Spain.
- [17] Kostenko, D., Kudryashov, N., Maystrishin, M., Onufriev, V., Potekhin, V., & Vasiliev, A. (2018). DIGITAL TWIN APPLICATIONS: DIAGNOSTICS, OPTIMISATION AND PREDICTION. *Annals of DAAAM & Proceedings*, 29.
- [18] Corradini, F., & Silvestri, M. (2021). A DIGITAL TWIN BASED SELF-CALIBRATION TOOL FOR FAULT PREDICTION OF FDM ADDITIVE MANUFACTURING SYSTEMS. *Annals of DAAAM & Proceedings*, 10(2).
- [19] Rasheed, A., San, O., & Kvamsdal, T. (2019). Digital Twin: Values, challenges and enablers. *arXiv preprint arXiv:1910.01719*.
- [20] Wright, L., & Davidson, S. (2020). How to tell the difference between a model and a digital twin. *Advanced Modeling and Simulation in Engineering Sciences*, 7(1), 1-13.
- [23] Osho, J., Hyre, A., Pantelidakis, M., Ledford, A., Harris, G., Liu, J., & Mykoniatis, K. (2022). Four Rs Framework for the development of a digital twin: The implementation of Representation with a FDM manufacturing machine. *Journal of Manufacturing Systems*, 63, 370-380.
- [24] Liu, C., Le Roux, L., Körner, C., Tabaste, O., Lacan, F., & Bigot, S. (2020). Digital Twin-enabled collaborative data management for metal additive manufacturing systems. *Journal of Manufacturing Systems*.
- [25] Moretti, M., Rossi, A., & Senin, N. (2021). In-process monitoring of part geometry in fused filament fabrication using computer vision and Digital Twins. *Additive Manufacturing*, 37, 101609
- [26] Klingaa, C. G., Mohanty, S., Funch, C. V., Hjerimitslev, A. B., Haahr-Lillevang, L., & Hattel, J. H. (2021). Towards a Digital Twin of laser powder bed fusion with a focus on gas flow variables. *Journal of Manufacturing Processes*, 65, 312-327.
- [27] Stavropoulos, P., Papacharalampoulous, A., & Tzimanis, K. (2021). Design and Implementation of a Digital Twin Platform for AM processes. *Procedia CIRP*, 104, 1722-1727.

- [28] Moyne, J., Qamsane, Y., Balta, E. C., Kovalenko, I., Faris, J., Barton, K., & Tilbury, D. M. (2020). A requirements driven Digital Twin framework: Specification and opportunities. *IEEE Access*, 8, 107781-107801.
- [29] Baumann, F., Schön, M., Eichhoff, J., & Roller, D. (2016). Concept development of a sensor array for 3D printer. *Procedia CIRP*, 51, 24-31.
- [30] Chhetri, S. R., Faezi, S., Canedo, A., & Faruque, M. A. A. (2019, April). QUILT: Quality inference from living Digital Twins in IoT-enabled manufacturing systems. In *Proceedings of the International Conference on Internet of Things Design and Implementation* (pp. 237-248).
- [31] Tan, Y., Yang, W., Yoshida, K., & Takakuwa, S. (2019). Application of IoT-aided simulation to manufacturing systems in cyber-physical system. *Machines*, 7(1), 2.
- [32] Liu, M., Fang, S., Dong, H., & Xu, C. (2021). Review of Digital Twin about concepts, technologies, and industrial applications. *Journal of Manufacturing Systems*, 58, 346-361.
- [33] Zhang, H., Liu, Q., Chen, X., Zhang, D., & Leng, J. (2017). A Digital Twin-based approach for designing and multi-objective optimization of hollow glass production line. *IEEE Access*, 5, 26901-26911.
- [34] Bartsch, K., Pettke, A., Hübert, A., Lakämper, J., & Lange, F. (2021). On the Digital Twin application and the role of artificial intelligence in additive manufacturing: a systematic review. *Journal of Physics: Materials*.
- [35] Kantaros, A., Piriomalis, D., Tsaramirsis, G., Papageorgas, P., & Tamimi, H. (2021). 3D Printing and Implementation of Digital Twins: Current Trends and Limitations. *Applied System Innovation*, 5(1), 7.
- [36] ISO. 2021. "ISO (DIS) 23247-1: Automation Systems and Integration - Digital Twin Framework for Manufacturing - Part 1: Overview and general principles"
- [37] Labuschagne, C., & Brent, A. C. (2005). Sustainable project life cycle management: the need to integrate life cycles in the manufacturing sector. *International Journal of Project Management*, 23(2), 159-168.
- [38] Ma, J., Harstvedt, J. D., Dunaway, D., Bian, L., & Jaradat, R. (2018). An exploratory investigation of Additively Manufactured Product life cycle sustainability assessment. *Journal of Cleaner Production*, 192, 55-70.
- [39] Cerdas, F., Juraschek, M., Thiede, S., & Herrmann, C. (2017). Life cycle assessment of 3D printed products in a distributed manufacturing system. *Journal of Industrial Ecology*, 21(S1), S80-S93.

- [40] Choudhari, C. M., & Patil, V. D. (2016, September). Product development and its comparative analysis by SLA, SLS and FDM rapid prototyping processes. In *IOP Conference Series: Materials Science and Engineering* (Vol. 149, No. 1, p. 012009). IOP Publishing.
- [41] Mourtzis, D. (2016). Challenges and future perspectives for the life cycle of manufacturing networks in the mass customisation era. *Logistics Research*, 9(1), 1-20.
- [42] Cai, Y., Wang, Y., & Burnett, M. (2020). Using augmented reality to build Digital Twin for reconfigurable additive manufacturing system. *Journal of Manufacturing Systems*, 56, 598-604.
- [43] Mandolla, C., Petruzzelli, A. M., Percoco, G., & Urbinati, A. (2019). Building a Digital Twin for additive manufacturing through the exploitation of blockchain: A case analysis of the aircraft industry. *Computers in Industry*, 109, 134-152.
- [44] Knapp, G. L., Mukherjee, T., Zuback, J. S., Wei, H. L., Palmer, T. A., De, A., & DebRoy, T. J. A. M. (2017). Building blocks for a Digital Twin of additive manufacturing. *Acta Materialia*, 135, 390-399.
- [45] Gaikwad, A., Yavari, R., Montazeri, M., Cole, K., Bian, L., & Rao, P. (2020). Toward the Digital Twin of additive manufacturing: Integrating thermal simulations, sensing, and analytics to detect process faults. *IISE Transactions*, 52(11), 1204-1217
- [46] Balta, E. C., Tilbury, D. M., & Barton, K. (2019, August). A Digital Twin framework for performance monitoring and anomaly detection in fused deposition modeling. In *2019 IEEE 15th International Conference on Automation Science and Engineering (CASE)* (pp. 823-829). IEEE.
- [47] Weiss, B., Storti, D. W., & Ganter, M. A. (2015). Low-cost closed-loop control of a 3D printer gantry. *Rapid Prototyping Journal*.
- [48] Santana, L., Ahrens, C. H., Netto, A. D. C. S., & Bonin, C. (2017). Evaluating the deposition quality of parts produced by an open-source 3D printer. *Rapid Prototyping Journal*.
- [49] Greeff, G. P., & Schilling, M. (2017). Closed loop control of slippage during filament transport in molten material extrusion. *Additive Manufacturing*, 14, 31-38.
- [50] Kousiatza, C., & Karalekas, D. (2016). In-situ monitoring of strain and temperature distributions during fused deposition modeling process. *Materials & Design*, 97, 400-406.

- [51] Anderegg, D. A., Bryant, H. A., Ruffin, D. C., Skrip Jr, S. M., Fallon, J. J., Gilmer, E. L., & Bortner, M. J. (2019). In-situ monitoring of polymer flow temperature and pressure in extrusion based additive manufacturing. *Additive Manufacturing*, 26, 76-83.
- [52] Pollard, D., Ward, C., Herrmann, G., & Etches, J. (2017). Filament temperature dynamics in fused deposition modelling and outlook for control. *Procedia Manufacturing*, 11, 536-544.
- [53] Dinwiddie, R. B., Love, L. J., & Rowe, J. C. (2013, May). Real-time process monitoring and temperature mapping of a 3D polymer printing process. In *Thermosense: Thermal Infrared Applications XXXV* (Vol. 8705, pp. 165-173). SPIE.
- [54] Wu, H., Wang, Y., & Yu, Z. (2016). In situ monitoring of FDM machine condition via acoustic emission. *The International Journal of Advanced Manufacturing Technology*, 84(5), 1483-1495.
- [55] Liu, J., Hu, Y., Wu, B., & Wang, Y. (2018). An improved fault diagnosis approach for FDM process with acoustic emission. *Journal of Manufacturing Processes*, 35, 570-579.
- [56] Kim, J. S., Lee, C. S., Kim, S. M., & Lee, S. W. (2018). Development of data-driven in-situ monitoring and diagnosis system of fused deposition modeling (FDM) process based on support vector machine algorithm. *International Journal of Precision Engineering and Manufacturing-Green Technology*, 5(4), 479-486.
- [57] Tlegenov, Y., Hong, G. S., & Lu, W. F. (2018). Nozzle condition monitoring in 3D printing. *Robotics and Computer-Integrated Manufacturing*, 54, 45-55.
- [58] principles, ISO. 2021. "ISO (DIS) 23247-2: Automation Systems and Integration - Digital Twin Framework for Manufacturing - Part 2: Reference architecture
- [59] Kaushish, J. P. (2010). *Manufacturing processes*. PHI Learning Pvt. Ltd..
- [60] Klocke, F., & Kuchle, A. (2009). *Manufacturing processes* (Vol. 2, pp. p-433). Berlin: Springer.
- [61] Rajput, R. K. (2007). *A textbook of manufacturing technology: Manufacturing processes*. Firewall Media.
- [62] Yossef, M., & Chen, A. (2015, June). Applicability and limitations of 3D printing for civil structures. In *Proceedings of the 2015 conference on autonomous and robotic construction of infrastructure* (pp. 237-246). USA: Ames.

- [63] Chen, Z., Li, Z., Li, J., Liu, C., Lao, C., Fu, Y., ... & He, Y. (2019). 3D printing of ceramics: A review. *Journal of the European Ceramic Society*, 39(4), 661-687.
- [64] Buchanan, C., & Gardner, L. (2019). Metal 3D printing in construction: A review of methods, research, applications, opportunities and challenges. *Engineering Structures*, 180, 332-348.
- [65] Basß H, Eleveli S, Yapıcı F. Fault tree analysis for fused filament fabrication type Three-dimensional printers. *J Fail Anal Prev* 2019;19(5):1389–400
- [66] Sun, Q., Rizvi, G. M., Bellehumeur, C. T., & Gu, P. (2008). Effect of processing conditions on the bonding quality of FDM polymer filaments. *Rapid prototyping journal*.
- [67] Fernandez-Vicente, M., Calle, W., Ferrandiz, S., Conejero, A. (2016). Effect of infill parameters on tensile mechanical behavior in desktop 3D printing. *3D printing and additive manufacturing*, 3(3), 183-192.
- [68] Singh, T., Kumar, S., & Sehgal, S. (2020). 3D printing of engineering materials: A state of the art review. *Materials Today: Proceedings*, 28, 1927-1931.
- [69] Fazzini, G., Paolini, P., Paolucci, R., Chiulli, D., Barile, G., Leoni, A., ... & Ferri, G. (2019, June). Print On Air: FDM 3D Printing Without Supports. In *2019 II Workshop on Metrology for Industry 4.0 and IoT (MetroInd4. 0&IoT)* (pp. 350-354). IEEE.
- [70] Dawood, A., Marti, B. M., Sauret-Jackson, V., & Darwood, A. (2015). 3D printing in dentistry. *British dental journal*, 219(11), 521-529.
- [71] Khoo, Z. X., Teoh, J. E. M., Liu, Y., Chua, C. K., Yang, S., An, J., ... & Yeong, W. Y. (2015). 3D printing of smart materials: A review on recent progresses in 4D printing. *Virtual and Physical Prototyping*, 10(3), 103-122.
- [72] Thompson, M. K., Moroni, G., Vaneker, T., Fadel, G., Campbell, R. I., Gibson, I., ... & Martina, F. (2016). Design for Additive Manufacturing: Trends, opportunities, considerations, and constraints. *CIRP annals*, 65(2), 737-760.
- [73] Sepasgozar, S. M., Shi, A., Yang, L., Shirowzhan, S., & Edwards, D. J. (2020). Additive manufacturing applications for industry 4.0: A systematic critical review. *Buildings*, 10(12), 231.
- [74] Gul, J. Z., Sajid, M., Rehman, M. M., Siddiqui, G. U., Shah, I., Kim, K. H., ... & Choi, K. H. (2018). 3D printing for soft robotics—a review. *Science and technology of advanced materials*, 19(1), 243-262.
- [75] Ahmed, A., Azam, A., Bhutta, M. M. A., Khan, F. A., Aslam, R., & Tahir, Z. (2021). Discovering the technology evolution pathways for 3D printing (3DP)

using bibliometric investigation and emerging applications of 3DP during COVID-19. *Cleaner Environmental Systems*, 3, 100042.

[76] Kidwell, J. (2017). Best practices and applications of 3D printing in the construction industry.

[77] Lemu, H. G. (2012, April). Study of capabilities and limitations of 3D printing technology. In *AIP Conference Proceedings* (Vol. 1431, No. 1, pp. 857-865). American Institute of Physics.

[78] Shahrain, M., Didier, T., Lim, G. K., & Qureshi, A. J. (2016). Fast deviation simulation for 'fused deposition modeling' process. *Procedia Cirp*, 43, 327-332.

[79] Errandonea, I., Beltrán, S., & Arrizabalaga, S. (2020). Digital Twin for maintenance: A literature review. *Computers in Industry*, 123, 103316.

[80] Wang, Z. (2020). Review of real-time three-dimensional shape measurement techniques. *Measurement*, 156, 107624.

[81] Peng, A., Xiao, X., & Yue, R. (2014). Process parameter optimization for fused deposition modeling using response surface methodology combined with fuzzy inference system. *The International Journal of Advanced Manufacturing Technology*, 73(1), 87-100.

[82] Padhi, S. K., Sahu, R. K., Mahapatra, S. S., Das, H. C., Sood, A. K., Patro, B., & Mondal, A. K. (2017). Optimization of fused deposition modeling process parameters using a fuzzy inference system coupled with Taguchi philosophy. *Advances in Manufacturing*, 5(3), 231-242.

[83] Qattawi, A., Alrawi, B., & Guzman, A. (2017). Experimental optimization of fused deposition modelling processing parameters: a design-for-manufacturing approach. *Procedia Manufacturing*, 10, 791-803.

[84] Tanoto, Y. Y., Anggono, J., Siahaan, I. H., & Budiman, W. (2017, January). The effect of orientation difference in fused deposition modeling of ABS polymer on the processing time, dimension accuracy, and strength. In *AIP Conference Proceedings* (Vol. 1788, No. 1, p. 030051). AIP Publishing LLC.

[85] Chuang, C. M., Chen, C. Y., & Yau, H. T. (2002). A reverse engineering approach to generating interference-free tool paths in three-axis machining from scanned data of physical models. *The International Journal of Advanced Manufacturing Technology*, 19(1).

[86] Yanamandra, K., Chen, G. L., Xu, X., Mac, G., & Gupta, N. (2020). Reverse engineering of additive manufactured composite part by toolpath reconstruction using imaging and machine learning. *Composites Science and Technology*, 198, 108318.

- [87] Rupal, B. S., Mostafa, K. G., Wang, Y., & Qureshi, A. J. (2019). A Reverse CAD approach for estimating geometric and mechanical behavior of fdm printed parts. *Procedia Manufacturing*, 34, 535-544.
- [88] Mohammed, A., & Abdullah, A. (2018, November). Scanning electron microscopy (SEM): A review. In Proceedings of the 2018 International Conference on Hydraulics and Pneumatics—HERVEX, Băile Govora, Romania (pp. 7-9).
- [89] Hermena, S., & Young, M. (2021). CT-scan Image Production Procedures. StatPearls.
- [90] Roschli A, Gaul KT, Boulger AM, Post BK, Chesser PC, Love LJ, et al. Designing for big area additive manufacturing. *Addit Manuf* 2019;25:275–85.
- [91] Dudescu C, Racz L. Effects of raster orientation, infill rate and internal structure on the mechanical properties of 3d printed materials. *ACTA Universitatis Cibiniensis* 2017;69(1):23–30.
- [92] Bourell, D.L., M.C. Leu, and D.W. Rosen, Roadmap for additive manufacturing: identifying the future of freeform processing. The University of Texas at Austin, Austin, TX, 2009
- [93] Minetola, P., Iuliano, L., & Marchiandi, G. (2016). Benchmarking of FDM machines through part quality using IT grades. *Procedia Cirp*, 41, 1027-1032.
- [94] Costa, S.F., Duarte, F.M., Covas, J.A., Estimation of filament temperature and adhesion development in Fused Deposition Techniques. *Journal of Materials Processing Technology* <http://dx.doi.org/10.1016/j.jmatprotec.2017.02.026>
- [95] Wong, K. V., & Hernandez, A. (2012). A review of additive manufacturing. *International scholarly research notices*, 2012.
- [96] Delda, R. N. M., Basuel, R. B., Hacla, R. P., Martinez, D. W. C., Cabibihan, J. J., & Dizon, J. R. C. (2021). 3D Printing Polymeric Materials for Robots with Embedded Systems. *Technologies*, 9(4), 82.
- [97] Faust, J. L., Kelly, P. G., Jones, B. D., & Roy-Mayhew, J. D. (2021). Effects of Coefficient of Thermal Expansion and Moisture Absorption on the Dimensional Accuracy of Carbon-Reinforced 3D Printed Parts. *Polymers*, 13(21), 3637.
- [98] Henson, C. M., Decker, N. I., & Huang, Q. (2021). A Digital Twin strategy for major failure detection in fused deposition modeling processes. *Procedia Manufacturing*, 53, 359-367.

- [99] Peng, A. H., & Wang, Z. M. (2010). Researches into influence of process parameters on FDM parts precision. In *Applied Mechanics and Materials* (Vol. 34, pp. 338-343). Trans Tech Publications Ltd.
- [100] Msallem, B., Sharma, N., Cao, S., Halbeisen, F. S., Zeilhofer, H. F., & Thieringer, F. M. (2020). Evaluation of the dimensional accuracy of 3D-printed anatomical mandibular models using FFF, SLA, SLS, MJ, and BJ printing technology. *Journal of Clinical Medicine*, 9(3), 817.
- [101] Popescu, D., Zapciu, A., Amza, C., Baci, F., & Marinescu, R. (2018). FDM process parameters influence over the mechanical properties of polymer specimens: A review. *Polymer Testing*, 69, 157-166.
- [102] Boschetto, Alberto, Luana Bottini, and Francesco Veniali. "Integration of FDM surface quality modeling with process design." *Additive Manufacturing* 12 (2016): 334-344
- [103] Garzón, E. O., Alves, J. L., & Neto, R. J. (2017). Post-process influence of infiltration on binder jetting technology. In *Materials design and applications* (pp. 233-255). Springer, Cham
- [104] Ullah, A. M. M., Kubo, A., & Harib, K. H. (2020). Tutorials for integrating 3D printing in engineering curricula. *Education sciences*, 10(8), 194.
- [105] Mourtzis, D., Toghias, T., Angelopoulos, J., & Stavropoulos, P. (2021). A Digital Twin architecture for monitoring and optimization of Fused Deposition Modeling processes. *Procedia CIRP*, 103, 97-102.
- [106] Yin, J., Lu, C., Fu, J., Huang, Y., & Zheng, Y. (2018). Interfacial bonding during multi-material fused deposition modeling (FDM) process due to inter-molecular diffusion. *Materials & Design*, 150, 104-112.
- [107] Vergara Gómez, S. (2020). Evaluation of digimat's thermomechanical analysis capabilities in the simulation of FDM process.
- [108] Armillotta, A., Bellotti, M., & Cavallaro, M. (2018). Warpage of FDM parts: Experimental tests and analytic model. *Robotics and Computer-Integrated Manufacturing*, 50, 140-152.
- [109] Kantaros, A., & Karalekas, D. (2013). Fiber Bragg grating based investigation of residual strains in ABS parts fabricated by fused deposition modeling process. *Materials & Design*, 50, 44-50.
- [110] Zhang, Y., & Chou, Y. K. (2006). Three-dimensional finite element analysis simulations of the fused deposition modelling process. *Proceedings of the Institution of Mechanical Engineers, Part B: Journal of Engineering Manufacture*, 220(10), 1663-1671.

- [111] Mahesh, M., Wong, Y. S., Fuh, J. Y. H., & Loh, H. T. (2004). Benchmarking for comparative evaluation of RP systems and processes. *Rapid Prototyping Journal*.
- [112] Coogan, T. J., & Kazmer, D. O. (2017). Healing simulation for bond strength prediction of FDM. *Rapid Prototyping Journal*
- [113] Courter, B., Savane, V., Bi, J., Dev, S., & Hansen, C. J. (2017, June). Finite element simulation of the fused deposition modelling process. In Proceedings of the NAFEMS World Congress (pp. 11-14).
- [114] Sun, Q., Rizvi, G. M., Bellehumeur, C. T., & Gu, P. (2008). Effect of processing conditions on the bonding quality of FDM polymer filaments. *Rapid prototyping journal*.
- [115] El Moumen, A., Tarfaoui, M., & Lafdi, K. (2019). Modelling of the temperature and residual stress fields during 3D printing of polymer composites. *The International Journal of Advanced Manufacturing Technology*, 104(5), 1661-1676.
- [116] Söderberg, R., Wärmefjord, K., Carlson, J. S., & Lindkvist, L. (2017). Toward a Digital Twin for real-time geometry assurance in individualized production. *CIRP annals*, 66(1), 137-140.
- [117] Zhang, Y., & Shapiro, V. (2018). Linear-time thermal simulation of as-manufactured fused deposition modeling components. *Journal of Manufacturing Science and Engineering*, 140(7).
- [118] Gouge, M., Denlinger, E., Irwin, J., Li, C., & Michaleris, P. (2019). Experimental validation of thermo-mechanical part-scale modeling for laser powder bed fusion processes. *Additive Manufacturing*, 29, 100771.
- [119] Shen, B., Shih, A. J., & Xiao, G. (2011). A heat transfer model based on finite difference method for grinding. *Journal of manufacturing science and engineering*, 133(3).
- [120] Zhou, Y., Nyberg, T., Xiong, G., & Liu, D. (2016, July). Temperature analysis in the fused deposition modeling process. In *2016 3rd international conference on information science and control engineering (ICISCE)* (pp. 678-682). IEEE.
- [121] Cattenone, A., Morganti, S., Alaimo, G., & Auricchio, F. (2019). Finite element analysis of additive manufacturing based on fused deposition modeling: distortions prediction and comparison with experimental data. *Journal of Manufacturing Science and Engin*

- [122] Croccolo, D., De Agostinis, M., & Olmi, G. (2013). Experimental characterization and analytical modelling of the mechanical behaviour of fused deposition processed parts made of ABS-M30. *Computational Materials Science*, 79, 506-518.
- [123] Sonmez, F. O., & Hahn, H. T. (1998). Thermomechanical analysis of the laminated object manufacturing (LOM) process. *Rapid Prototyping Journal*.
- [124] Baronio, G., Harran, S., & Signoroni, A. (2016). A critical analysis of a hand orthosis reverse engineering and 3D printing process. *Applied bionics and biomechanics*, 2016.
- [125] Chen, H., Yang, X., Chen, L., Wang, Y., & Sun, Y. (2016). Application of FDM three-dimensional printing technology in the digital manufacture of custom edentulous mandible trays. *Scientific reports*, 6(1), 1-6.
- [126] Nancharaiah, T. R. D. R. V., Raju, D. R., & Raju, V. R. (2010). An experimental investigation on surface quality and dimensional accuracy of FDM components. *International Journal on Emerging Technologies*, 1(2), 106-111.
- [127] Johnson, W. M., Rowell, M., Deason, B., & Eubanks, M. (2014). Comparative evaluation of an open-source FDM system. *Rapid Prototyping Journal*.
- [128] Pei, E., Campbell, R.I. and Beer, D. (2011), "Entry-level RP machines: how well can they cope with geometric complexity?", *Assembly Automation*, Vol. 31 No. 2, pp. 153-160
- [129] Pratt, M. J., Bhatt, A. D., Dutta, D., Lyons, K. W., Patil, L., & Sriram, R. D. (2002). Progress towards an international standard for data transfer in rapid
- [130] Ameta, G., Lipman, R., Moylan, S., & Witherell, P. (2015). Investigating the role of geometric dimensioning and tolerancing in additive manufacturing. *Journal of Mechanical Design*, 137(11).
- [131] Zharylkassyn, B., Perveen, A., & Talamona, D. (2021). Effect of process *Today: Proceedings*, 44, 1307-1311
- [132] Erdemir, A., Guess, T. M., Halloran, J., Tadepalli, S. C., & Morrison, T. M. (2012). Considerations for reporting finite element analysis studies in biomechanics. *Journal of biomechanics*, 45(4), 625-633.
- [133] Paul, S. (2021). Finite element analysis in fused deposition modeling research: A literature review. *Measurement*, 178, 109320.
- [134] Domingo-Espin, M., Puigoriol-Forcada, J. M., Garcia-Granada, A. A., Lumà, J., Borros, S., & Reyes, G. (2015). Mechanical property characterization

and simulation of fused deposition modeling Polycarbonate parts. *Materials & Design*, 83, 670-677.

[135] Salonitis, K., & Al Zarban, S. (2015). Redesign optimization for manufacturing using additive layer techniques. *Procedia Cirp*, 36, 193-198.

[136] Garg, A., & Bhattacharya, A. (2017). An insight to the failure of FDM parts under tensile loading: finite element analysis and experimental study. *International Journal of Mechanical Sciences*, 120, 225-236.

[137] Qattawi, A., & Ablat, M. A. (2017). Design consideration for additive manufacturing: fused deposition modelling. *Open Journal of Applied Sciences*, 7(6), 291-318.

[138] Hambali, R. H., Celik, H. K., Smith, P. C., Rennie, A. E. W., & Ucar, M. (2010, September). Effect of build orientation on FDM parts: a case study for validation of deformation behaviour by FEA. In IN: Proceedings of IDECON 2010—international conference o

[139] Hopkinson, N., & Dicknes, P. (2003). Analysis of rapid manufacturing—using layer manufacturing processes for production. *Proceedings of the Institution of Mechanical Engineers, Part C: Journal of Mechanical Engineering Science*, 217(1), 31-39.

[140] Baikerikar, P. J., & Turner, C. J. (2017, August). Comparison of as-built FEA simulations and experimental results for additively manufactured dogbone geometries. In *International Design Engineering Technical Conferences and Computers and Information in Engineering Conference* (Vol. 58110, p. V001T02A021). American Society of Mechanical Engineers.

[142] Zhou, M., Yan, J., & Feng, D. (2019). Digital Twin framework and its application to power grid online analysis. *CSEE Journal of Power and Energy Systems*, 5(3), 391-398.

[141] Lalegani Dezaki, M., & Mohd Ariffin, M. K. A. (2020). The effects of combined infill patterns on mechanical properties in fdm process. *Polymers*, 12(12), 2792.

[152] Martínez, J., Diéguez, J. L., Ares, E., Pereira, A., Hernández, P., & Pérez, J. A. (2013). Comparative between FEM models for FDM parts and their approach to a real mechanical behaviour. *Procedia Engineering*, 63, 878-884.

[143] Abbas, T., Othman, F. M., & Ali, H. B. (2017). Effect of infill Parameter on compression property in FDM Process. *dimensions*, 12(12.7), 25-4.

[144] Naranjo-Lozada J, Ahuett-Garza H, Orta-Castañón P, Verbeeten WMH, SáizGonzález D. Tensile properties and failure behavior of chopped and

continuous carbon fiber composites produced by additive manufacturing. *Addit Manuf* 2019;26:227–41.

[145] Forcellese A, Simoncini M, Vita A, Di Pompeo V. 3D printing and testing of composite isogrid structures. *Int J Adv Manuf Tech* 2020;109(7-8):1881–93.

[146] Blok LG, Longana ML, Yu H, Woods BKS. An investigation into 3D printing of fibre reinforced thermoplastic composites. *Addit Manuf* 2018;22:176–86.

[147] Günaydın K, Türkmen HS. Common FDM 3D printing defects. In *International Congress on 3D Printing (Additive Manufacturing) Technologies and Digital Industry*, 2018.

[148] Fayazbakhsh K, Movahedi M, Kalman J. The impact of defects on tensile properties of 3D printed parts manufactured by fused filament fabrication. *Mater Today Commun* 2019;18:140–8.

Published papers

Guajardo-Trevino, A. M., Ahuett-Garza, H., Orta-Castanon, P., Urbina-Coronado, P. D., Saldana, C., & Kurfess, T. R. (2022). Effects of deposition-strategy-induced raster gaps and infill voids on the compressive strength of 3D printed isogrid structures. *Manufacturing Letters*, 31, 15-19.

<https://doi.org/10.1016/j.mfglet.2021.12.001>

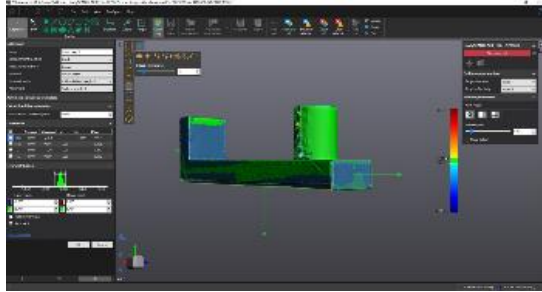
Curriculum Vitae

Alan Mauricio Guajardo Treviño born in Monterrey, México, on October 07, 1991. He earned the Mechanical Engineering degree from the *Universidad Autonoma de Nuevo Leon*, in June 2014. He earned his Master's Degree in Production Management, in Donosti, Spain in 2016. He was accepted in Science doctorate in Jan 2018.

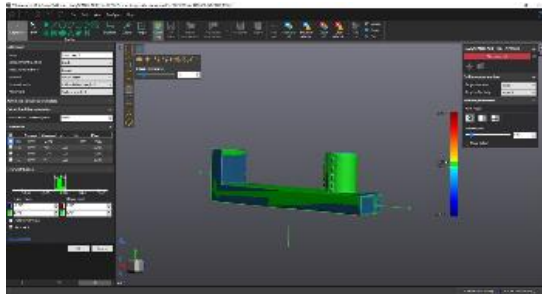
This document was typed in using Microsoft Word by Alan Mauricio Guajardo Treviño

Appendix A

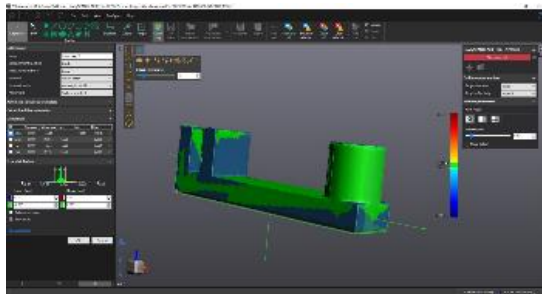
The following appendix contains images of the point cloud difference between the CAD model.



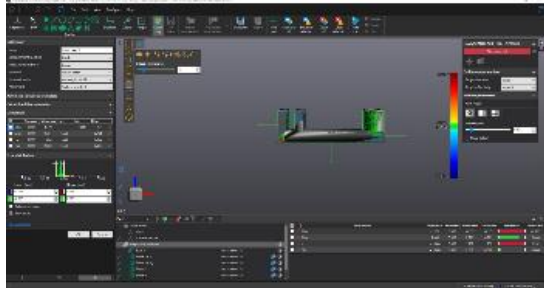
Scan 1W onyx side s4 measured 2.0



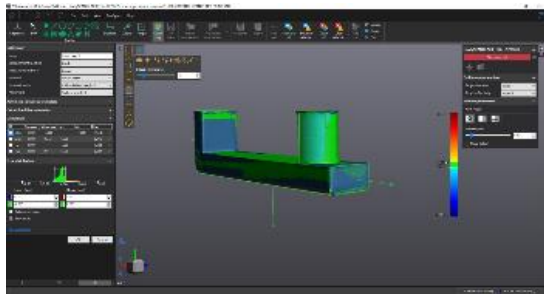
Scan 1W onyx side s5 measured 2.0



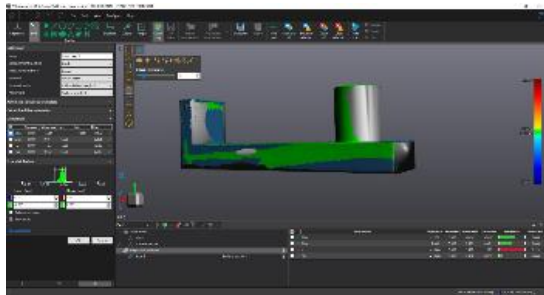
Scan 2W onyx side s4 measured 2.0



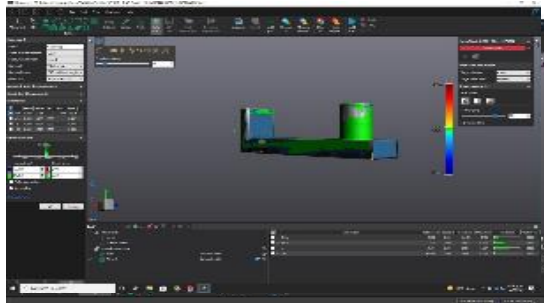
Scan 2W onyx side s5 measured 2.0



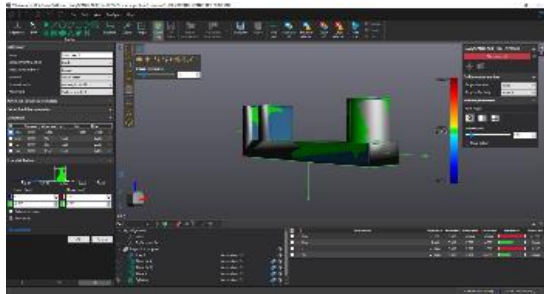
Scan onyx 1W up s4 measured 2.0



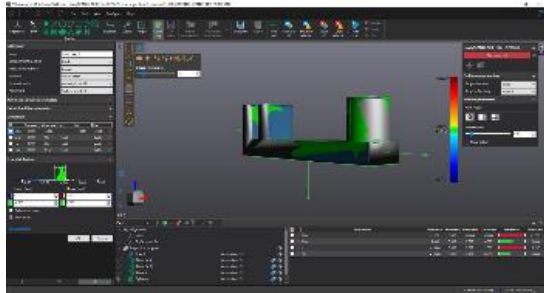
Scan onyx 1W up s5 measured 2.0



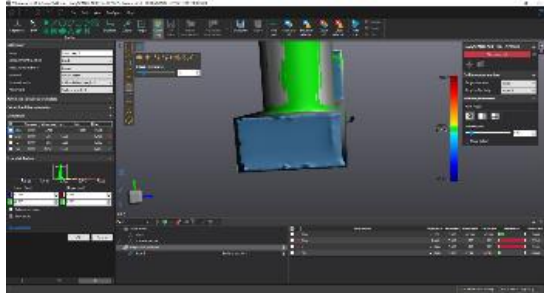
Scan onyx 2W up s3 measured 2.0



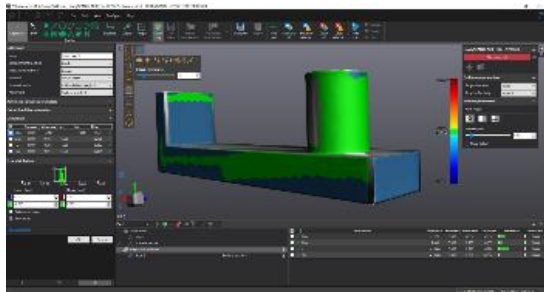
Scan onyx 2W up s4 measured 2.0



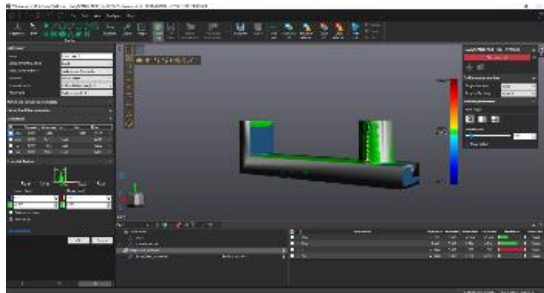
scan onyx 2W up s5 measured 2.0



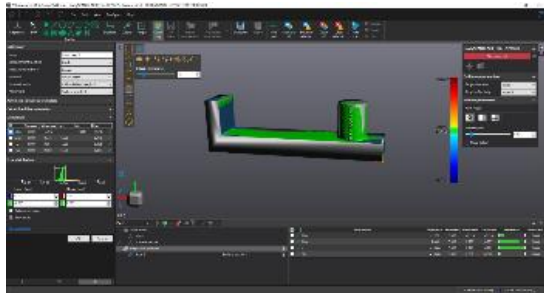
Scan onyx 1W up s1 measured 2.0



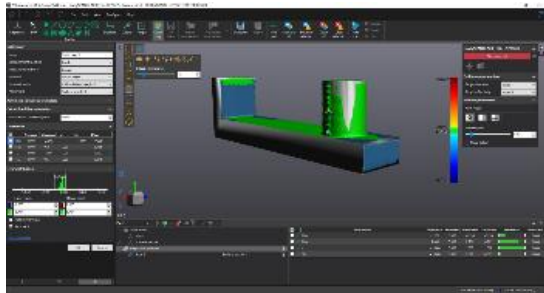
Scan onyx 1W up s2 measured 2.0



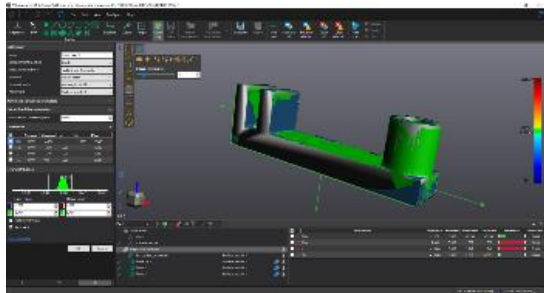
Scan onyx 1W up s3 measured 2.0



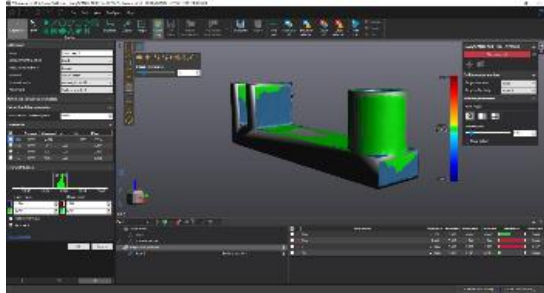
Scan 1W onyx side s1 measured 2.0



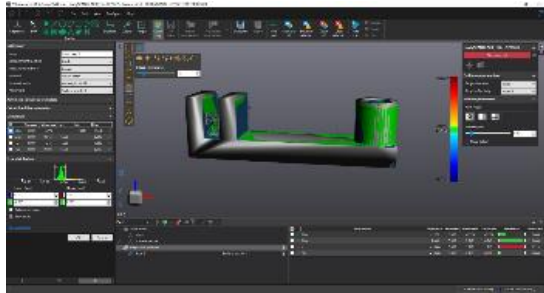
Scan 1W onyx side s2 measured 2.0



Scan 1W onyx side s3 measured 2.0



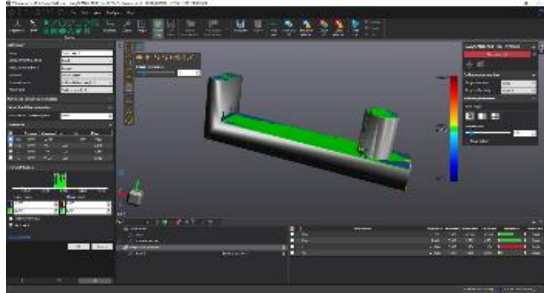
Scan 2W onyx side s1 measured 2.0



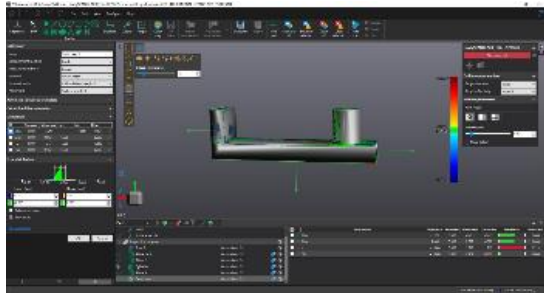
Scan 2W onyx side s2 measured 2.0



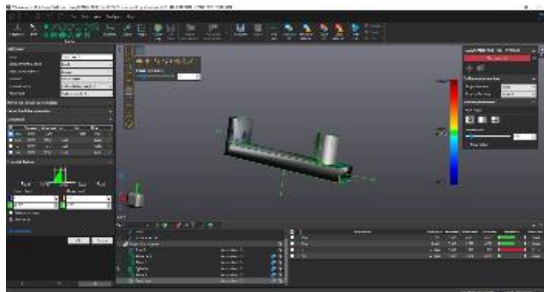
Scan 2W onyx side s3 measured 2.0



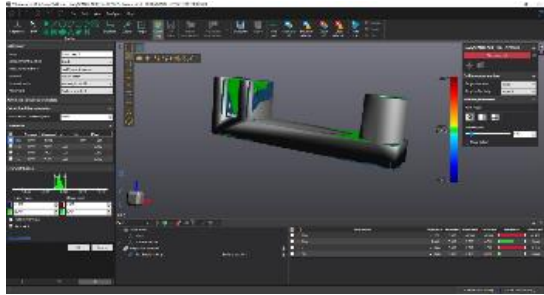
Scan PLA 1W up s1 measured 2.0



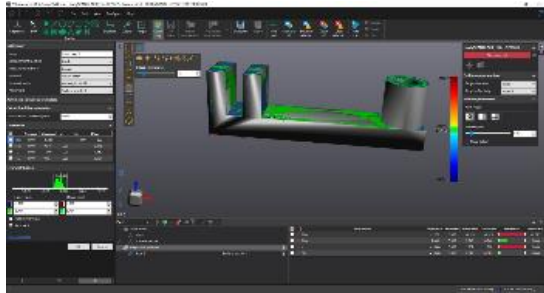
Scan PLA 1W up s3 measured 2.0



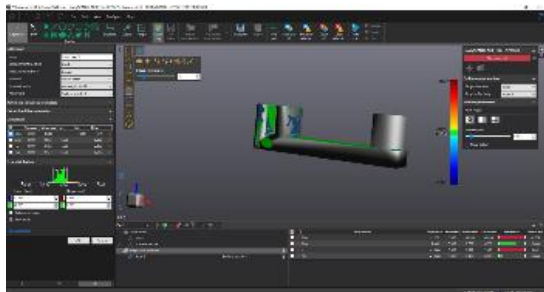
Scan PLA 1W up s4 measured 2.0



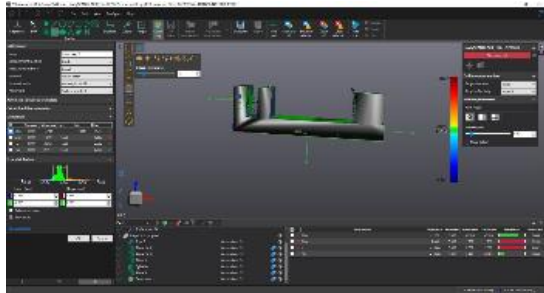
Scan PLA 1W up s5 measured 2.0



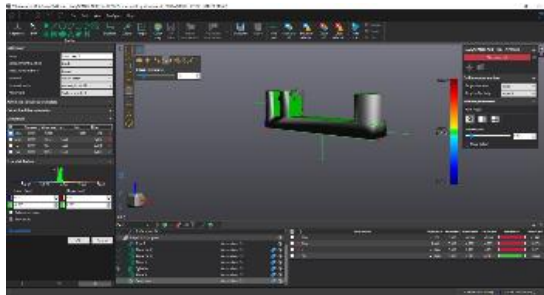
Scan PLA 2W up s1 measured 2.0



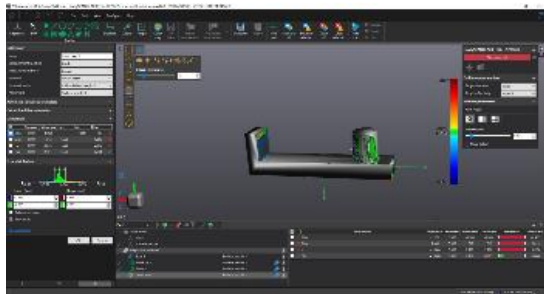
Scan PLA 2W up s2 measured 2.0



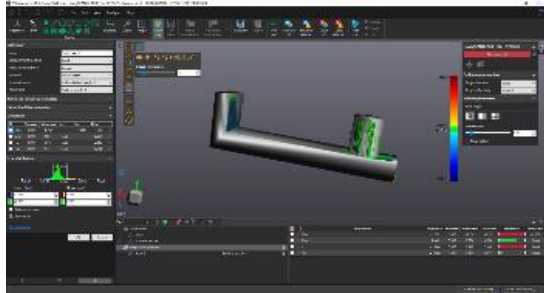
Scan PLA 2W up s3 measured 2.0



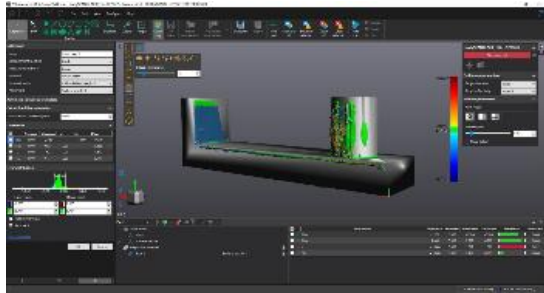
Scan PLA 2W up s4 2.0 measured 2.0



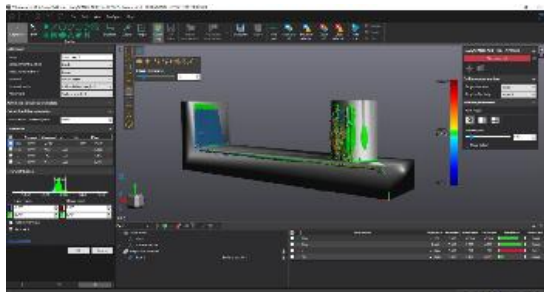
Scan PLA 2W up s5 measured 2.0



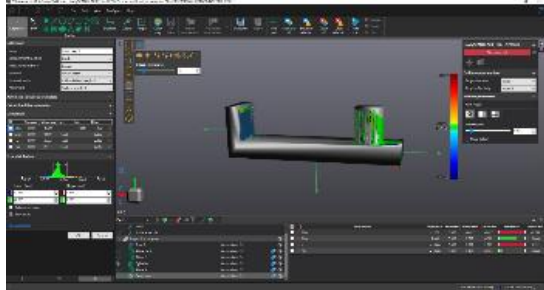
Scan PLA 1W side measured 2.0



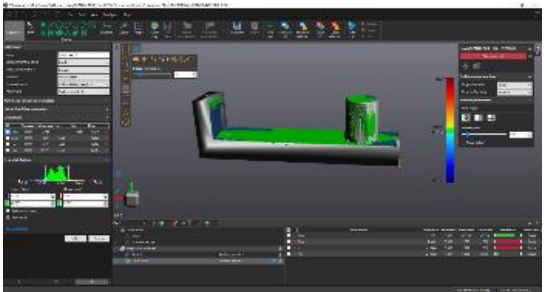
Scan PLA 1W side s2 measured 2.0



Scan PLA 1W side s3 measured 2.0



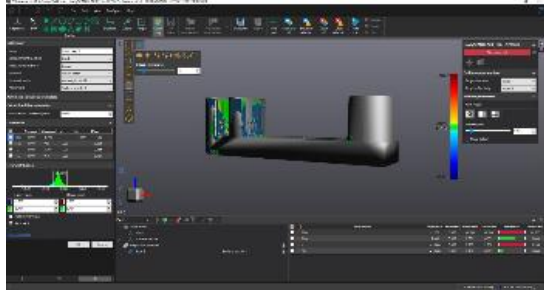
Scan PLA 1W side s4 measured 2.0



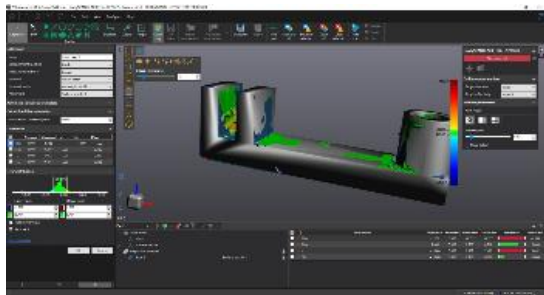
Scan PLA 1W side s5 measured 2.0



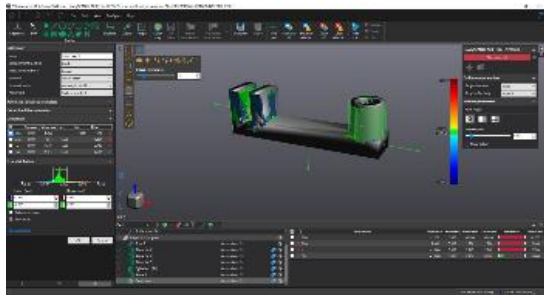
Scan PLA 2W side measured 2.0



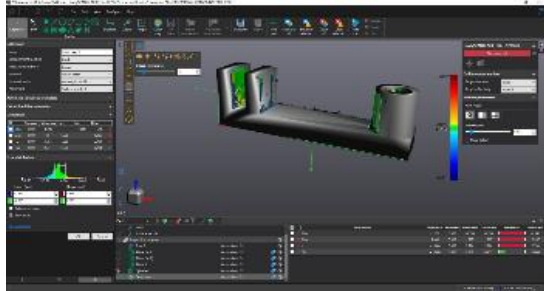
Scan PLA 2W side s2 measured 2.0



Scan PLA 2W side s3 measured 2.0



Scan PLA 2W side s4 measured 2.0



Scan PLA 2W side s5 measured 2.0